A study of the non-linear dynamics of vortex flows by numerical methods

by

Jes Peter Christiansen

A dissertation submitted to the University of Warwick for admission to the degree of Doctor of Philosophy

MEMORANDUM

This dissertation is submitted to the University of Warwick in support of my application for admission to the degree of Doctor of Philosophy. It contains an account of my own work performed at Culham Laboratory, Abingdon and at the School of Physics of the University of Warwick in the period September 1969 to January 1972 under the general supervision of Doctor K.V. Roberts of Culham Laboratory and Doctor G. Rowlands of the University of Warwick. No part of this dissertation has been used previously in a degree thesis submitted to this or any other University. The work described in this thesis is the result of my own independent research except where specifically acknowledged in the text.

J. P. Christiansen

ACKNOWLEDGEMENTS

The author wishes to express his deep gratitude to Dr K V Roberts and Dr G Rowlands for their continued interest and encouragement throughout the course of this work. I wish especially to thank Dr J B Taylor and Dr N J Zabusky for their cooperation and helpful assistance. I would also like to thank all those members of the Computational Physics Group and Applied Mathematics Group at Culham Laboratory, who have been available for discussions. Furthermore, I would like to thank the computing staff at Culham Laboratory for helpful assistance.

I gratefully acknowledge the financial support provided by the United Kingdom Atomic Energy Authority and by my father L.Christiansen.

Finally, I wish to thank Mrs H B Pengelly for her skill and patience in typing this thesis.

ABSTRACT

The subject of motions in two-dimensional ideal fluids is treated by numerical methods and the results given an interpretation based on theories as well as numerical experiments. Phenomena in ideal fluids have relevance to flows in realistic fluids when the flow speeds encountered are much smaller than the speed of sound and when dissipative mechanisms play a negligible role. The restriction to consider only motions of two dimensions is established and the resulting mathematical description yields a classical formalism. In terms of the scalar vorticity the motion of a two-dimensional ideal fluid can be interpreted by the flow in phase space of a classical phase fluid. The scalar stream function acts as a Hamiltonian for a system whose phase space corresponds to real space. Two models with respectively an infinite and a finite number of degrees of freedom are used to picture the evolution with time of the vorticity distribution. The former model, the field model, is used in analytic studies, and the latter model, the particle model, is employed in the numerical approach. The field model is reviewed as an introduction to the subject. The particle model is fitted into a numerical scheme that forms the basis of a computer simulation code VORTEX. This numerical scheme is presented in detail and made the subject of a numerical analysis. Controlled numerical experiments are carried out to establish possible inaccuracies of the scheme and the sources of these inaccuracies are revealed by means of the results from the numerical analysis. The general work of preparing controlled numerical experiments is briefly mentioned and by recording the experience from several numerical experiments the quality of these can be assessed. Results of several numerical experiments are then presented. The problem of two-dimensional turbulence is tackled by a precursory study of the interaction between finite area vorticity regions. An analytic calculation is made to support the

numerical simulations which demonstrate the non-linear aspects of vortex interactions: fusion of strongly interacting vortices of the same sign and large amplitude oscillations in the flow from two vortices of opposite sign. The numerical experiments that follow, treat the stability and long time evolution of laminar wakes, and heuristic comparisons are made with wind tunnel experiments that minimise three-dimensional effects. A model of four finite-sized vortices is used to study the stability of von Kármán vortex streets. Comparisons with theory are made and the results show fusion of like-signed vortex regions as well as fission of a vortex in the presence of other vortices. The final study comprises numerical experiments with a model approximating vortex flows in jets. It is concluded that much insight can be gained by using relatively simple flow models combined with a suitable numerical scheme in order to understand the non-linear dynamics of vortex flows.

Publications

Various aspects of the work described in this thesis have been published, or are in the course of publication in the scientific literature. With reference to the chapters of this thesis the relevant publications are:

CHAPTER 1 : CHRISTIANSEN, J P and ROBERTS, K V , 1969. Paper 40 in the Proceedings of the Computational Physics Conference at Culham Laboratory, July 1969. Available from HMSO.

CHAPTER 2 : CHRISTIANSEN, J P and HOCKNEY, R W , 1971. Comp.Phys.Comm. 2, 127.

CHRISTIANSEN, J P and HOCKNEY, R W , 1971. Comp.Phys.Comm. 2, 139.

CHRISTIANSEN, J P , 1971. Numerical simulation of hydrodynamics by the method of point vortices. UKAEA Culham Report CLM-P282 submitted for publication in Journal of Computational Physics.

CHRISTIANSEN, J P and ROBERTS, K V , 1969. Numerical simulation techniques applied to incompressible hydrodynamic flows. 3rd Annual Conference on Plasma Simulation at Stanford University, September 1969.

CHRISTIANSEN, J P and ROBERTS, K V , 1969. Paper 51 in the Proceedings of the Computational Physics Conference at Culham Laboratory, July 1969. Available from HMSO.

ROBERTS, K V and CHRISTIANSEN, J P , 1972. Topics in Computational Fluid Mechanics. Comp.Phys.Comm. 3. Suppl.

CHAPTER 4 : CHRISTIANSEN, J P and ROBERTS, K V , 1970. The non-linear development of modes on the surface of circular vortices. Conference Digest, Computational Physics, The Institute of Physics and the Physical Society, London.

CHRISTIANSEN, J P and ROBERTS, K V , 1971. Simulation of hydrodynamic systems oscillating with large amplitudes around stationary equilibrium states. 5th Annual Conference on Plasma Simulation at University of Iowa, Nov.1971.

CHAPTER 5 : CHRISTIANSEN, J P and ZABUSKY, N J , 1972. Instability, fission and fusion of asymmetric vortex structures. UKAEA Culham Report CLM-P306. Submitted for publication in Journal of Fluid Mechanics.

APPENDIX : CHRISTIANSEN, J P , 1970. VORTEX, a two-dimensional hydrdynamics simulation code. UKAEA Research Report CLM-R106. Available from HMSO.

CONTENTS

INTRODUCTION

The introduction to this thesis outlines our approach to Computational Physics. The combination of Hydrodynamics and Computational Physics is treated in a short review of previous relevant work. An account of the research carried out is given as a survey of the work presented in each chapter.

Approach to Computational Physics

The advent of high-speed computers has over the last decade exerted an influence on practically every science. The almost explosion-like evolution of computer technology has made it difficult to forecast what future role computers will play. In some areas of experimental sciences analogue computers have replaced human beings, whilst in other areas a digital computer merely acts as a fast slide rule or graph plotter. It is quite clear that a variety of views on the significance of computers must exist amongst the people who design them, use them and those whose work can be computerised. We shall not attempt to promote any of these views, but only try to briefly establish the areas covered by Computational Physics.

By definition we think of Computational Physics as the discipline in which the elementary operations inherited from Applied Mathematics are processed by computing machinery to produce results of a physics calculation. At its inception this discipline was conceptually identical to Applied Mathematics. Today, some 10-15 years later, Computational Physics is in the process of being established as a self-contained discipline. Although several classical areas of physics are involved in one way or another, it is generally accepted that Computational Physics mainly interacts with the following branches of science:

1. Theoretical Physics and Mathematics
2. Experimental Physics
3. Applied Mathematics and Numerical Analysis
4. The general science of computers.

Many opinions exist as to how emphasis should be placed on each of these areas. The rank of priorities given to the work in this thesis follows from the list above and is put "in manifesto" by the division of the research work into distinctly separate chapters. The time and effort spent

in each of these four areas are however not proportionally represented in this thesis, as it would change the rank of priorities given above. It is the opinion of the author that at present too much time and effort are often spent in the area of computing science, the handling of computers and the writing of computer programs. Not surprisingly one finds in the scientific community a widespread lack of distinction between computing science and computational physics. It is the author's hope that the work presented in this thesis will do justice to making that distinction clear.

Hydrodynamics and Computational Physics

Hydrodynamics is one of the oldest disciplines in modern physics, yet with a rather peculiar history. To review its history is beyond the scope of this thesis and therefore only features of relevance to the present work will be mentioned. - The initial interest in hydrodynamics arose from attempts to describe the dynamics of continuous media, e.g. fluids. The present interest establishes itself through many disciplines associated with hydrodynamics: "The development of aircraft has caused an interest in aerodynamics and hydraulics. The exploration of the solar system and advances made in astrophysics have developed magneto-hydrodynamics. Nuclear fusion research has pushed forward theories in plasma physics. The construction of large ships and submarines has intensified experimental hydrodynamic studies".

The area in which these disciplines overlap is characterised by the problem of describing motions occurring in media which for all practical purposes are regarded as continuous in structure. There is a great variety of media (ultra-dense stellar matter, water, a rarefied plasma) whose motions can be treated hydrodynamically. The more complex a structure of a medium becomes, the more comprehensive a parametric description becomes. Yet irrespective of its actual material composition a medium will funda-

mentally exhibit dynamical properties described by the partial differential equations of hydrodynamics. These equations were formulated in 1760 by Euler with applications to a simple fluid model. Since then Euler's idealised model has been superseded by more realistic and also more complicated models. These latter models introduce concepts like compressibility of a fluid, viscous forces, electromagneto-dynamic forces, oblique stresses etc. All these concepts serve to account for the complexity of the internal fluid structure; sometimes even more than one fluid is being introduced in a model. Research on such complex models is often confined to studying the influence of new features of the internal fluid structure rather than the general dynamics of the model.

In order to understand the dynamics of fluids it seems reasonable to consider first the motions that occur in simple fluids. The present work is conceived in the belief that many intricate and perplexing fluid motions can be explained by studies of idealised models. The most ideal model we can think of consists of a fluid whose material (molecular) composition has no effect whatsoever on any motion into which it can be set. Such a fluid is called an ideal fluid and it has been the subject matter of many investigations. Motions in ideal fluids will bear some relationship to flows in real fluids when the flow speed encountered are much smaller than the sound speed and dissipation of energy due to viscous forces can be neglected. An ideal fluid is incompressible such that any disturbance communicated travels at infinite speed. An ideal fluid is also inviscid (zero viscosity) and its density is usually assumed uniform.

Most of the flows occurring in fluids are rotational, e.g. two- or three-dimensional phenomena. This important feature is reflected in Kelvin's minimum theorem and also in a demonstration by Kirchoff and Kelvin stating that irrotational flows are in general impossible (see Lamb, 1932). The conceptual backbone of rotational motions is centered around the definition of vorticity, a quantity introduced by d'Alembert and now used by most authors

in hydrodynamics. The vorticity is a vector describing the instantaneous rate of rotation in a plane perpendicular to the vectorial direction. (The standard sign convention applies). Vortices are finite fluid regions that possess vorticity and a vortex can be shaped like a ring, a twisted tube, or a cylinder. The motion of the fluid can be described by the motion of vortices: knowing the vorticity distribution we can determine the resulting flow field.

When a motion is strictly two-dimensional then the description in terms of vorticity of a two-dimensional ideal fluid can be based on a Hamiltonian formalism, a feature discovered by Kirchoff. The vorticity becomes a scalar function whose evolution with time is governed by Poisson's and Liouville's equations. The scalar vorticity distribution behaves as a classical phase space distribution in a two-dimensional phase space. Such a situation has received attention from many authors and various models have been employed to picture the flow of an incompressible phase fluid. The vortices which are the sources of the flow field are now restricted to move about in a plane and correspond to rectilinear vortices in a three-dimensional flow. Although the mathematical description of two-dimensional ideal fluids in its classic formalism is attractive to employ for studies of hydrodynamic flows, we admit its inadequacy to represent more than a highly restricted class of phenomena whose dynamics becomes degenerate through the lack of the third space dimension.

The various models used to picture the flow of a phase fluid can be divided into two classes. In the first class the vorticity distribution is represented as a truly continuous function. In the second class the vorticity distribution is considered to arise from a finite number of point vortices which are analogous to point charges in electrostatics or point masses in gravitational problems. A point vortex can, like a point charge or mass, be represented by a Dirac delta-function and it induces an

irrotational motion with a singularity at its position. The two classes of models are based on two descriptions: field model (continuum) and action-at-a-distance model (point vortices).

A model of the first class, called "the constant vorticity model" is of particular interest to our work. In this model the vorticity takes constant values different from zero in areas confined by contours. If these contours are closed we think of the area as being a vortex. The constant vorticity model has been used in studies by Kirchoff, Kelvin, Love, Hill and later by Proudman and Lamb. Because of the non-linearity of the hydrodynamic equation only special systems involving simple contours are treated. Most of this work is reviewed in the books of Bassett (1888) and Lamb (1932).

The point vortex model originally introduced by Kirchoff is rigorously analysed by Lin (1943). It was used by von Kármán (1911) in a study of the stability of vortex streets (parallel arrays of oppositely-signed point vortices). Von Kármán's study was extended by Rosenhead (1929 & 1930) and is also treated in the book by Kochin, Kibel & Roze (1964). The most important work on the point vortex model is presented in a paper by Onsager (1949) who attempts to develop a theory of the statistical mechanics of ensembles of point vortices. This paper has been followed up by a study by Morikawa (1960) with applications to meteorology.

With the advent of computers it is possible to treat previously insolvable problems, e.g. non-linear problems, by applying suitable numerical methods to approximate the partial differential equations. A new subject, Computational Fluid Mechanics, has grown from the efforts made to understand the non-linear dynamics of fluid flows. A review of these efforts is given in the form of an annotated bibliography by Harlow (1970).

Recent work in the field of Computational Fluid Mechanics comprises a

study by Abernathy & Kronauer (1962) of the formation of the von Karman vortex street. Lately this study has been repeated by Kadomsev & Kostomarov (1972). Both studies employed the point vortex model treating the point-point interaction by an exact method, however for a small number ($\sim$ 50) of point vortices.

The majority of relevant numerical investigations have been based on transformations of the partial differential equations into finite difference forms. In most studies the effects from viscous forces are introduced as is the case in the work of Fromm & Harlow (1963), Leith (1969) and Zabusky & Deem (1971). The most intriguing problem dealt with is that of turbulence from a two-dimensional point of view (Kraichman, 1967) and a variety of approaches to this problem have been made. A straightforward finite difference attack on a three-dimensional turbulent flow (for example through a pipe) can never succeed in practice when the viscosity is small, as pointed out by Emmons (1970). This example serves to illustrate how Computational Fluid Mechanics and Computational Physics in general are confined to deal with abstract models (dimensionality, geometry, fluid properties etc.). Nevertheless much insight and qualitative understanding of real phenomena can be gained from numerical calculations and this leaves the field of Computational Fluid Mechanics open for innovations of both numerical and physical nature. The conclusion reached by most authors in the field is that much further work remains to be done.

Research carried out

The scope of the work has settled in various forms during the three-year period of research. The material presented in this thesis represents approximately a third of the research period. The remaining material comprises the design and testing of computer codes (see Appendix) and the work on two-dimensional guiding centre plasmas. The last item is summar-

ised in a paper by the author and J.B. Taylor (1972).

The work began with the development of a computer code, VORTEX, capable of simulating a restricted class of two-dimensional flows in ideal fluids. Its background, design and operation is presented in a report included as an appendix to this thesis. The operation of the code was carried out on the Culham Laboratory ICL KDF9 computer for which the VORTEX code had been specially designed. The graphical output presented as figures in this thesis was generated by a Benson-Lehner 120 microfilm recorder. -

In chapter 1 we set out to describe the basis of our work:"motions in ideal fluids of two dimensions". The concept of vorticity is introduced to demonstrate that the motion of ideal fluids of two dimensions can be pictured as the flow in phase space of an incompressible phase fluid. Our description adds no new contributions to the subject; it serves as a guide to the following chapters. In our work we have however aimed at expanding and elaborating the work of Onsager (1949).

Because a phase fluid of two dimensions is a classical system, one would expect to establish a theory of thermodynamic equilibria including concepts like temperature, entropy etc. When a point vortex model is studied we have a finite number N of degrees of freedom such that Gibbs general theory of thermodynamic equilibria applies. If the field model is studied we have a system with an infinite number of degrees of freedom, but such systems are well-known, the most familiar example being the classical electromagnetic field. By itself, a classical system with an infinite number of degrees of freedom behaves in a self-consistent way. If we follow principles laid down by Lynden-Bell (1967) it is possible to show even in the limit $N \to \infty$ that in equilibrium the vorticity distribution, when the entropy (suitably defined) is maximized, is that given by

Lynden-Bell. It should then be possible to define the usual thermodynamic quantities when $N \to \infty$. For a finite N Onsager (1949) defines temperature and shows that it can take positive and negative values. Our advances in the case $N \to \infty$ end at this point because the area-functions described at the end of chapter 1 enter all the mathematical expressions involved and we have had no success in determining these functions. Thus we have not found it worthwhile including this study in chapter 1.

Chapter 2 represents a self-contained description of the numerical method employed to approximate the partial differential equations. Although we aim at studying field models (continuous models) we have chosen to approximate these by a discrete set of point vortices which are then essentially regarded as particles. The particle model, which has found extensive use in Plasma Physics (see references at the end of chapter 2) is fitted into a numerical scheme which solves the appropriate equations on a square Cartesian mesh. All physical quantities (e.g. vorticity, velocity field) are then readily calculable. In order to understand the effects arising from the approximations made we perform a series of controlled numerical experiments on the flow induced by a single circular vortex of finite size (a Rankine vortex). The results from these experiments reveal certain undesired features of our numerical model and in the light of a numerical analysis of this model we explain the sources of the errors in the results. At the end of the chapter it is concluded that the numerical approach is suitable for our studies and the limitations on these is established to some extent. The numerical scheme we describe is a new scheme and like other schemes it has its advantages and deficiencies. We find that the studies made in the following chapters could not have been made with any other existing scheme.

Chapter 3 is intended to indicate the considerations that go ahead of implementing numerical experiments. This chapter is deliberately made as

short as possible, since it would excessively swell the bulk of this thesis if all numerical experiments performed were to be described in detail. We outline features that are common to most of our numerical experiments and discuss the initial vorticity distributions and boundary conditions used. To back up the conclusion of chapter 2 we comment in general on the quality of the numerical experiments by quoting results from these.

The work presented in chapter 4 is related to the problem of turbulence in ideal fluids of two dimensions (Kraichnan, 1967). To tackle this problem we have initially found it worthwhile studying the interaction properties of systems with two finite-sized vortices. The intention of the study is to establish some features of the large scale length behaviour of turbulent motions.

The first part of the chapter covers an analytic calculation of the interaction between two vortices. Such a calculation applies to weak interactions over a longer time-scale or strong interactions over a short time-scale. The analysis demonstrates that finite-sized vortices undergo a motion as if they were point vortices. However, because they are of finite size their shapes depart from the initial circular shape. The deformation is explained by the presence of surface waves that carry negative energy. The calculation yields formulae for the amplitudes and frequencies of these surface waves. Because of the growth of surface waves energy is released and made available for the vortices to approach or move away from each other.

The numerical experiments on vortex interactions are described in the second part of chapter 4. For experiments on weak interactions we find agreement with the theory. For strong interactions we find that like-signed vortices (same direction of rotation) approach and fuse together to form a single vortex. Strong interactions between oppositely-signed

vortices lead to a peculiar dynamic situation: large amplitude oscillations of the surface waves are found to agree with theory and an apparent restoration of their initial circular shape is established after one rotation period of the vortex.

We believe that these non-linear phenomena can be given an interpretation in terms of the thermodynamic quantities mentioned earlier: "At a given energy of a system of n_1 vortices a particular number n_2 of vortex regions will maximize the entropy S(e.g. S = S(n)). The final equilibrium state with n_2 vortices or vortex regions can be reached, if sufficient free energy (released by the growth of negative energy waves) is made available for the transition $n_1 \rightarrow n_2$ to occur". This statement generalizes the transition $2 \rightarrow 1$ observed in the numerical experiments of chapter 4. In chapter 5 we observe the transitions $4 \rightarrow 3$ and $4 \rightarrow 3 \rightarrow 2$ both corresponding to fusion of nearby vortex regions, but also the transition $4 \rightarrow 5$ is found corresponding to the fission of a vortex. Obviously a further study in this area is required. Ultimately one would like to describe the onset of two-dimensional turbulence in terms of an increase in entropy and to predict whether such an increase is possible. Unfortunately our statements about this are as inconclusive as those of Onsager (1949).

Chapter 5 treats the stability and long-time evolution of two-dimensional wakes. Numerical experiments on shear unstable velocity profiles of laminar flows are described. The results lead to a study of an asymmetric four-vortex finite area system corresponding to a von Karman street of point vortices. The critical parameter of this system is b/a, the initial transverse-to-longitudinal separation of vortex centres. At b/a = 0.281 the four-vortex system is stable in agreement with the von Karman theory for a point vortex system. We observe that negative energy waves develop on the surface of the vortices due to self-consistent interactions. At b/a = 0 and at b/a = 0.6 the measured growth rates of an

instability are smaller/larger respectively than that predicted by the theory of von Karman. Fusion and fission of vortices are observed in these experiments and we make heuristic comparisons with those two-dimensional tunnel experiments that are described in the beginning of the chapter. Finally we look at numerical experiments on a model approximating the vortex flows arising from jets which escape nozzles. A comparison is made with an analytic study by Michalke & Timme (1967). A certain measure of disagreement between the growth rates of an instability as predicted by the theory and the growth rates measured is established. A tentative explanation for this is given.

At the end of this thesis we summarize the work presented and we attempt to draw conclusions about its future prospects.

CHAPTER 1

TWO-DIMENSIONAL IDEAL FLUIDS

An ideal fluid is an abstraction from a real fluid but is considered a useful concept from an analytical and computational point of view. This chapter describes the details of the abstractions made. It is shown that strictly two-dimensional motions of ideal fluids can be interpreted via the motion in phase space of a classical phase fluid. This phase fluid is the part of the ideal fluid which possesses vorticity. The particular vorticity models used in the research work are introduced.

1.1 Material, kinematical and dynamical preliminaries

The fundamental assumption on which hydrodynamics relies is that the matter dealt with can be regarded as continuous in structure. A motion of a continuum is taken to be a one-parameter family of mappings of the continuum on to other continua. The parameter is time t with a continuous domain of variation, $-\infty < t < \infty$, $t = 0$ being an arbitrary initial instant. The continuum is occupied by a fluid whose molecular composition remains invariant with time. A finite set of quantities are assumed to describe the state of the fluid exhaustively. These quantities are presented as mathematical functions $Q_i(\underline{r},t)$ giving the value of Q_i at time t at a point with coordinates $\underline{r}$. The coordinate $\underline{r}$ is measured in a coordinate system at rest and the description in terms of $Q_i(\underline{r},t)$ is called Eulerian. An alternative description called Lagrangian expresses Q_i as $Q_i(\underline{R}(t))$ where $\underline{R}(t)$ is the coordinate of a point moving with the fluid. In both descriptions we chronicle the history of Q_i.

In order to establish a pattern of histories common to fluids of different molecular composition it seems natural to consider only properties common to all fluids. Logically there are only two such properties: the space coordinate $\underline{r}$ and time t. A fluid whose history in all possible circumstances can be described in terms of these two quantities as well as properties derived from $\underline{r}$ and t is called an ideal fluid.

Although the molecular composition of an ideal fluid need not be specified, its invariance with time implies that no finite portion of the ideal fluid can be created or destroyed during any motion. A volume $dV = d^3|\underline{R}|$ which at time t occupies the spatial volume $dv = d^3|\underline{r}|$ remains invariant throughout any motion ($dV = dv$) which then is called isochoric (volume preserving). A fluid susceptible of isochoric motions only is normally called an incompressible fluid. Ideal fluids are also often called

incompressible, inviscid fluids. The familiar concepts like fluid density, temperature, viscosity etc. all refer to fluids that are non-ideal. Throughout the rest of this thesis we shall concern ourselves with the behaviour of ideal fluids.

The motion of an ideal fluid was defined as a one-parameter family of mappings of a configuration $C_1(\underline{R},t_1)$ on to other configurations. A motion is necessarily reversible with respect to time, e.g. the mappings of $C_1(\underline{R},t_1)$ on to $C_2(\underline{R},t_2)$ and vice versa can be distinguished only by the arrow of time. In order to describe motions Euler introduced the velocity field

$$\underline{u}\,(\underline{r},t) = \frac{d}{dt}\,\underline{r} \qquad (1.1)$$

where as before $\underline{r}$ is the coordinate in a coordinate system at rest. $\underline{u}(\underline{r},t)$ describes the motion completely and we can regard it as the dependent variable (state variable) with $\underline{r}$ and t being the independent variables. The equation of state that $\underline{u}$ must satisfy at all times is

$$\underline{\nabla} \cdot \underline{u} = 0 \ , \qquad (1.2)$$

in the sense that all motions must be isochoric (no divergence of points that form an infinitesimal portion of fluid). The velocity field is a vector field whose lines of constant $|\underline{u}|$ are called streamlines. A motion for which

$$\underline{u} = \underline{u}(r) \qquad (1.3)$$

is said to be a steady motion and the streamlines remain fixed in the coordinate system at rest. If a motion is not steady we write

$$\frac{d\underline{u}}{dt} = \underline{a}(\underline{r},t) \ . \qquad (1.4)$$

$\underline{a}(\underline{r},t)$ is called the acceleration field in analogy with particle accelerations in Newtonian mechanics. Equation (1.4) was written by Euler and

d'Alembert as

$$\frac{\partial}{\partial t}\,\underline{u} + \underline{u} \cdot \underline{\nabla}\,\underline{u} = \underline{a}(\underline{r},t) \ , \qquad (1.5)$$

and is called Euler's equation for an ideal fluid. Its first term is called the local acceleration which represents the change of $\underline{u}$ in a rest frame of reference. In a steady motion (eq.1.3) it vanishes. The second term is called the convective acceleration, because it represents the acceleration required to convect a portion of the fluid from one region to another which has a different value of $\underline{u}$. The acceleration field which determines the dynamics of a motion can in the Stokes representation be expressed as a sum of a lamellar field and a solenoidal field, e.g.

$$\underline{a} = - \underline{\nabla} b + \underline{\nabla} \times \underline{c} \ . \qquad (1.6)$$

b and $\underline{c}$ are called the scalar and the vector potential of $\underline{a}$ respectively. The solenoidal field $\underline{\nabla} \times \underline{c}$ will <u>not</u> be considered in the rest of this work. It is a non-conservative field as opposed to the lamellar field $\underline{\nabla} b$. $(\oint \underline{a} . d\underline{s} = \oint (\underline{\nabla} \times \underline{c}) \cdot d\underline{s} \neq 0)$.

This preliminary description of motions in ideal fluids demonstrates that these are described by functions $\underline{u}(\underline{r},t)$ that satisfy equations (1.2) and (1.5). If $\underline{a}$ or b is specified then it is necessary to select from a wide class of solutions to equation (1.5) the one that is consistent with an initial state $\underline{u}(\underline{r},0)$. The selection of a solution $\underline{u}(\underline{r},t)$ must be supplemented by a geometrical description of the ideal fluid. If the latter is confined to a finite region $\underline{u}$ must be prescribed at the boundaries of this region. Otherwise the desired behaviour of $\underline{u}$ for $\underline{r} \to \infty$ must be established.

Any motion we may wish to study is thus based on a particular solution $\underline{u}$ of an <u>initial-boundary value problem</u>.

1.2 Rotational and irrotational motions. Definition of vorticity

The velocity field can just like the acceleration field be decomposed as

$$\underline{u} = - \underline{\nabla} \phi + \underline{\nabla} \times \underline{\psi} \quad . \tag{1.7}$$

ϕ is called the velocity potential and $\underline{\psi}$ the stream function. When $\underline{\psi} = 0$ the motion is called irrotational, otherwise rotational. If we insert equation (1.7) in equation (1.2) we get

$$\nabla^2 \phi = 0 \quad . \tag{1.8}$$

The classical theory of irrotational motions in ideal fluids is thus a branch of potential theory. Authors like d'Alembert and Euler at first contended that all motions in ideal fluids are irrotational. Although these authors later admitted rotational motions to be possible, but unusual, efforts were concentrated on studying irrotational motions. A century later Kelvin (1849) and Helmholtz (1858) demonstrated the impossibility of irrotational motions in general: "There is no steady irrotational motion, other than a state of rest, within a finite simply connected region with a steady boundary". The proof of this theorem was supplemented by an interpretation of Kelvin's minimum theorem (Lamb, 1932) : "Consider any motion 1 within a finite simply connected region resulting in an amount of energy E_1. For any irrotational motion of energy E_2 and with the same motion at the boundaries as 1 we shall always have $E_2 < E_1$." It was then natural to start investigations of rotational motions.

As mentioned in the introduction, rotational motions are based on the concept of vorticity. The vorticity is a vector $\underline{\zeta}$ defined by

$$\underline{\zeta}\,(\underline{r},t) = \underline{\nabla} \times \underline{u}(\underline{r},t) \quad . \tag{1.9}$$

The kinematical significance of the vorticity vector has been given

essentially four different interpretations by Cauchy, Stokes, Hankel and Kelvin. Without going too much into the details of these interpretations which may seem somewhat mystifying, we simply interpret vorticity as follows:

"The value $|\underline{\zeta}(\underline{r})|$ is twice the instantaneous rate of rotation in a plane perpendicular to $\underline{\zeta}$ going through the point $\underline{r}$".

The importance of the vorticity vector is that knowing $\underline{\zeta}$ then, in principle, any state of motion is known to within the gradient of a harmonic function ϕ. If we ignore ϕ our results will be determined to within an irrotational motion, but in view of what was said above this irrotational motion is a state of rest because we shall deal with fixed boundaries (chapter 3). We can regard $\underline{\zeta}$ as a state variable satisfying

$$\nabla \cdot \underline{\zeta} \equiv 0 \tag{1.10}$$

which follows from (1.9). By inserting $\underline{u}$ given by (1.7) with $\phi \equiv 0$ into (1.9) we find

$$\underline{\zeta} = \underline{\nabla} \times \underline{\nabla} \times \underline{\psi} = - |\underline{\nabla}|^2 \underline{\psi} \quad , \tag{1.11}$$

that is, the vorticity and the stream function are related by a vectorial form of Poisson's equation. In order to express the dynamics of the vorticity vector we transform equation (1.5) by applying the operation $\underline{\nabla}\times$ on both sides. This results in

$$\frac{\partial}{\partial t} \underline{\zeta} + \underline{u} \cdot \underline{\nabla}\, \underline{\zeta} - \underline{\zeta} \cdot \underline{\nabla}\, \underline{u} = 0 \quad . \tag{1.12}$$

This equation does not contain any term associated with the acceleration field $\underline{a}$ because of our restriction to consider conservative fields ($\underline{\nabla} \times \underline{a} \equiv 0$) only. Equations (1.9) to (1.12) now form a closed set in the variables $\underline{\zeta}$, $\underline{\psi}$ and $\underline{u}$ and it is this set of equations we shall study.

The modern theory of vorticity which was initiated by Helmholtz will not be presented here since it is the subject matter of many treatises

(see Introduction for references). It is however worthwhile stating the two fundamental theorems both enunciated by Lagrange (1783):

I. Any volume of an ideal fluid once in irrotational motion will always remain in irrotational motion.

II. A rotational motion of an ideal fluid cannot be generated by impulsive pressures.

Theorem I can be found in a complimentary form called Helmholtz theorem stating that the lines of constant $\underline{\zeta}$ in a given motion will remain attached to the fluid. Theorem II vaguely hints at the creation of vorticity, a problem which caused a great deal of controversy amongst authors like Stokes, St.Venant, Boussinesq, and in this century by Poincaré, Hadamard and Duhem. Classically, vorticity was thought to be generated at the boundaries of a fluid and then only by viscous forces. Vorticity would then diffuse inwards if viscosity was present. Hadamard (1901) states: "Vorticity is generated by viscous forces via mechanisms which cannot be represented by analytic functions". (The decay of vorticity in a viscous fluid is on the other hand an analytic process). This incomplete understanding of the generation of vorticity was not altered until Lighthill (1963) solved the problem by introducing boundary layers.

Ideal fluids are inviscid fluids. They cannot generate nor diffuse vorticity. The study of ideal fluids is therefore concerned with only the convection of vorticity. Hence the study of ideal fluids applies to situations in real fluids where the rate of convection of vorticity by far dominates that of diffusion. We must give an initial distribution of vorticity $\underline{\zeta}(\underline{r},0)$ without accounting for how such a distribution is generated. Solutions to equations (1.9) - (1.12) will then describe motions that are consistent with this initial distribution. As mentioned earlier we shall choose that solution which satisfies a set of prescribed boundary conditions.

The set of equations (1.9) - (1.12) contain no parameters that describe characteristic lengths or time intervals. The equations cannot themselves introduce any scaling in space and time. The scale lengths and typical time periods are implicitly imposed by specifying the initial vorticity distribution $\underline{\zeta}(\underline{r},0)$. The following investigations shall deal with two basically different types of initial distribution. The first represents the flow of a subdomain and we shall call this distribution a vortex. The second type of distribution is intended to represent a flow extending over the entire domain concerned and rather than studying the flow itself we follow the time evolution of the vorticity distribution which produces the flow.

1.3 Two-dimensional motions. Hamiltonian equations

In the previous two sections we have made some restrictions on our investigations by ignoring certain features of real fluids. This is quite a common procedure and it leads to the concept of an ideal fluid whose motion can be fully described by the corresponding vorticity distribution. We shall now make the most severe restriction on our studies by confining these to consider two-dimensional motions only. In the introduction we attempted to justify such a restriction; in this section we shall discuss some of its implications.

A motion for which

$$\underline{u} = (u_x, u_y, 0) \ , \ u_x = u_x(x,y) \ , \ u_y = u_y(x,y) \tag{1.13}$$

is said to be a two-dimensional motion. Since it is the same for all planes parallel to the x-y plane, z = 0, we need only concern ourselves with that plane. To give quantities their right dimensions we can think of a slab of thickness a unit length in the z-direction. A unit length is whatever we care to choose, but is the same for all three directions $\hat{x},\hat{y},\hat{z}$. ($\hat{x},\hat{y},\hat{z}$ are the unit vectors with respect to x,y,z).

With $\underline{u}$ given by (1.13) we see that the vorticity vector and the stream function will have z-components only

$$\underline{\zeta} = \zeta(x,y)\ \hat{z} \quad , \quad \underline{\psi} = \psi(x,y)\ \hat{z} \quad .$$

The vorticity and the stream function are from now on regarded as <u>scalar</u> quantities related by equation (1.11) which then becomes

$$\nabla^2 \psi = -\zeta \quad \text{or} \quad \frac{\partial^2\psi}{\partial x^2} + \frac{\partial^2\psi}{\partial y^2} = -\zeta \quad . \tag{1.14}$$

Because the velocity can be expressed as

$$u_x = \frac{\partial\psi}{\partial y} \quad , \quad u_y = -\frac{\partial\psi}{\partial x} \tag{1.15}$$

we can write equation (1.12), in the compact form

$$\frac{\partial\zeta}{\partial t} + [\zeta,\psi] = 0 \quad . \tag{1.16}$$

The Poisson bracket $[\zeta,\psi] = \frac{\partial\zeta}{\partial x}\frac{\partial\psi}{\partial y} - \frac{\partial\zeta}{\partial y}\frac{\partial\zeta}{\partial x}$ and we notice that the third term of (1.12) $\underline{\zeta} \cdot \nabla\underline{u} \equiv 0$.

It can be seen from (1.15) that the scalar stream function ψ behaves as a Hamiltonian for a system with an infinite number of degrees of freedom. We have an unusual degree of symmetry in that real space (x,y) act as phase space. Equation (1.16) is Liouville's equation describing the motion of a two-dimensional phase fluid whose density is ζ . In classical particle dynamics we speak of a Hamiltonian and usually think of this as representing the total energy of a particle system. The particle analogue is called a point vortex (see also chapter 2) and can be represented by a Dirac delta function in real space resulting in a Hamiltonian given by equation (2.3). ψ can be interpreted as an energy density rather than the total energy of the system as we shall see below. By thinking of the vorticity distribution in terms of point vortices (chapter 2) Kirchoff was able to present the point vortex equations in Hamiltonian form. The true structure of the equations was later

elaborated on by Lin (1943), Onsager (1949) and Morikawa (1960) all of whom adopted the concept of point vortices.

For the case of a continuous vorticity distribution, the total energy, which is purely kinetic, can be written as

$$E = \tfrac{1}{2}\rho_o \int_A |\underline{u}|^2 \, d\underline{r} \quad , \quad (d\underline{r} = dxdy) \, , \tag{1.17}$$

where A denotes the domain occupied by an ideal fluid whose physical density takes the constant value ρ_o. Substituting for $\underline{u}$ and using Green's first identity we find

$$E = \tfrac{1}{2}\rho_o \int_A \zeta \, \psi \, d\underline{r} \quad , \tag{1.18}$$

provided we meet the boundary condition

$$\oint_C \psi \frac{\partial \psi}{\partial n} \, ds = 0 \quad . \tag{1.19}$$

C is the contour bounding A and $\frac{\partial}{\partial n}$ denotes differentiation with respect to the normal $\hat{n}$ of C. Equation (1.18) shows us that the energy of the subdomain $d\underline{r}$ is proportional to $\psi(\underline{r})$ which via equation (1.14) is expressed as

$$\psi(\underline{r}) = \int_A \zeta(\underline{r}') \log|\underline{r}-\underline{r}'| \, d\underline{r}' \, , \tag{1.20}$$

and thus thought of as an energy density.

Although the equations of motion (1.15) are Hamiltonian we shall use the symbols (x,y) instead of (q,p). However, when polar coordinates (r,θ) are used rather than (x,y) we use (q,p) since now $q = \frac{1}{2} r^2, p = \theta$. (Chapter 4 uses (q,p)).

1.4 Classical phase fluids and their invariants of motion

There is a wide class of classical dynamical systems exhibiting a time evolution which can be pictured as the flow of an incompressible self-interacting fluid in a $2n$-dimensional phase space (typically $n \leq 3$). The phase fluid density normally denoted by f, but in our case by ζ,

obeys the usual form of a dynamical equation of motion (1.16). The self-interaction property is expounded by ψ (normally H) being a functional of ζ (see equation 1.20).

We have just seen that the system of a two-dimensional ideal fluid belongs to this class and we shall emphasize the inherent analogy with other systems distinguished from the former (ζ,ψ) system by being called (f,H) systems. Such systems are found in plasma physics: A one-dimensional collisionless plasma, an electron beam or a system consisting of a beam interacting with a plasma are described in two-dimensional phase space (x,v) and the Hamiltonian is written as

$$H = \tfrac{1}{2} m v^2 + e \phi (x) \qquad (1.21)$$

where ϕ is the electrostatic potential given by

$$\frac{d^2\phi}{dx^2} = - e \int f(x,v)\, dv \,. \qquad (1.22)$$

We have systems of bodies interacting via gravitational forces. These can also be described in a two-dimensional phase space (x,v) and H,ϕ are obtained from (1.21) and (1.22) by replacing -e by m.

For all these systems whether they are made up of particles or fluids we think of their motion as being represented by a phase fluid of density ζ (or f). It is important to notice that the total energy is uniquely determined by this density function. Such a property makes the behaviour of a phase fluid much simpler to analyse than that of a real fluid, whose density does not uniquely determine the energy.

Consider now a system consisting of a domain A, finite or infinite, occupied by an ideal fluid and suppose there is no interaction with any other dynamical system. If A is finite it is bounded by a contour C, if infinite C will formally indicate the limit $r \to \infty$. The laws of Newtonian mechanics can be applied to the system as a whole.

Since we exclude all dissipative mechanisms we have conservation of energy (equation 1.18), linear and angular momentum. The linear momentum

$$\underline{p} = \rho \int_A \underline{u}\, d\underline{r} \tag{1.23}$$

and the angular momentum

$$\underline{L} = \rho \int_A (\underline{r} - \underline{r}_o) \times \underline{u}\, d\underline{r} \tag{1.24}$$

are calculated with respect to a point P_o (or axis $\hat{z}$ through P_o) with coordinates $\underline{r}_o$ given by

$$\underline{r}_o = \frac{\int_A \zeta\, \underline{r}\, d\underline{r}}{\int_A \zeta\, d\underline{r}} \quad . \tag{1.25}$$

The point P_o may conveniently be called the point at rest since the velocity $\underline{u}(\underline{r}_o)$ is zero during the whole motion (Lamb, 1932). If $\int_A \zeta\, d\underline{r} = 0$, then P_o moves to infinity or becomes indeterminate.

As opposed to the (f,H) system we have an extra constant of motion, namely L, which emphasizes the unusual symmetry present. When $\frac{\partial}{\partial t} \equiv 0$ for (f,H) systems these are said to be in equilibrium and we have $f = f(H)$. In the case of an ideal fluid, $\frac{\partial}{\partial t} \equiv 0$ corresponds to a steady state flow (section 1.1); the vorticity distribution does not change with time but the fluid itself is in motion. We can also find the phase fluid (vorticity distribution) in a steady state of motion whilst the corresponding real fluid is <u>not</u> undergoing a steady motion (see for example Kirchoff's elliptic vortex, Lamb 1932).

Along with an infinite number of degrees of freedom we have an infinite number of invariants of motion written in the form $g(\zeta)$, where g is any functional of ζ. By this we mean that the value $g(\zeta)$ occurring in one or more subdomains remains invariant with time. In the next section we shall look at one particular functional $g(\zeta)$.

1.5 The area functions. The constant vorticity model.

We learned that in an ideal fluid vorticity cannot be created or destroyed. The total amount of vorticity must therefore remain constant, e.g.

$$\Gamma = \int_A \zeta \, d\underline{r} \tag{1.26}$$

is an invariant of motion and Γ is called the circulation of A. Since that part of the fluid which has $\zeta \neq 0$ behaves like a second incompressible fluid (equation 1.10) susceptible to ishochoric motions only, we have an area conservation law: let $A_1(\zeta)d\zeta$ designate the area between contours in the xy-plane of constant ζ and $\zeta+d\zeta$. Then $A_1(\zeta)d\zeta$ is a conserved quantity for all values of ζ, as well as $A_1(\zeta)$. We call $A_1(\zeta)$ the area function of the first kind and we shall meet this quantity again in chapter 3. Similarly we speak of an area function of the second kind $A_2(\psi)$, where $A_2(\psi)d\psi$ denotes the area between contours of constant ψ and $\psi+d\psi$. This last quantity is <u>not</u> an invariant of motion except when $\zeta = \zeta(\psi)$ in which case the vorticity contours and streamlines coincide :

$$A_1(\zeta)d\zeta = A_1(\ )\frac{d\zeta}{d\psi}\,d\psi = A_2(\psi)d\psi \tag{1.27}$$

The reason why we introduce the two area-functions $A_1(\zeta)$ and $A_2(\psi)$ is our interest in a particular model called "the constant vorticity model" dealt with in detail in chapters 4 and 5. Our aim has been to establish some general theory for this model and, as mentioned in the introduction, our attempts to do so have only been partially successful. A main difficulty has been that of determining $A_2(\psi)$ for equilibrium distributions $\zeta = \zeta(\psi)$.

In the constant vorticity model we assume that the vorticity distribution everywhere takes one of the constant values $-\zeta_0$, 0 or $+\zeta_0$. The vorticity distribution can then be described in terms of a set of

contours (open or closed) which confine fluid areas of constant vorticity. This model which has found extensive use in plasma physice (de Packh 1962, Dory 1964, Berk,Nielsen and Roberts 1970) is referred to as "the Waterbag model".

Suppose a set of contours C_i confining areas of constant vorticity are expressed by equations of the form

$$G_i(x,y,t) = 0 \tag{1.28}$$

such that $G_i > 0$ inside C_i and $G_i < 0$ outside C_i. Subscript i refers to contour number i. The vorticity distribution can then be written as

$$\zeta(x,y) = \sum_i \Theta(G_i) , \tag{1.29}$$

where Θ denotes the Heaviside function. Inserting (1.29) in (1.16) and integrating the lefthand side of the resulting equation we find that each contour has an equation of motion of the type

$$\frac{\partial G_i}{\partial t} + [G_i,\psi] = 0. \tag{1.30}$$

(Use $\frac{\partial}{\partial w}(G_i) = \delta(G_i)\frac{\partial G_i}{\partial w}$ for $w = t,x$ and y and form $\int_{-\varepsilon}^{+\varepsilon} \delta(G_i)\frac{\partial G_i}{\partial w}\,dG_i$). Equation (1.30) will be used in chapter 4.

In this chapter we have seen that the description of an ideal fluid can be based on the concept of vorticity. For two-dimensional motions this description yields a classical formalism that features many analogies with systems in plasma physics and elsewhere. We have finally chosen a model whose applications to realistic situations are limited in a number of ways, but on the other hand this model proves to be convenient to work with analytically and computationally.

CHAPTER 2

NUMERICAL SIMULATION OF TWO-DIMENSIONAL HYDRODYNAMIC MOTIONS BY THE METHOD OF POINT VORTICES

We have shown that the motion of a two-dimensional incompressible, inviscid and homogeneous fluid can be thought of in terms of the gradual evolution of a continuous vorticity distribution. This chapter describes how a computational model can be obtained if we first replace the continuous vorticity distribution by a finite set of point vortices interacting through a stream function which satisfies Poisson's equation. We first study the effects of replacing the exact relevant equations by suitable finite difference forms. These effects are used to explain numerical errors arising in a series of computer simulations on a fast model in order to acquire a quantitative estimate for possible inaccuracies. It is concluded that the particle model presented is useful for solving a variety of problems.

2.1 Point vortices

In chapter 1 we realized why vortices are important in hydrodynamics in that they are the sources for the incompressible flow field; if we are given the vorticity distribution at any instant of time then both the current state of the system and its future evolution are in principle determined subject to appropriate boundary conditions. This property is reminiscent of any system that can be cast into a Hamiltonian form (section 1.3). Analogies with systems in plasma physics and gravitational theory were also mentioned in chapter 1. These suggest that an incompressible flow field can be thought of in terms of the mutual interaction of a set of vortex elements (action-at-a-distance model as in electrostatics),

rather than in terms of the velocity field itself (field model). A much clearer picture of the flow is often obtained in this way.

The method of solution described in this chapter differs from those commonly adopted in numerical fluid dynamics (Harlow 1970). It resembles more closely the particle simulation techniques employed in plasma physics (Methods of Computational Physics, volume 9, 1970). The method starts from a physical model in which the continuous vorticity distribution $\zeta(x,y)$ is approximated by a large number of point vortices

$$\zeta(x,y) = \sum_{n=1}^{N} \zeta_n \delta(x-x_n)\ \delta(y-y_n) \tag{2.1}$$

where $\zeta_n = \pm 1$. Each pair of coordinates refers to a point vortex and satisfies the equations (1.15)

$$\dot{x}_n = \frac{\partial \psi}{\partial y_n} \quad , \quad \dot{y}_n = -\frac{\partial \psi}{\partial x_n} \tag{2.2}$$

where the Hamiltonian (section 1.3) now takes the form

$$\psi = \frac{1}{2\pi} \sum_{n=1}^{N} \zeta_n \log|\underline{r}-\underline{r}_n| \ . \tag{2.3}$$

The approximation (2.1) is very similar to those made in studies of one-dimensional collisionless plasmas. However, the situation there is that a large number of ions and electrons with coordinates (x_n,v_n) can be thought of as a continuous distribution function which then satisfies a Vlasov equation, e.g. the reverse approximation is made.

It is quite important to notice that the approximation (2.1) differs conceptually from the approximations we shall make to equations (2.2) and (2.3) in terms of finite difference forms. The former approximation is based on a particular way of dealing with a continuum, analytically or numerically and it is the number N, of point vortices which determines the accuracy of such an approximation. The approximations that can be

made to equations (2.2) and (2.3) are based on numerical methods and they are independent of N. In the next section we shall see how (2.2) and (2.3) can be approximated quite independently of the existence of point vortices. To study the effects from all our approximations we therefore treat these one by one and isolate the effects from the remainders.

The discretization of time and (x,y) space which takes place when we approximate (2.2) and (2.3) naturally suggests that the spacings Δt and $(\Delta x, \Delta y)$ should be as small as possible. Ideally, therefore, we can view the hydrodynamics model described in chapter 1 as the limit

$$N \to \infty \quad , \quad \Delta t \to 0 \quad , \quad (\Delta x, \Delta y) \to 0 \quad ,$$

of our approximated model. The interesting problem of solving for an optimum set $(N, \Delta t, \Delta x, \Delta y)$ that will produce a minimum error in a given situation remains unresolved. The capacity of a computer memory required depends on N and $(\Delta x, \Delta y)$ whereas the cost of a calculation will depend also on Δt as well as the complexity of the numerical algorithms. Little is known as to how to select the right optimum, since it may depend strongly on the physical problem that is being studied. The model described in this chapter has in fact been used by Taylor and McNamara (1971) to study two-dimensional guiding-centre problems in magnetized plasmas. They reached the conclusion that in their studies the value of N had little influence on the errors. For the test model described in section 2.8 we have a much stronger dependence on N of the inaccuracies but this will not be dealt with further until chapter 3.

We shall therefore carry out an analysis of our approximations and leave out the optimum choice of N, Δt, $(\Delta x, \Delta y)$ + algorithms. Our main concern has been the applications of a particular model rather than finding its optimum form for each application.

2.2 A numerical scheme for the motion of point vortices

Suppose we are given an ensemble of N point vortices with coordinates (x_n, y_n) lying inside a rectangular region covered by a Cartesian mesh of size N_x by N_y. To evaluate the vorticity $\zeta(i,j)$ at the mesh point (i,j) we use the cloud-in-cell (CIC method (Harlow, 1964). This method assumes each 'point' vortex to possess uniform vorticity within a unit square such that the corresponding unit amount of vorticity can be credited to surrounding mesh points through a bilinear interpolation. A smoothing of the vorticity distribution will result from the bilinear interpolation and section 2.6 describes the numerical effect of this.

Let us assume that the coordinates of a point vortex are written as $x_n = i + dx$ and $y_n = j + dy$. The CIC method credits vorticity to the 4 surrounding meshpoints by

$$\begin{aligned} \zeta(i,j) &= (1-dx)(1-dy) = A_1 , \quad \zeta(i+1,j) = dx(1-dy) = A_2 , \\ \zeta(i,j+1) &= (1-dx)\,dy = A_3 , \quad \zeta(i+1,j+1) = dx\,dy = A_4 . \end{aligned} \tag{2.4}$$

The quantities A_1-A_4 represent 4 areas of intersection between the mesh and the square-shaped vortex, and the CIC method is often referred to as the area-weighting technique. When the vorticity from all N point vortices has been credited to the mesh points using (2.4), Poisson's equation (1.14) can be solved by the usual 5-point approximation

$$\frac{\psi(i,j+1) + \psi(i,j-1) - 2\psi(i,j)}{(\Delta y)^2} + \frac{\psi(i+1,j) + \psi(i-1,j) - 2\psi(i,j)}{(\Delta x)^2} = -\zeta(i,j) \tag{2.5}$$

where Δx, Δy are the mesh spacings. Equation (2.5) is solved by the Hockney method (Hockney, 1965) allowing for a variety of boundary conditions. The velocity field is evaluated by centered differences

$$u_x(i,j) = \frac{\psi(i,j+1) - \psi(i,j-1)}{2\Delta y}; \quad u_y(i,j) = -\frac{\psi(i+1,j) - \psi(i-1,j)}{2\Delta x} . \quad (2.6)$$

To advance the set of positions (x_n,y_n) one timestep a leapfrog scheme is used. Two sets of coordinates $(x_n,y_n)_{even}$ and $(x_n,y_n)_{odd}$ are introduced in order to express the coordinates at alternate times $s\Delta$ and $(s+1)\Delta t$ (s even). The equations (2.2) then become, letting superscript s denote the time $s\Delta t$

$$\begin{aligned} x_n^{s+1} &= x_n^{s-1} + u_x^s\,(x_n^s,\, y_n^s)\; 2\Delta t \\ y_n^{s+1} &= y_n^{s-1} + u_y^s\,(x_n^s,\, y_n^s)\; 2\Delta t \quad . \end{aligned} \quad (2.7)$$

The set of coordinates $(x_n^s,\, y_n^s)$ determines the velocity field (also ζ^s, ψ^s) which is used to move the other set. The velocity $\underline{u} = (u_x,u_y)$ used in (2.7) is evaluated by the CIC method according to

$$\underline{u}(x_n^s,y_n^s) = A_1^s\,\underline{u}(i,j) + A_2^s\,\underline{u}(i+1,j) + A_3^s\,\underline{u}(i,j+1) + A_4^s\,\underline{u}(i+1,j+1) \quad (2.8)$$

where the 4 areas $A_1^s - A_4^s$ at time $s\Delta t$ are given by (2.4). Equations (2.4) and (2.8) form a consistent set of interpolations in the sense that a single point vortex will not move in its own velocity field.

2.3 The effects of the finite difference formulation

The numerical scheme described in section 2.2 approximates a truly continuous system (Eqs.(1.16) and (1.18) by a particle model and finite differences in space and time. We are primarily interested in the effects of numerical errors introduced by the following 3 approximations:

1. The square-shaped boundary.
2. The time integration (Δt finite).
3. The mesh (square mesh, Δx and Δy finite).

In the following we shall briefly examine each approximation and apply our

results to the solution of a particular flow problem discussed in section 2.7.

2.4 The square-shaped boundary

Imagine that our simulation problem is that of following the motion of a number of contours enclosing areas of constant $\zeta = \pm\zeta_o$. Initially our distribution function is described by a set of contours expressed by functions

$$G_j(x,y) = 0 \ .$$

The solution to Laplace's equation in a suitable coordinate system is ($\tilde{}$ denotes value outside any contour j)

$$\tilde{\psi} = \tilde{\psi}(x,y) \tag{2.9}$$

where $\frac{\partial}{\partial \underline{r}}(\tilde{\psi}) \to 0$ (say) for $|\underline{r}(x,y)| \to \infty$. The solution $\tilde{\psi}$ of Laplace's equation satisfies the set of conditions

$$\tilde{\psi}(G_j = 0) \ = \ \psi(G_j = 0)$$

where ψ is a solution of (1.14).

We then introduce a square boundary and require that $\tilde{\psi} = \psi_1$, a constant, along this square G_o . The solution (2.9) can be expanded in the normal way

$$\tilde{\psi} = \sum_{k=o}^{\infty} \tilde{\psi}_k \tag{2.10}$$

with

$$\tilde{\psi}_o = \frac{-1}{4\pi} \log r \int_A \zeta(x,y)da = \frac{-1}{4\pi}(\log r)\ \zeta_o \Sigma A_j + \psi_c$$

where r is the distance from the origin to the variable point P and A_j is the area enclosed by contour j. A_j is positive if $\zeta = \zeta_o$ and negative if $\zeta = \zeta_o$. In general the kth term of the expansion (2.10) is

$$\psi_k = \frac{(k-1)!(-1)}{k+1} \left\{\nabla^k r\right\} . \left\{D^{(k)}\right\}$$

where the bracketed quantities are tensors of rank k. If $\sum_j A_j \neq 0$, ψ_o will no-mally be the dominant term for sufficiently large r values. This means that, regardless of the choice of coordinate system, $\tilde{\psi}$ exhibits rotational symmetry. Thus the contour C_o should approximately be a circle. The introduction of a square boundary can now be interpreted as a super-position of four images of the set of contours. The images further away are neglected. The resulting potential can be calculated as a super-position of 5 pctentials arising from the actual system of contours (i=o) and four image systems (i = 1,2,3,4) placed symmetrically with respect to each of the four boundaries.

If we look at distances r inside the square but far from any contour the dominant term in the expansions (2.10) is ψ_o. This gives

$$\psi_o = \sum_{i=0} \alpha \frac{1}{\pi} \zeta_o (\Sigma_j A_j) \log r_i$$

where $\alpha = -1$ for i = 0 otherwise $\alpha = +1$. Inserting r_i as $r_i^2 = r^2+4L^2 - 4Lr \cos(\theta+\phi)$, $\phi = 0, -\frac{\pi}{2}, \pi, \frac{\pi}{2}$ for i = 1,2,3,4 we get when expanding the log term

$$\tilde{\psi}_o = - K \log r + K \sum_{m=1}^{\infty} \frac{1}{2m} \left(\frac{r}{2L}\right)^{4m} \cos(4m\theta) \qquad (2.11)$$

with

$$K = \frac{1}{4\pi} \zeta_o \sum_j A_j \ .$$

Eq.(2.11) shows that rotational modes m=4, 8, 12 .... have been imposed on the original solution.

For higher order terms in the expansion (2.10) we find that

$$\psi_k = \beta_o^{(k)} \frac{1}{r^k} + \sum_{m=1}^{\infty} \beta_{4m}^{(k)} \cos 4m\theta) \left(\frac{r}{2L}\right)^{4m}$$

where coefficients $\beta_{4m}^{(k)}$ as functions of cos (4mθ) arise from the expansion of $\frac{1}{r_i^k}$. For k=1, $\beta_{4m}^{(1)}$ become the Legendre polynomials.

In order to evaluate the effect of introducing a square boundary we see that first we must estimate the relative weight of the terms $\tilde{\psi}_k$ for $k=0,1,2 \ldots$. Once this is done we must evaluate the coefficients for $m=4, 8, 12$ modes in the expansion of $\tilde{\psi}_k$ and compare their amplitudes with the log r term. The maximum effect on the distribution of vorticity will occur when the coefficients are evaluated at the largest r for which $\zeta \neq 0$.

2.5 The effect of the discretization of time

We are primarily interested in the stability of the finite time integration implemented by the leapfrog scheme. To examine this assume that we move two independent sets e and o of points. We assume for simplicity that the points move in a time independent velocity field so that ψ is constant in time. As a result of applying finite Δt to the motion of the points e and o we imagine that the limit $\Delta t \to 0$ results in a symmetrical displacement around the correct value $\underline{R}_c$

$$\underline{r}_e(t) = \underline{R}_c + \underline{\delta}, \quad \underline{r}_o(t) = \underline{R}_c - \underline{\delta} \ .$$

Inserting for $\underline{r}_e$ and $\underline{r}_o$ in $\frac{d\underline{r}}{dt} = \underline{u}$ and subtracting we get

$$\frac{d\underline{\delta}}{dt} = -\frac{d\underline{u}}{d\underline{r}}\,\underline{\delta} \ . \qquad (2.12)$$

Suppose $\underline{\delta} = (\delta_x \hat{\underline{x}} + \delta_y \hat{\underline{y}})\, e^{ist}$ where both δ_x, δ_y may be functions of x,y and $\hat{x}$ and $\hat{y}$ are the base unit vectors of an orthogonal coordinate system. To find whether s can become complex we insert for δ in Eq.(2.12)

$$\frac{d}{dt}(\delta_x \hat{\underline{x}}) + \frac{d}{dt}(\delta_y \hat{\underline{y}}) + is(\delta_x \hat{\underline{x}} + \delta_y \hat{\underline{y}}) + \delta_x \nabla u_x + \delta_y \nabla u_y = 0 \ . \qquad (2.13)$$

Eq.(2.13) will express the eigenvalues λ of s as $g(\underline{\delta}) = \lambda\underline{\delta}$, through a quadratic equation in s which, since $\nabla.\underline{u} = 0$ becomes

$$-s^2 + S\,(u_x,\, u_y) = 0 \quad .$$

The condition for stability is then

$$S(u_x,u_y) = \frac{\partial u_x}{\partial x}\frac{\partial u_y}{\partial y} - \frac{\partial u_x}{\partial y}\frac{\partial u_y}{\partial x} \geqslant 0 \quad .$$

In polar coordinates Eq.(2.13) becomes

$$\tfrac{1}{2}\frac{1}{r}\frac{\partial(u_r^2 + u_\theta^2)}{\partial r} + \frac{1}{r}\frac{\partial u_r}{r}\frac{\partial u_\theta}{\partial\theta} - \frac{1}{r}\frac{\partial u_r}{\partial\theta}\frac{\partial u_\theta}{\partial r} \geqslant 0 \quad .$$

We notice that for a simple steady state flow described by $\underline{u} = \underline{\omega}(r) \times \underline{r}$ with $u_r = 0$ $u_\theta = \omega(r)r$ the above condition corresponds to

$$\left[\omega^2(r)\;\; 1 + r\,\frac{d\ln\omega(r)}{dr}\right] \geqslant 0 \quad .$$

From this we deduce that the leapfrog scheme causes the frequently encountered irrotational flow $\omega \sim r^{-2}$ to become unstable. The implications of this result will be dealt with in the description of the test model.

2.6 Effects introduced by the mesh

In section 2.2 we have presented the finite difference forms used to approximate Eqs.(2.2) and (1.14).

Let us look at each difference form separately to see how good an approximation it is. Throughout this section we will consider functions represented by a finite series of harmonics. For simplicity we choose

$$\cos rx \quad \cos sy$$

with $r = \frac{\pi\ell}{N_x}$ or $\frac{2\pi\ell}{N_x}$ and $s = \frac{\pi k}{N_y}$ or $\frac{2\pi k}{N_y}$ depending on which type of

boundary condition is imposed on the functions.

a) Poisson's equation

Consider a mesh function represented correctly at all meshpoints as

$$\zeta = \sum_{\ell} \sum_{k} \cos\ rx\ \cos\ sy\ .$$

The analytic solution to Eq.(1.14) is for a particular mode ℓ,k

$$\psi = \left[r^{-2} + s^{-2}\right]\left[\cos\ rx\ \cos\ sy\right]\ .$$

We insert this expression in Eq.(2.5) and get the solution ζ_Δ . We then form the ratio $\frac{\zeta\Delta}{\zeta}$ and get

$$\frac{\zeta_\Delta}{\zeta} = K\left[2\cos r + 2\cos s - 4\right] \qquad (2.14)$$

where $K = r^{-2} + s^{-2}$.

b) Evaluation of fluid velocity

Similarly for Eq.(2.6) we can assume that say $u_x = \cos\ rx\ \cos\ sy$ with the analytic solution

$$\psi = \frac{1}{s}\ \cos\ rx\ \sin\ sy\ .$$

Substitution in Eq.(2.6) gives

$$u_x^\Delta = \frac{1}{s}\cos\ rx\ \cos\ sy\ \sin\ s \qquad (2.15)$$

such that $\frac{u_x^\Delta}{u_x} = \frac{1}{s}\sin\ s \approx 1$ when s is small. Exactly the same relation holds for $\frac{u_y^\Delta}{u_y}$ with x inserted for y on the righthand side.

To get an idea of the truncation of harmonics caused by the difference forms (2.6, 2.7) we assume that we are given

$$\zeta = 2\,\frac{s}{r^2+s^2}\cos\ rx\ \cos\ sy$$

which results in a velocity

$$u_x = -\cos\ rx\ \sin\ sy\ .$$

Combining Eqs.(2.14) and (2.15) gives

$$u_x^{\Delta} = \eta_x \cos rx \sin sy$$

where

$$\eta_x = \frac{\sin s}{s} \frac{r^2 + s^2}{2(\cos r + \cos s - 2)}$$

and similarly

$$\eta_y = \frac{\sin r}{r} \frac{r^2 + s^2}{2(\cos r + \cos s - 2)} \quad .$$

Set $r = \frac{\pi \ell}{64}$ and $s = \frac{\pi k}{64}$ (VORTEX Code) and let us see how many modes are subject to a truncation less than 5%, i.e. $\eta \geq 0.95$. A rough estimate gives $\ell = k = 16$.

c) Area weighting of velocities

The approximation (2.8) finds an interpolated velocity (u_x, u_y) at the position (x_n^s, y_n^s) by the CIC method. To find the effect of this interpolation we assume that u is correctly given at all meshpoints as

$$u_x = \cos rx \cos sy \quad .$$

Setting as before the positions inside the box to dx, dy then the analytically correct velocity at $(x,y) = (i + dx, j + dy)$ is

$$u_x = \cos r\,(i + dx) \cos s\,(j + dy) \quad . \tag{2.16}$$

The velocity found by Eq.(2.8) is

$$u_x^{\Delta} = A_1 \cos(ri)\cos(sj) + A_2 \cos(ri+r)\cos(sj) + A_3 \cos(ri)\cos(sj+s) + A_4 \cos(ri+r)\cos(sj+s) \quad , \tag{2.17}$$

where superscript Δ denotes the interpolated value.

To find the net difference between u_x and u_x^{Δ} we perform a Taylor expansion of u_x at the point (i,j) .

$$u_x(i+dx,j+dy) = u_x(i,j) + \frac{\partial u_x}{\partial x}\,dx + \frac{\partial u_x}{\partial y} + dy + \tfrac{1}{2}\left(\frac{\partial^2 u_x}{\partial x^2}\,dx^2 + \frac{\partial^2 u_x}{\partial y^2}\,dy^2 + 2\,\frac{\partial^2 u_x}{\partial x \partial y}\,dxdy \right).$$

The form u^{Δ} can similarly be written in terms of the finite difference forms of the derivatives

$$u_x^{\Delta}(i+dx,j+dy) = u_x(i,j) + \left[\frac{\partial u_x^{\Delta}}{\partial y}\right]_{\frac{1}{2},0} dx + \left[\frac{\partial u_x^{\Delta}}{\partial y}\right]_{0,\frac{1}{2}} dy + \left[\frac{\partial^2 u_x^{\Delta}}{\partial x \partial y}\right]_{\frac{1}{2},\frac{1}{2}} dxdy \,.$$

It is apparent from this last expression that the term $\frac{1}{2}\frac{\partial^2 u_x}{\partial x^2}\,dx^2 + \frac{1}{2}\frac{\partial^2 u_x}{\partial y^2}\,dy^2$ has disappeared in the finite difference approximation. The area-weighting is just a bilinear interpolation which introduces an artificial viscosity with no physical counterpart.

The interpolated velocity at a point inside a mesh cell is now written as

$$\frac{d\underline{r}}{dt} = \underline{u}_c + \underline{u}_\nu = \underline{u}_M$$

where $\underline{u}_c$ is the correct velocity for an incompressible inviscid fluid, i.e. a solution to

$$\frac{\partial \underline{u}_c}{\partial t} + \underline{u}_c \cdot \nabla \underline{u}_c = -\frac{1}{\rho}\nabla P \,.$$

The velocity $\underline{u}_M = \underline{u}_c + \underline{u}_\nu$ is, however, a solution to

$$\frac{\partial \underline{u}_M}{\partial t} + \underline{u}_M \cdot \nabla \underline{u}_M = -\frac{1}{\rho}\nabla P - \nabla(\nu_M \nabla \underline{u}_M)$$

with ν_M being the kinematic viscosity $(\frac{\mu}{\rho})$.

The velocity $\underline{u}_\nu$ caused by area-weighting can be calculated assuming again that the correct velocity $\underline{u}_c$ is given by Eq.(2.16).

We expand the coefficients of the terms in Eqns.(2.16) and (2.17). This gives for the x component for mode (r,s) taking terms of second order

$$u_\nu = \left[\tfrac{1}{2}r^2 dx(dx-1) + \tfrac{1}{2}s^2 dy(dy-1) \right] \cos ri \quad \cos sj$$

such that

$$u_\nu = \xi\, u_c(i,j) \ .$$

The coefficients for sin cos, sin sin, cos sin result in higher order terms. The coefficient of u_ν represents a non-physical viscosity that depends on the position (dx, dy) within a mesh cell as well as on the mode number (r, s). Since this non-physical viscosity depends on (x, y), the velocity $\underline{u}_M$ does not satisfy Eq.(1.2), and the interpolation used to evaluate $\underline{u}_M$ will introduce a non-physical compression of the fluid. The point vortices therefore experience a compressible flow field which will cause them to cluster.

We notice that if dx = 0 or 1 or dy = 0 or 1 then the corresponding dependence of r or s respectively vanishes. Since

$$\xi = \tfrac{1}{2}r^2 dx(dx-1) + \tfrac{1}{2}s^2 dy(dy-1) \ ,$$

we find that $\xi \leq 0$ for all r,s,dx,dy. We also notice the quadratic dependence of the mode numbers ℓ, k. For a given mode ξ_{max} occurs for dx = dy = $\frac{1}{2}$.

We can then roughly state that there is little interference from the interpolation on the long wavelength modes (r, s small), whereas the amplitudes of the short wavelength modes will be diminished. In Fig.2.1 we assume that y is kept constant and plot u_c and u_ν as functions of i and dx for a long and a short wavelength mode. The maximum amplitude of u_ν is for a given mode $\frac{1}{8}\, r^2$.

Notice how the short wavelength mode is virtually reduced to zero over the length of a mesh cell.

d) Area-weighting of vorticity

In the approximation (2.4) ζ is made up of area contributions as indicated. Analytically we regard a point vortex as described by a Dirac Delta function. Hence the contribution from a point vortex at $(x_n,y_n) = (i+dx,j+dy)$ is

$$\zeta = \delta(x- i-dx)\ \delta(y-j-dy)\ .$$

This function can be Fourier analysed and written as

$$\zeta = \frac{2}{N_x}\frac{2}{N_y}\sum_{\ell}\sum_{k} a_{\ell k}\cos rx\ \cos sy \qquad (2.18)$$

where we have chosen a cosine expansion in both directions. The coefficient $a_{\ell k}$ is

$$a_{\ell k} = \int_0^{N_x}\int_0^{N_y} \zeta \cos rx \cos sy\, dx\, dy - \frac{1}{rs}\cos r(i+dx)\cos s(i+dy). \qquad (2.19)$$

The area-weighting method credits to the surrounding points amounts A_n given by Eq.(2.4). Each contribution can be expressed by Eq.(2.18) but with a coefficient $a_{\ell k}$, obtained from (2.19) by setting $(\delta x,\delta y) = (0,0)$, $(0,1)$,(1.0) and $(1,1)$ respectively. The procedure is therefore quite analogous to the one before and the difference between ζ^{Δ} and ζ for mode (r,s) is then to second order

$$\delta\zeta = \zeta^{\Delta}-\zeta = \tfrac{1}{2}\frac{1}{r}\frac{1}{s}\left[r^2dx(dx-1) + s^2dy(dy-1\right]\cos rx\cos sy\ .$$

The question of interest is now: how many modes in the expansion (2.18) are required to produce ζ^{Δ} ? Or conversely: how many modes in the expansion of ζ^{Δ} differ from those of (2.18) by an amount which is less than a given Δ ? A comparison between the expansions for ζ^{Δ} and ζ gives

approximation	analytic
$(1 - dx + dx\cos r)^D$	$(\cos(rdx))^D$
$(dx \sin r)^D$	$(\sin(rdx))^D$

where D is the dimension of the system.

We form the difference Δ^r between the upper two terms and let D=1 for simplicity,

$$\Delta^r = dx\cos r+1-dx-\cos(rdx) = \sum_n \frac{r^{2n}}{(2n)!}(-1)^n\left[dx-dx^{2n}\right].$$

As an example we can ask how many modes are reproduced to within 5% if N is say 64 as in VORTEX. The first two leading terms in the above expansion are

$$\Delta_1^r = -\tfrac{1}{2}\frac{\pi^2\ell^2}{64^2}\left[dx-dx^2\right]$$

$$\Delta_2^r = \frac{1}{24}\frac{\pi^4\ell^4}{64^4}\left[dx-dx^4\right] .$$

We notice that $\Delta_2^r << (\Delta_1^r)^2$. If we roughly set $\Delta_1^r = 0.05$ then $\Delta_2^r < 0.0005$. For $dx = \frac{1}{2}$ we derive

$$\ell = \sqrt{\frac{8.64^2\Delta_1^r}{\pi^2}} \quad \underline{\ell = 12} \quad ,$$

i.e. the 12 first modes deviate less than 5% from their correct values.

2.7 Properties of the test system

To obtain a quantitative measure of the effects of the approximations mentioned in sections 2.2 to 2.6 we apply the numerical scheme described in section 2.2 to a simple and fully understood flow problem. By choosing a time-independent flow as a test problem for the scheme we can be sure that any time variation occurring in the numerical results must be ascribed to the approximations made.

A system in which $\zeta = \zeta_o$ inside a circle of radius R_o and $\zeta = 0$ elsewhere is called Rankine's combined vortex (Lamb 1932, Bassett 1888), when the solutions to Poisson's and Laplace's equations inside and outside the circle respectively are fitted properly at $r = R_o$:

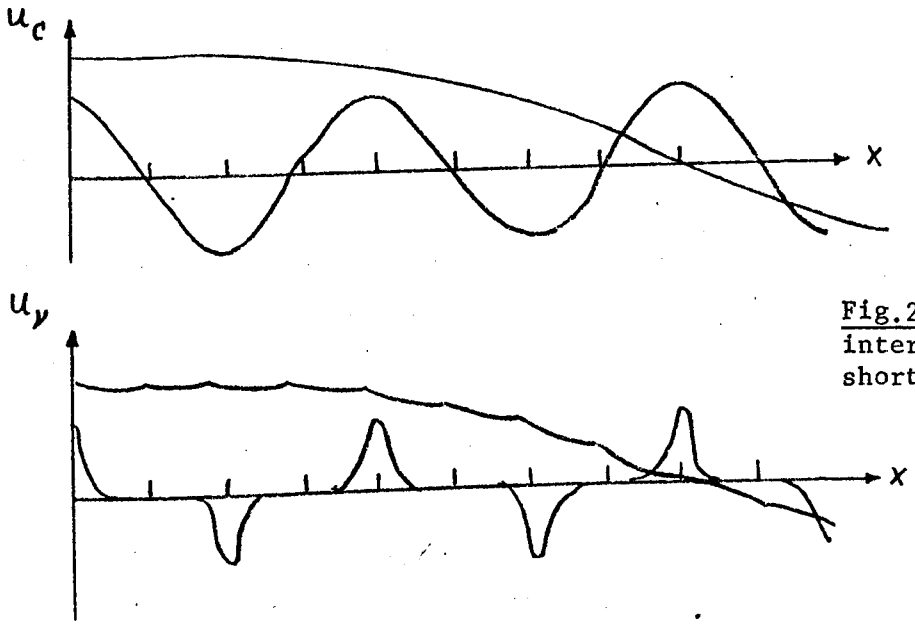

Fig.2.1 Effect of CIC interpolation on long and short wavelength modes.

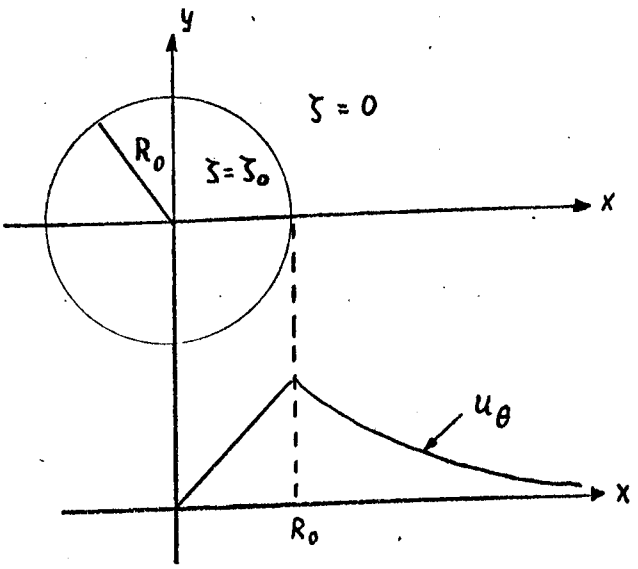

Fig.2.2 Rankine's combined vortex as test model.

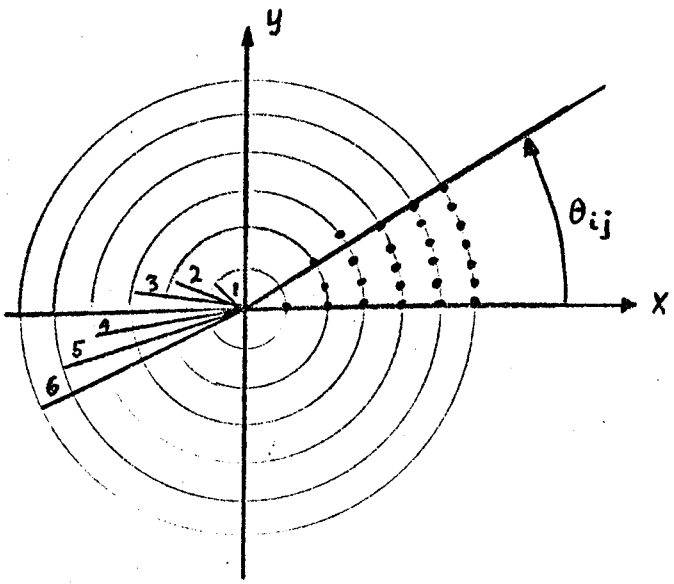

Fig.2.3 Point vortices arranged to simulate Rankine's combined vortex.

$$\psi = \psi_o - \tfrac{1}{4}\zeta_o (r^2 - R_o^2) \qquad r \leqslant R_o$$

$$\psi = \psi_o - \tfrac{1}{4}\zeta_o R_o^2 \log \frac{r}{R_o} \qquad r \geqslant R_o$$

The fluid velocity is everywhere azimuthal :

$$\begin{aligned} u_r &= 0 \\ u_\theta &= \tfrac{1}{2}\zeta_o r \qquad r \leqslant R_o \\ u_\theta &= \tfrac{1}{2}\zeta_o \frac{R_o^2}{r} \qquad r \geqslant R_o \end{aligned} \tag{2.20}$$

which is indicated in Fig.2.2. Since the vorticity ζ is a function of the stream function ψ only, i.e. $\zeta = \zeta(\psi)$, we have a steady state flow as the Poisson bracket $[\zeta,\psi]$ of eq.(1.16) is zero. Rankine's combined vortex is an analytic approximation to a motion often encountered in real fluids, although the viscous effects present in real fluids will eventually smooth out the discontinuous ζ distribution, vorticity diffusing through the surrounding irrotationally-moving fluid according to $\frac{d\zeta}{dt} = \nu^2 \nabla^2 \zeta$ so that the vortex decays exponentially and in the limit $t \to \infty$ the flow is fully irrotational (Ting and Tung 1965).

If a small-amplitude irrotational disturbance (see chapter 4)

$$\Delta\psi = A_m e^{i(m\theta - \omega_m t)} \begin{Bmatrix} r^m & r \leqslant R_o \\ r^{-m} & r \geqslant R_o \end{Bmatrix}$$

is imposed it will cause a stable azimuthal corrugation to travel around the interface $r = R_o$ with an angular velocity (Lamb 1932)

$$\frac{\omega_m}{m} = \tfrac{1}{2}\zeta_o \frac{m-1}{m} \quad . \tag{2.21}$$

The equilibrium steady-state flow is thus linearly stable, an important feature in view of the results presented in section 2.9 .

2.8 The set-up for numerical simulation

To obtain a circular region of constant $\zeta = \zeta_o$ we distribute point vortices as shown in Fig.2.3. On J rings of radii $r_j = jd$, $j = 1,J$

we place point vortices at angles $\theta_{ij} = i\,\frac{2\pi}{jM}$, $i = 1, jM$. This distribution credits a constant area $\pi d^2\,\frac{2J}{(J+1)M}$ to each point vortex.

In the experiments we set $d = 0.3$, $J = 24$, $M = 10$. The total number of particles is 3,000 plus 2 particles in the centre. The area is 163 and the period of rotation is $T_o = \frac{4\pi}{\zeta_o} = 0.682$. We have chosen $\Delta t = \frac{16}{3002}$, such that the approximate number of timesteps for one rotation is 128. The maximum velocity occurring at $r = R_o$ is $V_{max} = \frac{1}{2}\zeta_o R_o = 66.4$ so that the Courant Friedrichs-Lewy condition is satisfied ($V_{max}\,\Delta t = 0.35$).

A system of point vortices resembling the arrangement in Fig.2.3 has been examined by Morikawa and Swenson (1971). They study N point vortices, geostrophic or logarithmic, distributed on a circle. Their stability analysis of this system is already quite complex as N varies from 2 to 10, and with 24 rings present in our experiment we shall make no attempt to analyse the stability.

In the first series of experiments we place the vortex made up of particles in the centre of a square mesh and normally restrict ψ to be a constant (0) along the perimeter of the square. The simulation is run for about 1,000 timesteps. Ideally all jM point vortices on ring j should remain on this ring. To see whether this is the case we define the radius function for ring j as

$$r_j(\theta) = |\underline{r}_n - \underline{r}_g|$$

where $\underline{r}_g$ is the fixed centre of gravity of the jM points on ring j :

$$\underline{r}_g = \frac{1}{jM} \sum_{n=1}^{jM} \underline{r}_n \,.$$

The radius function can be represented by a finite Fourier series

$$r_j(\theta) = \sum_{m=2}^{L} a_m \, e^{im\theta}$$

where a_m is complex. Evidently $a_o = a_1 = 0$. Since at $t=0$ $a_m = 0$ for all m, any developments of an azimuthal mode will represent effects that are due to the finite difference formulation or the arrangement of points as explained above.

Analysis of the positions $\underline{r}_i$, $i = 1, jM$ provides us with a_m $(m=1,16)$ as well as the perimeter and area enclosed by the curve they define. The last two quantities are conserved in all experiments to within the level of rounding off errors. In order to assign the anomalies detected to any one of the difference approximations we carry out a number of experiments which are all like Experiment I apart from what is outlined below.

Experiment I: Standard experiment on the vortex as described above.

Experiment II: Along the square boundary ψ becomes a function of the distance from the centre of the vortex.

Experiment III: Δt is varied.

Experiment IV: A single ring of radius $R_d = 6.0$ is moved in a time independent velocity field inherited from Experiment I.

Experiment V: As IV but with $R_d = \frac{7.2^2}{6.0}$.

Experiment VI: As IV but with $R_d = R_o = 7.2$.

Experiment VII: Test of area weighting method for analytic velocity field.

2.9 Results of the numerical experiments

The standard Experiment I exhibits an anomalous instability at $r = R_o$ accounted for by a growth with time of the azimuthal modes a_4, a_8, a_{12} as shown in Fig.2.4. All other modes remain at the level of truncation errors. In order to assign this anomaly to any one of the effects mentioned earlier in this paper we performed the Experiments II-VII guided by the principle of elimination.

A study of Experiment I reveals a deviation in the azimuthal velocity profile as indicated qualitatively in Fig.2.5. First we look at the effect from using a square boundary since this seems most likely to cause the anomaly. The amplitudes b_4, b_8 ... of the potential $\tilde{\psi}_o$ (Eq.2.11) are linearly related (Lamb 1932, Bassett 1888), by

$$a_m = \frac{2m}{\zeta_o} b_m \quad .$$

With our data $a_4 \approx 10^{-5}$. Because of the vector integration technique (Boris and Roberts 1969) the positional accuracy is given by 18 bits or 10^{-5} (in cell length units). We can, therefore, expect the influence of a square boundary to be negligible and indeed Experiment II verifies this since a_4 develops in the same way as in Experiment I. We might now expect that the time integration method could cause the anomalous behaviour in face of the instability described in section 2.5. We have however devised a method (see Appendix) of preventing the 2 sets of coordinates from getting out of step. The method can be applied at a variable frequency during the time integration and whether used at any frequency or not the development of a_4, a_8 is still present (Experiment III).

In Experiments IV, V and VI we eliminate all calculations except for the time integration and the area-weighting of velocities (Eq.2.8). It is now found that inside the vortex the azimuthal modes oscillate with their

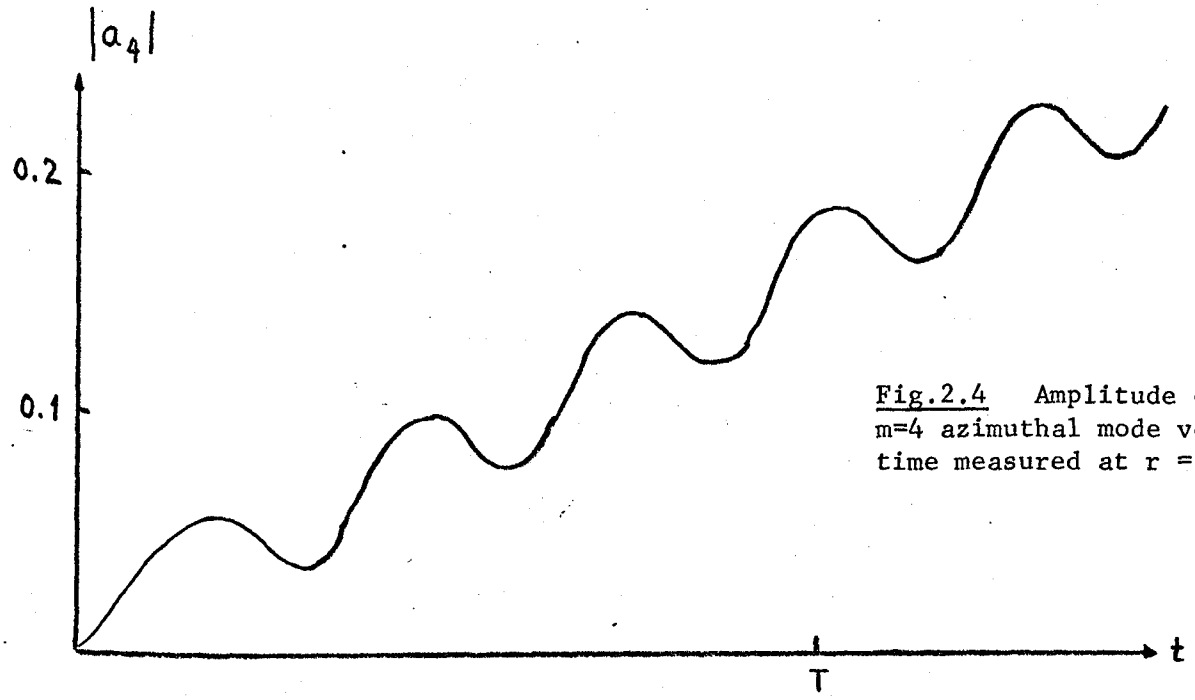

Fig.2.4 Amplitude of the m=4 azimuthal mode versus time measured at r = 7.2.

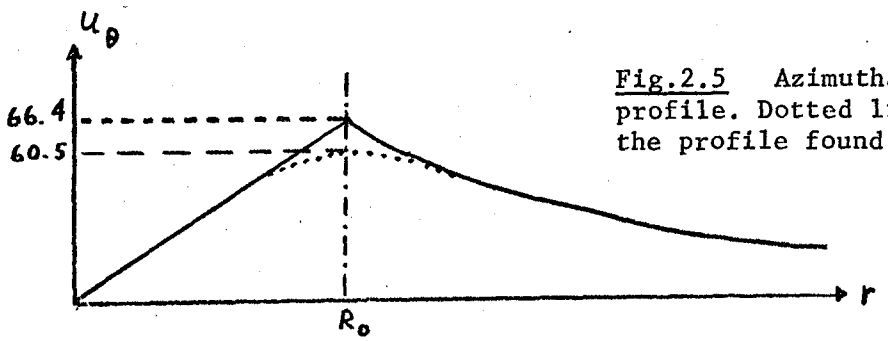

Fig.2.5 Azimuthal velocity profile. Dotted line indicates the profile found in the experiment.

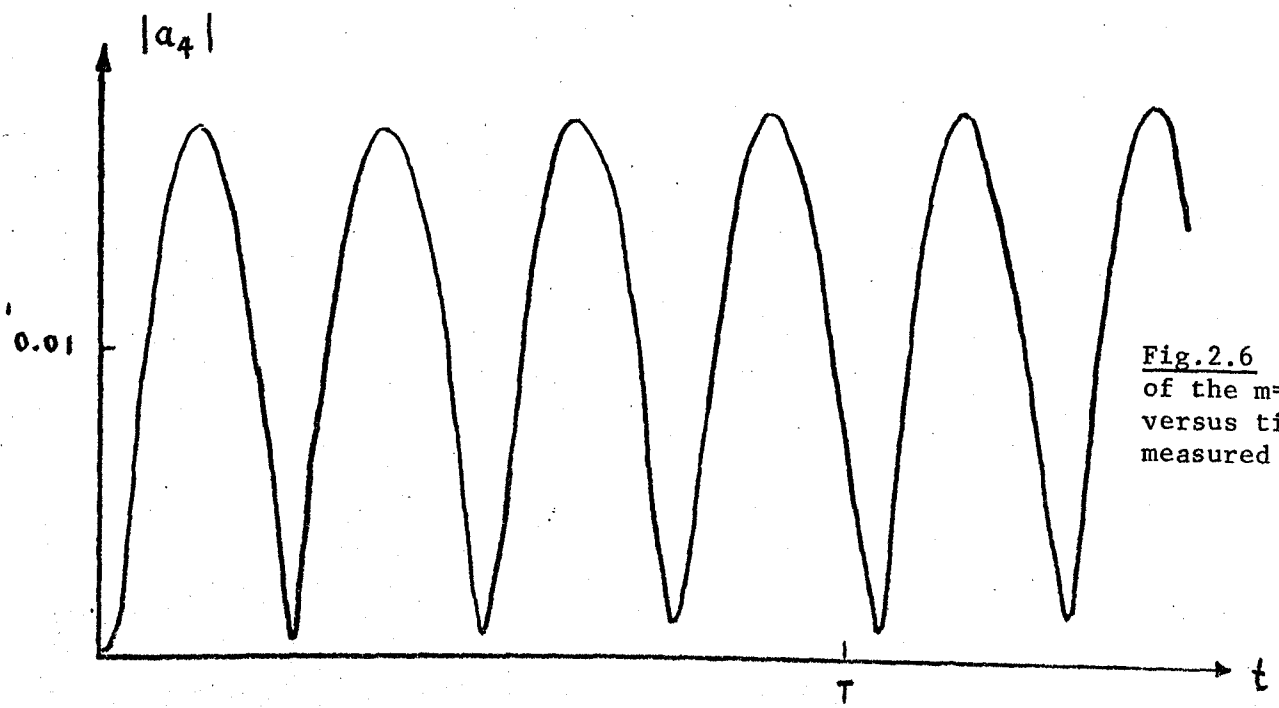

Fig.2.6 Amplitude of the m=4 azimuthal versus time, measured at r = 6.0

eigen-frequencies given by Eq.(2.21) without growing in time as shown in Fig.2.6. On the edge and outside the vortex we get the same growth as in Experiments I-III.

One might have been tempted to attribute the results given above to the leapfrog scheme, since we have shown in section 2.5 that this is unstable for irrotational flows, and the outermost ring of the vortex is partly moving irrotationally. However, the area-weighting method can equally well contribute to the results of Experiments IV, V and VI. As noticed earlier the area-weighting is a linear interpolation and is thus an exact method when dealing with a flow where u varies linearly as is the case inside the vortex. In Experiment VII we move a particle in a velocity field which is exactly represented at all mesh points. To find the particle velocity we use the formula for area-weighting (Eq.2.8), and as a trivial test of the method we find an exact representation for a flow described by a linearly varying azimuthal velocity. When moving a particle in a flow field with $u_x = 0$ and $u_y = \frac{1}{2}\zeta_o \frac{R_o^2}{r}$ (Eq.2.20) it is found that the area-weighting pushes a particle off the circle it should remain on. The radial velocity component that is introduced by the interpolation will change the radius of the particle orbit by an amount up to 1% during half the rotation period. This is roughly equal to the amplitude of a_4 by that time. Moreover, Experiment VII confirms the necessity of preventing the two sets of positions from getting out of step as indeed they should in an irrotational motion. The reason why the m=4, 8, 12 ... modes are enhanced is not as we thought initially the introduction of a square boundary. The circular geometry interacts with the square mesh producing a four-fold symmetry so that only modes with this symmetry can be present. The growth of these modes is caused by the area-weighting and one way to remove this anomaly would be to adopt a higher order interpolation scheme for evaluating the particle velocity.

It would be interesting to see whether a change in the structure of the mesh (hexagonal, triagonal etc.) would improve on the accuracy rather than employing more mesh points in the interpolation.

2.10 Advantages and deficiencies of a particle approach

Two questions that inevitably arise from the foregoing discussions are: How useful is the particle model for a further study of hydrodynamics? And how does it compare with other numerical techniques?

The answer to the first question is based on our experience from a series of numerical simulations on a variety of hydrodynamic problems. (See chapters 3, 4 and 5). The particle model has proved useful and reliable within a time range that naturally depends on what accuracy is needed and what kind of distribution is required. Good agreement has been achieved between theory and a number of experimental results. For a given flow problem that can be described analytically in the linear regime we can by comparing theory and experiment acquire a quantitative understanding of how the inaccuracies are related to the length of the time integration. In most of the cases that we have encountered the prominent part of the evolution takes place before the accumulation of errors can distort the result. For example, in our study of the interaction between vortices the picture of evolution is almost complete within 3, 4 or 5 periods of rotation of a single vortex, limiting the anomalous growth of azimuthal modes to say 5-6%. The most serious deficiency is, however, a consequence of using a finite number of particles to describe a continuum (hydrodynamic case). The area-weighting inherent from the particle approach introduces local compressions and rarefactions of the fluid, i.e. changes in particle density, and with this effect present the quality of simulating a waterbag system (ζ constant inside a contour) by a discrete distribution of points is

lost. A study of the area function $A_1(\zeta)$ which in the waterbag case should be a delta-function reveals an undesired relaxation of its initial peaked form (chapter 3).

The main alternative to our method seems to be a mesh method like the one used by Fromm and Harlow (1963) or by Zabusky and Deem (1971), which is subject to conditions for numerical stability analogous to those outlined in section 2.5 but causes vorticity to diffuse very quickly so that pictures such as those in chapters 4 and 5 could not be obtained in this way. During the development of our technique the accurate graphical display of the particle positions seemed an attractive feature, and we were also attracted by the particle method when it became clear how to optimize the equations of motion for particles (Boris and Roberts, 1969) so that the amount of computer time required for either method is much the same.

CHAPTER 3

GENERAL DISCUSSION OF IMPLEMENTING NUMERICAL EXPERIMENTS

This chapter representing the most time-consuming part of the research work is deliberately made as short as possible. The work with the computer codes is discussed and references are made to the Appendix. The problem of setting up the initial configuration of point vortices is outlined and the boundary conditions available are mentioned. The final discussion of the quality of the numerical experiments records the experience from a large number of different numerical exercises.

3.1 The computer codes

In the Appendix we present a detailed description of the "VORTEX" computer code. This computer code was originally intended for solving problems in hydrodynamics by the method described in chapter 2. In Table A.1 of the Appendix we list the most prominent features of the history of development. This hopefully emphasizes the considerable time spent in designing and implementing a computer code.

Table A.2 of the Appendix lists all the computer codes we found necessary to develop in order to interpret the results generated by the VORTEX code. The running of all codes on different experiments by which we mean numerical/computational experiments, made it necessary to organize and administrate the data produced in a proper fashion. From Table A.3 of the Appendix it can be seen that several hundred runs on the computer have been performed and each of these has been recorded in a diary just as one would do in experimental physics. Table A.3 can be regarded as an extract of the diary.

We have had to check the validity of the data generated by the computer codes. Obviously we cannot study the individual motion of thousands of point vortices in each run. Instead two different methods of controlling and checking the evolution of an experiment have been employed.

The first method produces diagnostic information either whilst the experiment is going on or at a later stage. The diagnostics are concerned with monitoring the time invariance of certain quantities (those described in chapter 1). We shall not describe the details of the diagnostics since it plays only a supporting role in conducting numerical experiments. We shall just emphasize as we did above that a considerable time has been spent in extracting the relevant information.

In the second method we purport to visualize the flow fields arising from the computations. Usually we do so by plotting the positions of the point vortices and many of the figures in chapters 4 and 5 are examples thereof. Light grey areas made up of small dots represent regions of positive vorticity (counter-clockwise rotation). Dark areas made up of asterisks represent regions of negative vorticity (clockwise rotation). Apart from displaying the vorticity distribution we can visualize a flow field by plotting the stream function (see for example Figure 4.2) or follow the motion of marker particles.

Much of the additional information presented in chapters 4 and 5 comes from the "analyser" codes listed in Table A.2. It would excessively swell the bulk of this chapter to describe the numerical methods used by these "analyser" codes. However we shall in the conclusion to this chapter discuss the reliability or validity of the numerical experiments in view of the diagnostics obtained from the "analyser" codes.

Although the work behind the material presented in this chapter has consumed by a wide margin most of the human efforts involved we shall not dwell on any detailed specifications. When Computational Physics can be fully established as a discipline and its terminology adopted by the scientific community it may well be superfluous to describe material of the kind to follow. One may simply use terms like "quiet starts", "random perturbations", "semi-conservation" etc., without elaborating their significance.

In this short chapter we shall indicate some of the considerations that go ahead of implementing numerical experiments. The methods of arranging point vortices to approximate given distributions are reviewed to avoid repetition thereof in chapters 4 and 5. Our restricted choice of boundary conditions is briefly mentioned. Finally we go through a short

general discussion of the reliability of the results from the numerical experiments of chapters 4 and 5.

3.2 General data for numerical experiments. Units.

All the numerical experiments listed in Table A.3 have been carried out with the VORTEX code in the versions Mk I, Mk II or Mk III (Table A.1). In this short section we shall outline the data that is common to most of the calculations performed.

As we have already described in chapter 2, the calculations take place within a square region covered by a cartesian mesh. The dimensions of this mesh are 64 by 64 unit lengths. The number N of point vortices used does vary, but is usually chosen as close as possible to 3200 which is the maximum number allowed by the computer memory. When both positive and negative point vortices are used the total vorticity is <u>always</u> zero. The finite value of the timestep Δt also varies from project to project. Its value is automatically chosen by the VORTEX code as a "convenient" value close to

$$\Delta t = \tfrac{1}{4} \frac{\Delta x}{\langle |\underline{v}| \rangle} \text{ , where } \langle |\underline{v}| \rangle = \frac{1}{N} \sum_{i=1}^{N} |\underline{v}_i| \text{ ,}$$

thereby satisfying the Courant-Friedrichs-Lewy condition (Richtmeyer, Mortion 1964) by a wide margin ($\frac{1}{4} < \frac{1}{\sqrt{2}}$).

In section 2.4 we noticed that the leapfrog time integration scheme will exhibit a numerical instability when applied to irrotational flows. To suppress this incipient instability we have devised a procedure that will average alternate time levels (even and odd levels) at a given frequency. This procedure is referred to as matching of particle positions and is mentioned in section 2.8 with a reference to the Appendix. In most of the numerical experiments the matching is done either once every 16 timesteps or once every 8 timesteps.

The length of a given calculation naturally depends on which phenomena

are studied. However Table A.3 indicates (column 3)the number of simulations carried out for a given project. We think of an experiment as consisting of one or more calculations. The experiment may cover a time period τ corresponding to $N_R = \frac{\tau}{\Delta t}$ timesteps. This number N_R is then broken down into units of 192 timesteps for technical reasons. An experiment may thus comprise several units (calculations).

The unit of time is arbitrary in the sense that it depends only on the strength Γ_i of a point vortex. This can be seen from the equation of motion of section 2.1, for example

$$\frac{d}{dt} x_i = \Gamma \sum (\hat{e}_z \times \underline{r}_{ij}) \frac{1}{|\underline{r}_{ij}|^2} \text{ sign } \Gamma_j$$

where $\hat{e}_z$ is a unit vector in the z-direction and $\underline{r}_{ij}=(x_i-x_j, y_i-y_j)$. The Mk I and Mk II versions of VORTEX assume

$$\sum |\Gamma_i| = 64 \ , \ |\Gamma_i| = \frac{164}{N}$$

whereas the Mk III version assumes $|\Gamma_i| = 1$ for all i . The relation between the time t_{II} of the calculations by the Mk I and Mk II versions and the corresponding time t_{III} of the Mk III version is thus

$$t_{III} = \frac{64}{N} t_{II} \ .$$

We have deliberately elaborated this minor item, since in all its simplicity it has caused a great deal of confusion. It is the time t_{III} that will be used in the following and referred to by the symbol t. The unit of time is thus the time taken for a positive and a negative point vortex separated by a unit length to travel a distance $\frac{1}{2\pi}$ in the direction perpendicular to the line adjoining them.

3.3 Initialization procedures

The numerical experiments encountered in chapters 4 and 5 employ the "constant vorticity" model described in chapters 1 and 2. Already in

section 2.7 we saw how point vortices were distributed to approximate a circular vortex of constant vorticity. The general problem to be dealt with in this section is how to effect distributions of point vortices so that the vorticity functions in question are represented well. With the errors arising from a finite difference representation of the partial differential equations (chapter 2) it seems quite obvious that the initial conditions of a numerical experiment ought to bear a close resemblance to the true situation that is being studied. A comparison between theory and experimental results should then produce some agreement. However trivial this point may seem it has nevertheless been overlooked by many authors in the field. In computer simulations of electrostatic and magnetized plasmas the genuine thermal fluctuations ($\sim N^{-\frac{1}{2}}$, N particle number) can become impossible to detect if an assembly of particles (ions and electrons) is distributed initially in some random fashion. Such a situation is referred to as a "noisy" start.

A "quiet" start (Byers, 1969) refers to an initial uniform loading of particles in phase space. In the plasma case particles are distributed on surfaces of constant energy and their positions in phase space are then (usually) altered by a small prescribed perturbation. Equally well one speaks of a "silent" start when particles during the first few timesteps of their motion will remain on the surfaces of constant energy.

The literature available on the "start" problem does not deal with the particle model described in chapter 2. However it is easy to guess that in our case one should attempt to place point vortices uniformly on the streamlines. The set-up of point vortices in section 2.7 represents a "silent" start since the streamlines are concentric circles. It is the finite difference forms (interpolations etc.) that eventually push particles off their streamlines, as we described in section 2.9.

In our studies involving vortices or rings of constant vorticity we consistently employ the "silent" start approach. However in the case of two or more vortices the initial streamlines are no longer concentric circles. The deviations from the circular shape raise the noise level and our point vortex distribution is reduced to that of the "quiet" start. But the latter is still far better than the "noisy" starts employed in the very early experiments with the VORTEX code. Point vortices were then distributed at random inside a circular region. ('Random' here and in the following refers to a sequence of numbers produced by a random number generator). With a "noisy" start it is impossible to monitor the surface motion of the vortices or to check the centroid motion (the motion of the vortex centre).

In our studies of laminar flows we have steady states in which all streamlines are straight. This situation is ideally suited for a numerical simulation on a cartesian mesh. Figure 5.1 shows how in one case point vortices are aligned at equidistant positions thereby producing an exact and constant value of ζ at all mesh points. (The case of the circular arrangement in Figure 2.3 produces the exact constant value at most mesh points, but introduces a smoothing near the edge of the vortex).

In order to examine the stability and long time evolution of a laminar flow this becomes subject to some kind of perturbation. Only irrotational disturbances, e.g. disturbances without sources of vorticity, are considered. This enables us to compare experimental results with those obtained from linear stability analysis of laminar flows (Chandrasekhar, 1961). The total amount of vorticity is that of the steady state and the disturbance becomes a stream function $\delta\psi$ which satisfies Laplace's equation $\nabla^2 \delta\psi = 0$. The associated velocity field

$$\delta\underline{u} = \underline{\nabla} \times \delta\underline{\psi} \quad , \quad (\delta\underline{\psi} = (0,0,\delta\psi))$$

is used to move point vortices a distance $\delta\underline{r} = \delta\underline{u}\,\Delta t$ away from their positions in the steady state.

We notice that whereas $\delta\underline{u}$ expressed at all mesh points has zero divergence the velocity field $\delta\underline{u}(\underline{r}_i)$ extracted at a particle position $\underline{r}_i$ is not divergence-free (section 2.5). The finite divergence $\nabla\cdot\delta\underline{u}$ obtained when interpolating to find $\delta\underline{u}(\underline{r}_i)$ (section 2.6) is however so small that its effect on the perturbation itself can be neglected. Let us assume that $\delta\underline{u}$ is represented by a sequence of random numbers such that $|\delta\underline{u}|_{max} \approx 1.0$. Then the effect of interpolating as described in section 2.6 causes a deviation in $\delta\underline{u}$ which is of the order

$$\Sigma\, \xi_{\ell,k}\ \delta\underline{u}_{\ell,k} \quad ,$$

a result obtained in section 2.5. If we assume all modes in the random perturbation field have the same amplitude, then the error in $\nabla\cdot\delta\underline{u}$ is to second order in (ℓ,k) $\frac{1}{8}\left[\left(\frac{2\pi\ell}{Nx}\right)^2 + \left(\frac{2\pi k}{Ny}\right)^2\right]$ for a mode (ℓ,k). In the long wavelength limit this error becomes of the order 10^{-2} in $\delta\underline{u}$. $\delta\underline{u}\,\Delta t$ itself is of the order 10^{-2} units of a cell length, such that the absolute error becomes approximately 10^{-4} cell lengths or close to the rounding off level 10^{-5}, arising from using 18 bits to represent $\delta\underline{u}$ (see beginning of section 2.8 and the Appendix).

The above-described method of perturbing a laminar flow is also applied to the ring problem discussed in section 5.8. In the studies of vortex streets we initially distribute points as described earlier in order to approximate circular vortices. If the vortices initially are of elliptic shape we distribute point vortices on "like" ellipses by mapping the equivalent positions on a circle into the ellipse, i.e. simply

$$y_{ellipse} = \frac{b}{R}\, y_{circle} \qquad x_{ellipse} = \frac{a}{R}\, x_{circle}$$

where a,b are the major/minor axes and R the radius of the circle.

($\sqrt{ab} = R^2$). This arrangement of point vortices results in a reasonably constant vorticity value at the mesh points (checked by analyser codes), provided the eccentricity, ε, of the ellipse is not too large ($\varepsilon < 0.95$). Numerical experiments on Kirchoff's elliptic vortex (Lamb, 1932, p.230) with $\varepsilon = 0.98$ have revealed that the arrangement of point vortices in this case causes large variations in the vorticity values at the mesh points. A different and much more complicated distribution of point vortices is then required to produce constant values of ζ at the mesh points. We shall not describe the method since none of the experiments dealt with in this thesis have used the method.

3.4 Boundary conditions

In chapter 1 we stated that to specify a given system completely it is necessary to include a prescription of its behaviour at the boundaries. Since all our numerical experiments take place within a square we need only specify the stream function ψ along two x-boundaries and two y-boundaries. The conditions for the vorticity ζ and the fluid velocity follow automatically (see below). When solving Poisson's equation by the method described in chapter 2, only 3 different types of boundary conditions are dealt with. These are:

A : ψ is constant (say zero) along all four boundaries.

B : ψ is constant along the y-boundaries and is assumed periodic in the x-direction.

C : ψ is assumed periodic both in the x- and the y-directions.

The corresponding behaviour of ζ and u along the boundaries is as follows: when ψ is a constant along a boundary $\zeta=0$ and $u = (\nabla x \psi).\hat{n} = 0$ at that boundary. When ψ is assumed periodic both ζ and $\underline{u}$ are periodic functions.

These three boundary conditions are simple and obviously restrictive in describing realistic flows. When ψ is constant along a boundary we speak of a fixed boundary with free slip, since we normally have a tangential motion along the boundary, e.g. $v \neq 0$. The free slip is of course only feasible in inviscid fluids. For realistic fluids (viscous fluids) conditions A and B must be extended to include the condition $v = (\nabla x \psi) \cdot \hat{t} = 0$ along the boundary, that is the fluid adheres to the boundary (no slip). We have vorticity actually being generated in a thin boundary layer and diffusing inwards in accordance with the prescription put forward by Lighthill (1963).

In section 2.3 we studied the effects of using condition A and based our calculation on images being present. When periodicity is being assumed we essentially attempt to study a system of infinite extent, but the finite box size L excludes phenomena characterised by wavelengths larger than L. In one particular case (see section 5.6) we perform the same experiment twice using boundary conditions B and C in order to demonstrate the lack of influence of the fixed boundaries on a given instability.

If we were to employ complex boundary conditions (special geometry of system, obstacles etc.) it would in general involve the construction of a new computer code every time a new set of conditions was considered. Quite apart from this any analytical theory would become more difficult to develop. Nevertheless it would be interesting to study the flows presented in chapters 4 and 5 for the case of free boundaries occurring for example between air and water. Unfortunately our numerical approach is not at all suitable for dealing with free boundaries. Although the presence of free boundaries is common to many problems in hydrodynamics, not much has been done in the field of numerical fluid dynamics as

regards calculations on this rather fundamental situation. However a very recent method developed by Zarodny and Greenberg (1972) for a study of water waves in ideal fluids may prove a promising step forward towards the understanding of free boundary problems.

3.5 The quality of the numerical experiments

Normally one would interpret the quality of a numerical experiment in terms of its ability to reproduce the properties of the system that is being studied. This makes an interpretation somewhat ambiguous, since the time evolution of the system is the object of the research. All we know for certain are the quantities that remain invariant as time proceeds. Our discussion of the quality of numerical experiments is therefore based on measurements of the invariants of motion which are described in section 1.4.

It is well known (Richtmeyer and Morton 1964) that most numerical schemes of practical use will conserve certain quantities for all times. Other quantities are "semi-conserved" by which is meant that they are identically conserved in the limit $\Delta t \to 0$. The numerical scheme described in chapter 2 will only conserve the total vorticity (total number of point vortices) and also satisfy the condition $\underline{\nabla} \cdot \underline{u} = 0$ at all mesh points. All other invariants of motion are semi-conserved.

The quality of an experiment can then to some extent be interpreted by the development with time of departures from the initial values of quantities like energy, linear and angular momentum. Instead of introducing large tables giving such deviations we shall briefly sum up the results extracted from every experiment performed. Let us look at each invariant of motion separately.

a) Energy: $E_1 = \sum_{i,j} |\underline{u}(i,j)|^2$; $E_2 = \sum_{i,j} \zeta(i,j)\psi(i,j)$;

The experiments of chapter 4 exhibit temporal variations of the order up to 0.1%. E_1 and E_2 differ constantly by 1-2% reflecting the effects from the numerical differentiation of ψ to get $\underline{u}$ (see section 2.3). When circular vortices persist as observed in some of the experiments of chapter 5 or when we study laminar flows we find variations in E_1 of the order 6-7% (max.).

b) Linear momentum: $\underline{p} = \sum_{i,j} \underline{u}(i,j)$.

The total linear momentum $\underline{p}$ is always chosen to be zero. Variations in $\underline{p}$ are due to rounding off errors only and no information is obtained by measuring p.

c) Enstrophy*: $\langle \zeta^2 \rangle = \sum_{i,j} \zeta^2(i,j)$.

The variations in enstrophy can become of the order 0.1-0.2% for experiments in which circular vortices persist, otherwise they may become $\sim$ 2%. The experiment on laminar wakes exhibits variations of up to 45% over long times. This violent variation reflects the inadequacy of our numerical model to represent the mixing of positive and negative vorticity accurately. In regions where thin slivers of vorticity should be found (continuum) too few point vortices are available to represent this short-wavelength-type distribution.

d) Area:

The conservation of the area of a circular or elliptic vortex has been found to be surprisingly good; in many experiments a variation as small as 0.01% has been measured. No attempt has been made to monitor the vorticity areas for laminar flows, understandably in view of what was said above.

---

*By definition enstrophy is vorticity squared.

c) The area function of the first kind:

The quantity $A_1(\zeta)$ (see chapter 1) is a very sensitive measure of how the vorticity function $\zeta(x,y)$ is treated by the mesh techniques of chapter 2. In all numerical experiments undertaken (except for I and II of chapter 4) we have

$$A(\zeta) = \delta(\zeta-\zeta_o) + \delta(\zeta+\zeta_o) .$$

δ represents the Dirac-delta function and the second term is present only when the vorticity takes the two values $\pm \zeta_o$. Because of the effective interaction between the geometry of the vorticity distribution (circles, ellipses etc.) and the square mesh, we get initially a spectrum with an extra peak near $\zeta=0$. This peak is present because the mesh points just outside the vortex boundaries are credited with a small amount of vorticity via the interpolation techniques. There is no cure for this misrepresentation of the "constant" vorticity model apart from adopting an altogether different numerical approach. Unfortunately the $\zeta=0$ peak broadens as time progresses and to prevent it from colliding with the peaks at $\zeta = \pm\zeta_o$, ζ_o should be chosen with some care (really as large a value as is possible).

In conclusion we can state the limitations on our numerical model as follows: Experience shows that experiments with circular vortices produce results of good overall quality for a time length of up to at least 5 rotation periods of the vortex and often longer. Experiments on laminar flows exhibit a reasonable quality of the results for the same time period. When mixing of positive and negative vorticity prevails the results are rather inaccurate and no conclusions can be drawn about small scale-length phenomena. These statements refer to experiments in which N has been chosen as close as possible to its maximum value 3200. Experiments for which $N \sim 1600$ have shown errors more than twice as large as those for

which $N \sim 3200$. Other experiments seem to be almost unaffected by variations in N (within certain limits). We have no definite explanation for this behaviour, as mentioned in section 2.1 .

CHAPTER 4

THE INTERACTION BETWEEN VORTICES OF FINITE SIZE

This chapter studies the interaction between vortices that initially are of circular shape and of constant vorticity. A useful model "the constant vorticity" model as used by many classic authors is briefly described. This model is first employed in an analytic study of weak interactions between 2 vortices. The distortion of each vortex boundary resulting from the interaction can be thought of as the presence of surface waves that carry negative energy. The analytic study yields explicit formulae for the amplitudes of the surface waves when these are confined to the linear regime. The analytic study supports the understanding of a series of controlled numerical experiments on relatively weak interactions; some measure of agreement between theory and experiment is established. Numerical experiments on strong interactions show results that can be partially explained via the conservation laws implied. The material presented in this chapter forms an introduction to that of the following chapter.

4.1 Introduction

The work presented in this chapter is related to the problem of turbulence from a two-dimensional point of view as mentioned in the introduction to this thesis. We have initially found it worthwhile studying the interaction properties of finite-area vorticity regions. The model we use in these studies is the field model with an infinite number of degrees of freedom. This model was employed in chapter 2 to study the effects of the numerical approximation. In the first part of this chapter we study the interaction between finite-area vortices from an analytic point of view. Consequently the numerical experiments presented in the second part of this chapter are based on approximations made to a field model with an infinite number of degrees of freedom. We emphasize this point since the particle model employed (chapter 2) could equally well lead us to make analytical studies of a particle model with a finite number of degrees of freedom.

The particular field model chosen is the "constant vorticity" model used by Kirchoff, Kelvin, Love, Hill and later by Proudman and Lamb (see Introduction and chapter 1). In the constant vorticity model we deal with a set of contours (open or closed) confining areas of constant vorticity $\pm\zeta_0$. The vorticity thus becomes a step-function taking the values $-\zeta_0$, 0 or $+\zeta_0$. The constant vorticity model is analogous to the so-called "water-bag model" which has found extensive use in Plasma Physics (De Packh 1962, Dory 1964, Berk, Nielsen & Roberts 1970).

The simplifications made in using the constant vorticity model are not as restrictive as might be apparent. Since we are dealing with ideal fluids we know that the vorticity contours remain attached to the fluid (Helmholtz theorem). Systems with smoothly varying vorticity distributions will exhibit a large scale behaviour very similar to that of our

model. The large scale dynamics is a function of the shape of the contours more so than the precise functional form of the vorticity inside these contours (except for extreme cases like boundary layer phenomena).

Our studies of vortex interactions as well as the resulting flow pattern comprise three situations :

a) The properties of a single vortex

b) The interaction between two nearby vortex regions

c) The properties of systems with several vortices.

The third situation will be dealt with in chapter 5, whereas we shall concentrate on the second situation in this chapter. The case of a single circular vortex was used in chapter 2 as already mentioned.

In the following we shall again look at a single circular vortex (a Rankine vortex) and briefly outline the basic properties of this system. Next we look at the interaction between two vortices of different size and strength. The vortices are assumed circular initially and we compare the energy of two vortices with that of one which has the same total vorticity as the two. The interaction between two vortices can be thought of as the evolution with time of surface waves describing the distortion of each vortex. (These surface waves were already encountered in chapter 2). A section describes how the time variation of the amplitudes of the surface waves can be calculated analytically when the interaction is assumed to be of a weak nature. When the amplitudes are known it is possible to describe how energy is being distributed.

The analytical results obtained are then used to check the results from a series of numerical experiments presented in three different sections of this chapter. We have encountered several problems when trying to explain the numerical results which all extend well into the non-linear regime. Firstly we are faced with the difference between an

analytic model: "constant vorticity regions in an infinite medium" and a numerical model: "suitably arranged array of point vortices moving in a square box". The purpose of chapter 2 was to study this difference quantitatively and as a rough measure we can rely upon the approximations made to within 5% for a time covering 4-5 rotation periods of a vortex (section 2.10). Secondly we are interested in the non-linear properties of the interaction between vortices, otherwise theory would do better than computational experiments. This makes subsequent discussions and interpretations of numerical results somewhat qualitative.

The theory presented, states that interacting vortices will undergo the classical motion (as if they were point vortices), but they will also at the same time distort each other. The surface modes describing the distortion oscillate with time and the situation looks much like that of an infinite set of coupled harmonic oscillators (e.g. phase mixing etc.). This behaviour is ergodic, the vortices should never reach the circular shape again, since Poincaré's recurrence theorem does not apply (infinite number of degrees of freedom).

The numerical experiments confirm this picture for weakly interacting vortices. When the interaction reaches a certain strength the two like-signed vortices approach and finally fuse or coalesce to form one large vortex. Two oppositely-signed vortices develop large amplitude surface waves which oscillate, and recurrence to some approximation is established.

The second part of this chapter will describe our observations and only qualitatively explain them mainly by arguments based on energy principles. The same applies to our observations dealt with in chapter 5.

4.2 Rankine's combined vortex

The case of Rankine's combined vortex (Lamb, 1932, p.29 and p.230, and chapter 2) is obtained when the rotational flow inside a circle is properly fitted to the irrotational flow outside the circle (the vortex). Consider a circular region (radius R_o) of constant vorticity ζ_o. Using

$$q = \frac{1}{2} r^2 \quad , \quad p = \theta$$

as the Hamiltonian variables, we readily find from Poisson's equation (1.18)

$$\frac{\partial}{\partial q}\left(q \frac{\partial \psi}{\partial q}\right) + \frac{1}{4q} \frac{\partial^2 \psi}{\partial p^2} = - \frac{1}{2} \zeta_o \quad , \tag{4.1}$$

the fitted solution

$$\left.\begin{aligned} \psi &= \psi_o - \frac{1}{2} \zeta_o (q - q_o) \quad 0 \leq q \leq q_o \\ \psi &= \psi_o - \frac{1}{2} \zeta_o \, q_o \log \frac{q}{q_o} \quad , q_o \leq q \end{aligned}\right\} \tag{4.2}$$

where $q_o = \frac{1}{2} R_o^2$. The adjustable constant ψ_o is chosen to satisfy equation (1.21) along a contour $q = K$

$$\psi_o = \frac{1}{2} \zeta_o \, q_o \log \frac{K}{q_o} \quad , \quad \psi \to 0 \text{ for } q \to K \quad . \tag{4.3}$$

To deal with the infinite energy arising when $K \to \infty$ we set

$$E = \frac{\pi}{4} \rho \, \zeta_o^2 \, q_o^2 + \bar{E} = E_o + \bar{E} \tag{4.4}$$

with

$$\bar{E} = \pi \rho \, \zeta_o \, q_o \, \psi_o$$

(E is worked out by equation 1.18).

$\bar{E}$ represents the energy of the irrotationally moving fluid and becomes infinite for $K \to \infty$. In a similar way we write the z-component of the angular momentum as

$$L = \pi \rho \, \zeta_o \, q_o^2 + \rho \, A \, \zeta_o \, q_o = L_o + \bar{L} \tag{4.5}$$

where A is the area of the irrotationally moving fluid. For a given

amount of circulation $\Gamma_o = 2\pi q_o \zeta_o$, Rankine's vortex represents a state of minimum angular momentum and maximum energy. By this we mean that an arbitrary irrotational disturbance

$$h = \sum_m h_m = \sum_m A_m \left(\frac{\varsigma}{q_o}\right)^{|m/2|} e^{imp}, \quad q \leq q_o \tag{4.6}$$

satisfying $\nabla^2 h_m = 0$ and preserving A_o, the area of the rotationally moving fluid will cause changes $\delta L_m \geq 0$, $\delta E_m \leq 0$ in L and E respectively. Kelvin has shown (Lamb, 1932, p.230) that the disturbance (4.6) will cause stable waves to travel round the surface with an angular velocity

$$\frac{\omega_m}{m} = \frac{m-1}{m} \frac{1}{2} \zeta_o. \tag{4.7}$$

The disturbance is assumed small, e.g. $|A_m| << \Gamma_o$ such that $\alpha_m = \frac{2}{\zeta_o} |m| A_m << q_o$. The vortex boundary is expressed as (see equation 1.30)

$$G(q,p,t) = q_o + \sum \alpha_m e^{i(mp - \omega_m t)} - q = 0. \tag{4.8}$$

where α_m is complex. Although Kelvin's assumptions using (r,θ) in the expressions for h and G instead of $(q,p) = (\frac{1}{2} r^2, \theta)$ does not conserve the area A_o of the vortex, the dispersion relation (4.7) is still valid. The changes in energy and angular momentum due to H become

$$\frac{\delta E}{E_o} = -\sum_m \frac{1}{2} \frac{\alpha_m \alpha_{-m} (|m| - 2)}{q_o^2 |m|}, \quad \frac{\delta L}{L_o} = \sum_m \frac{1}{4} \frac{\alpha_m \alpha_{-m}}{q_o^2} \frac{1}{|m|} . \tag{4.9}$$

A disturbance h_m as given by (4.6) can be thought of as a wave that carries negative energy ($\delta E_m < 0$). Negative energy waves are encountered in many studies in Plasma Physics (Berk, Nielsen and Roberts, 1970); in the following we shall see the importance of negative energy waves that arise from interactions between vortices.

4.3 The interaction between vortices

Consider a situation in which we have two different-sized vortices of different but constant density as shown in Figure 4.1. When these two vortices interact they will disturb the confining contours of each other and their motion is described by two equations of the type (4.8). For simplicity we can assume both vortices to be initially circular so that all amplitudes of the surface waves are zero at $t = 0$.

Figure 4.1 shows the two vortices 1 and 2 whose centres C_1 and C_2 respectively are placed a distance D apart. This system consists of three regions 1, 2 and 3 where region 1 is confined by the contour

$$C_1(q,p,t) = q_1 + \sum_m \alpha_m(t)e^{imp} - q = 0 \quad , \tag{4.10}$$

and similarly region 2 is confined by the contour

$$C_2(q,p,t) = q_2 + \sum_m \beta_m(t)e^{imp'} - q' = 0, \tag{4.11}$$

whilst region 3 occupies the space outside these two contours. We have chosen to work with the Hamiltonian variables $(q,p) = (\frac{1}{2}r^2,\theta)$ and the significance of q_1, q_2, q', p' and p is made clear in Figure 4.1. Subscripts 1, 2 or 3 will then refer a quantity to regions 1, 2 or 3. With the origin of the coordinate system placed in the centre C of vortex 1 the stream function in the region becomes

$$\begin{aligned}
\psi_1 &= \bar{\psi} - \tfrac{1}{2}\ \zeta_1(q-q_1) - \tfrac{1}{2}\,\zeta_2 q_2 \log\frac{q'}{q_2}\ , \\
\psi_2 &= \bar{\psi} - \tfrac{1}{2}\ \zeta_2(q'-q_2) - \tfrac{1}{2}\,\zeta_1 q_1 \log\frac{q}{q_1}\ , \\
\psi_3 &= \bar{\psi} - \tfrac{1}{2}\ \zeta_1\, q_1 \log\frac{q}{q_1} - \tfrac{1}{2}\,\zeta_2\, q_2 \log\frac{q'}{q_2}\ ,
\end{aligned} \tag{4.12}$$

where the quantity q indicated in Figure 4.1 is given by

$$q' = q + Q - 2\sqrt{qQ}\cos p. \tag{4.13}$$

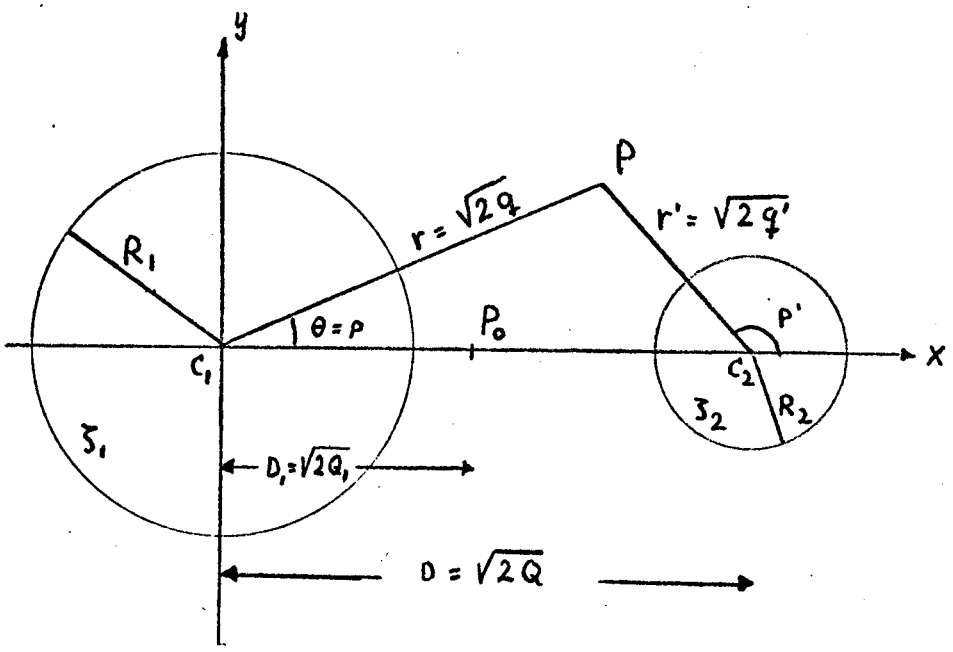

Figure 4.1. Two circular vortices of different size and different vorticity.

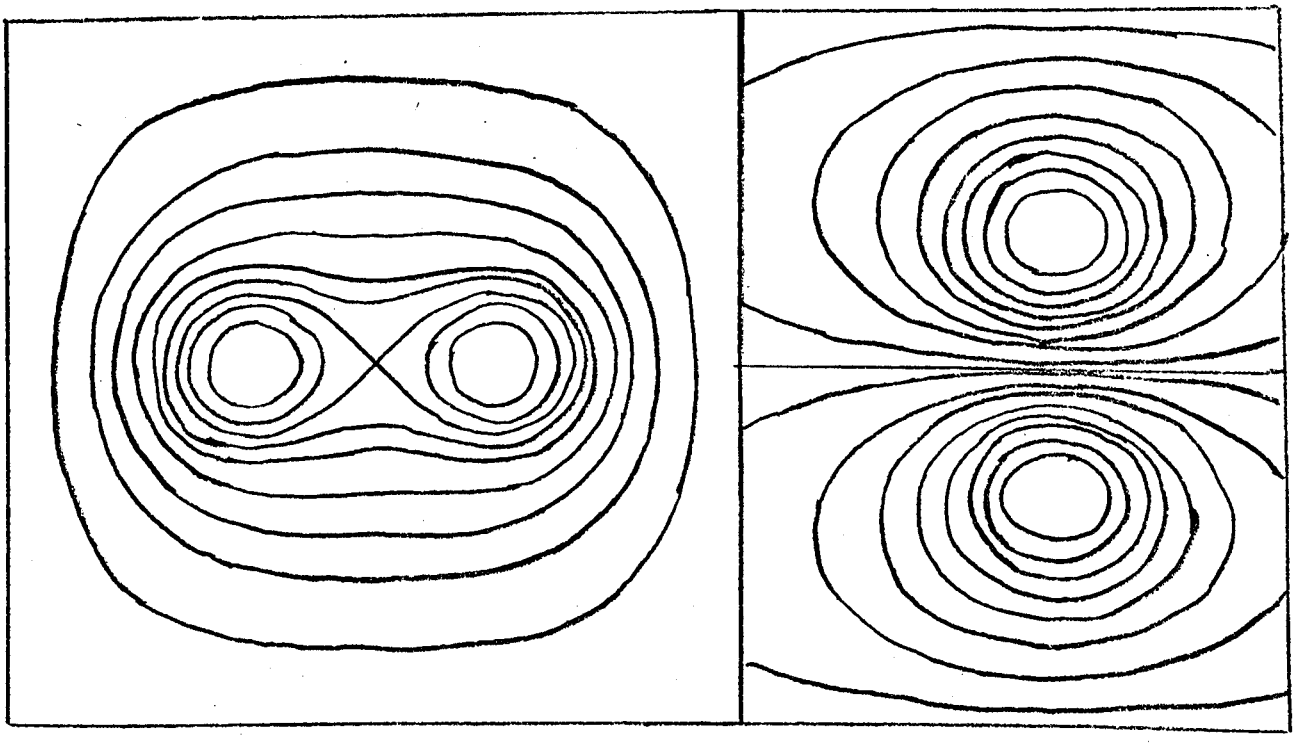

a: $\zeta_1 = \zeta_2$. $R_1 = R_2$ b: $\zeta_1 = -\zeta_2$. $R_1 = R_2$

Figure 4.2. The initial streamline configuration from two finite-sized vortices.

The initial streamline-configuration is shown in Figure 4.2a for the case $q_1 = q_2$ and $\zeta_1 = \zeta_2$ and in Figure 4.2b for the case $q_1 = q_2$ and $\zeta_1 = -\zeta_2$. (Since t = 0 we have $\alpha_m = \beta_m = 0$). Both configurations are well known from electrostatics, but Figures 4.2a and 4.2b obtained from numerical calculations have taken account of a finite value for q_1 and q_2. Also the stream function ψ is assumed to be a constant (zero) along a square in Figure 4.2a, whilst in Figure 4.2b ψ is assumed constant along the top and bottom boundaries and periodic in the horizontal direction.

Let us work out the energy of the system sketched in Figure 4.1. The circulations associated with each vortex become

$$\Gamma_1 = 2\pi\zeta_1 q_1 \quad \text{and} \quad \Gamma_2 = 2\pi\zeta_2 q_2$$

and we introduce two parameters η_1 and η_2, which measure the strength of interaction, by

$$\eta_1 = \frac{q_1}{Q} < 1 \quad \text{and} \quad \eta_2 = \frac{q_2}{Q} < 1 .$$

The total energy of the flow caused by two vortices is

$$E = E_1 + E_2 + E_{12} + E_{21} + \bar{E}$$

where $E_1 = \frac{1}{16\pi}\rho\,\Gamma_1^2$, $E_2 = \frac{1}{16\pi}\rho\,\Gamma_2^2$ and the barred quantity is $\bar{E} = \frac{1}{2}\rho\,(\Gamma_1 + \Gamma_2)\,\bar{\psi}$. The term E_{12} represents the "binding" energy between the vortices and is given by

$$E_{12} + E_{21} = +\frac{1}{8\pi}\rho\,\Gamma_1\,\Gamma_2 \log(\eta_1\,\eta_2) \quad . \qquad (4.14)$$

When $\Gamma_1\,\Gamma_2 > 0$ we have $E_{12} < 0$ and vice versa. If $\Gamma_1 = -\Gamma_2$ as in Figure 4.2b, $\bar{E} = 0$, and then the binding energy, $E_{12} > 0$, decreases when the vortices approach each other (dipole - analogy). If we assume $\zeta_1 = \zeta_2 = \zeta_0$ and also $\Gamma_1 + \Gamma_2 = \Gamma_0$, where the subscripts refer to a single circular vortex, then we can compare the energy $E^{(2)}$ of two vortices with that $(E^{(1)})$ of a single vortex having the same circulation,

e.g. $\Gamma_o = 2\pi\zeta_o q_o$ where $q_o = q_1 + q_2$. The constant $\bar{\psi}$ is compared with ψ_o of equation 4.3 and the difference becomes

$$\Delta E = E^{(1)} - E^{(2)} = \frac{1}{8\pi}\rho\,\Gamma_o^2\left[\frac{q_1 q_2}{q_o^2}(1 + \log(\eta_1\eta_2)) + \right.$$
$$\left. + \frac{q_1}{q_o}\log\frac{q_1}{q_o} + \frac{q_2}{q_o}\log\frac{q_2}{q_o}\right].$$

The difference is always positive for any set (q_1, q_2) subject to the condition $q_1 + q_2 = q_o$. The minimum value ΔE_{min} occurs when two identical vortices ($q_1 = q_2 = \frac{1}{2} q_o$) touch each other ($Q = 2 q_o$) in which case we have $\Delta E_{min} = \frac{1}{2} E_o$, where E_o is given by equation 4.4. From this we deduce that two vortices whether of circular shape or not cannot fuse together to form a single <u>circular</u> vortex since the energy would increase during this process. Naturally the opposite cannot occur. A similar argument will hold for the change in angular momentum.

In a situation with a large number N of finite-sized vortices the total energy is given by

$$E = \frac{1}{8\pi}\rho\left[\frac{1}{2}\sum_{j=1}^{N}\Gamma_j^2 + \sum_{i=1}^{N}\sum_{j=1}^{N}\Gamma_i\,\Gamma_j\log\,\eta_{ij} + 4\pi\,\bar{\psi}\sum_{j=1}^{N}\Gamma_j\right], \quad (4.15)$$

where $\eta_{ij} = \frac{q_i}{Q_{ij}}$, and $\bar{\psi}$ is the constant that makes ψ satisfy the condition $\int_C \psi\,\frac{\partial\psi}{\partial n}\,ds = 0$ along the boundary C of the system. If oppositely-signed vortices approach, equation 4.14 shows that the energy given by equation 4.15 will decrease and this can only be accounted for by letting like-signed vortices approach. On statistical grounds one may reason like Onsager (1949) that in most situations with many vortices a concentration of like-signed vortices will take place and the energy consumed in this way is released from regions where mixing of oppositely-signed vortices takes place. Our knowledge about the details of the

concentration and mixing can therefore be increased by studying simple types of interactions as shown in the following.

4.4 The weak interaction between two vortices

Our aim in this section is to study the situation in Figure 4.1 assuming that $\eta_1 << 1$ and $\eta_2 << 1$. This allows for an analytic treatment in the small amplitude regime. The problem has been studied using a similar assumption by Bassett (1888), but his treatment based on (r,θ) rather than $(\frac{1}{2} r^2,\theta)$ in the expressions for G_1 and G_2 introduces a $m = 0$ contribution to the area of the incompressible vortex regions, such that these expand.

The position of the point at rest P_o is found from equation 1.25. The distance $D_1 = |C_2 P_o|$ (Figure 4.1) is given by

$$D_1 = \frac{\Gamma_2}{\Gamma_1 + \Gamma_2} D$$

and lies to the left of C_1, between C_1 and C_2 or to the right of C_2 depending on the signs and values of Γ_1 and Γ_2. Figure 4.3 shows 4 different situations with two interacting vortices. If $\Gamma_1 = -\Gamma_2$ we have the case of a vortex pair travelling in the upwards ($\Gamma_1 > 0$) or downwards ($\Gamma_1 < 0$) direction. Otherwise the centres C_1 and C_2 of vortices 1 and 2 will rotate around the point p_o with an angular frequency given by

$$\Omega = \frac{\Gamma_1 + \Gamma_2}{2 \pi Q} = \frac{1}{2} \zeta_1 \eta_1 + \frac{1}{2} \zeta_2 \eta_2 \quad . \tag{4.16}$$

The quantity $Q_1 = \frac{1}{2} D_1^2$ can be written as

$$Q_1 = \left(\frac{1}{2} \frac{\zeta_2}{\Omega} \right)^2 q_2 \quad .$$

The distortion of the vortices due to their mutual interaction is described by the functions G_1 and G_2. If G_1 is known in a local

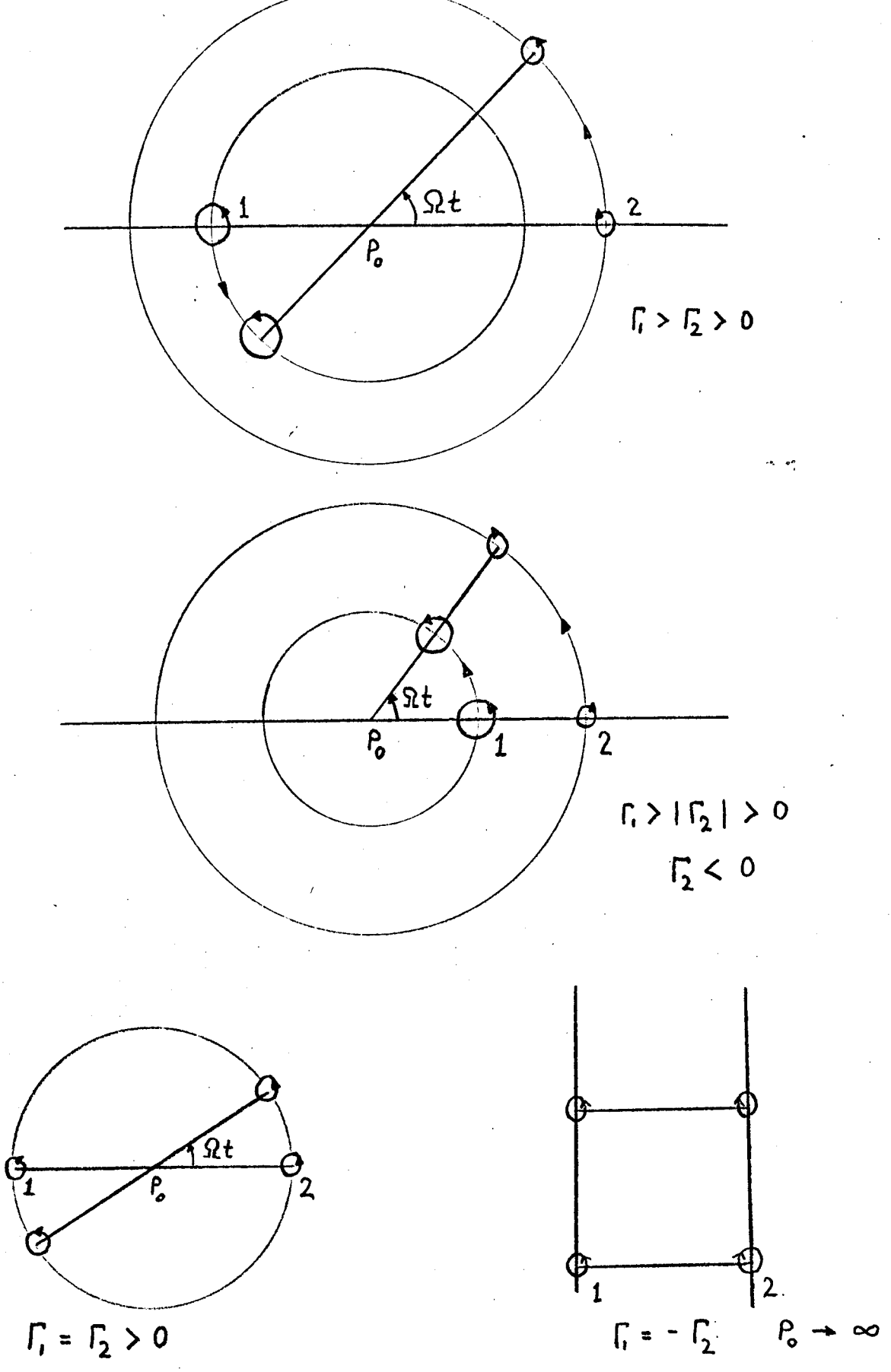

Figure 4.3. 4 different situations with two interacting vortices.

coordinate system whose origin is the moving centre C_1 of vortex 1, C_2 can be obtained in a local coordinate system whose origin is C_2 merely by interchanging indices 1 and 2 of the quantities referring to vortices 1 and 2. Let therefore equation 4.10 refer to the local coordinate system as indicated in Figure 4.4. In the following $(q,p) = (\frac{1}{2} r^2, 0)$ refer to the coordinate system with C_1 as origin thereby changing the terms $\frac{\partial \psi}{\partial p}$ and $\frac{\partial \psi}{\partial q}$ of equation 4.3. The velocity of point $P_1(q,p)$ defined by equation 4.10 relative to the moving centre is obtained by subtracting the velocity of C_1, $|\underline{u}_{c_1}| = \frac{1}{\sqrt{2}} \zeta_2 q_2 \frac{1}{\sqrt{Q}}$, from the actual velocity obtained from the stream function ψ as shown below. The values of the derivatives of the stream function along the contour of vortex 1 are modified by including the terms

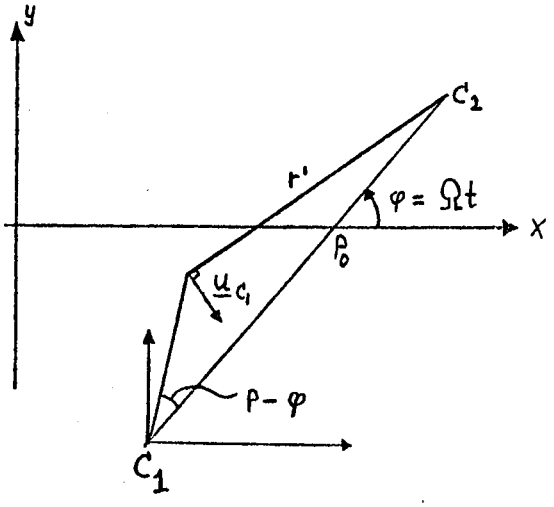

Figure 4.4. Local coordinate system with C_1 as origin.

$$\frac{\partial \psi}{\partial p} : \frac{1}{\sqrt{2}} |\underline{u}_{c_1}| \, q_1^{\frac{1}{2}} \, \frac{1}{i} \, (e^{i(p-\phi)})$$

$$\frac{\partial \psi}{\partial q} : \frac{1}{\sqrt{2}} |\underline{u}_{c_1}| \, q_1^{-\frac{1}{2}} \, (e^{i(p-\phi)} + e^{-i(p-\phi)})$$

where $\phi = \Omega t$ as shown in Figure 4.3. The stream-function from vortex 2 ψ^*, can be expanded for $q' < Q$ as

$$\psi^* = -\frac{1}{2} \zeta_2 \log \frac{q}{q_2} = \frac{1}{2} \zeta_2 q_2 \log \eta_2 +$$

$$+ \sum_m \frac{1}{|m|} \eta_1^{|m/2|} \left(\frac{q}{q_1}\right)^{|m/2|} e^{im(p-\phi)} \quad . \qquad (4.17)$$

Consistent with the distortions of both vertices the stream function ψ for regions 1, 2 and 3 given by equation (4.12) is changed by an amount $\delta\psi$ where $\nabla^2 \delta\psi = 0$. The solutions in regions 1, 2 and 3 that are continuous at $G_1 = 0$ and $G_2 = 0$ are chosen to keep the radial motion $(\frac{\partial}{\partial p} \delta\psi)$ continuous at $G_1 = 0$ and $G_2 = 0$

$$\begin{aligned}
\delta\psi_1 &= \sum_m \left[A_m \left(\frac{q}{q_1}\right)^{|m/2|} e^{imp} + B_m \left(\frac{q_2}{q'}\right)^{|m/2|} \right] \\
\delta\psi_2 &= \sum_m \left[B_m \left(\frac{q'}{q_2}\right)^{|m/2|} + A_m \left(\frac{q_1}{q}\right)^{|m/2|} e^{imp} \right] \qquad (4.18) \\
\delta\psi_3 &= \sum_m \left[A_m \left(\frac{q_1}{q}\right)^{|m/2|} e^{imp} + B_m \left(\frac{q_2}{q'}\right)^{|m/2|} \right]
\end{aligned}$$

where A_m, B_m are functions of time. The coordinate q' in the local coordinate system is shown in Figure 4.4. The $m = 0$ term is excluded from equations (4.17) and (4.18) and also from the expressions (4.10) and (4.11) as explained earlier.

In the following we encounter the quantity $\left(\frac{q}{q_1}\right)^{m/2}$ evaluated at $G_1 = 0$. Inserting from equation (4.10) we find

$$\left(\frac{q}{q_1}\right)^{|m/2|} = 1 + \left|\frac{m}{2}\right| \sum_m \frac{\alpha_m}{q_1} e^{imp} + \text{higher order terms.} \qquad (4.19)$$

As we are looking for linear relations with α_m, β_m, A_m and B_m only the first two terms of (4.19) are considered. Also the term $\left(\frac{q_2}{q'}\right)^{|m/2|}$ arising from the distortion of vortex 2 must be approximated in the small amplitude regime. Here we shall assume $B_m = 0$ for all m, corresponding to studying the interaction between the circular vortex 1 and a point vortex producing the same stream function as vortex 2 but without undergoing the resulting distortion. (This assumption was also made by Bassett (1888) to make the calculation possible). To get a rela-

tion between α_m and A_m we require that there is no slip along $G_1 = 0$, that is

$$\frac{\partial \psi_1}{\partial q} + \frac{\partial}{\partial q}\,\delta\psi_1 \quad = \quad \frac{\partial \psi_3}{\partial q} + \frac{\partial}{\partial q}\,\delta\psi_3 \quad .$$

Inserting and using equation (4.19) we get in the linear regime

$$A_m = \frac{1}{2|m|}\,\zeta_1\,\alpha_m \quad . \tag{4.20}$$

To find an equation for α_m we insert for G_1 and $\psi_1 + \delta\psi_1$ in equation (4.8). We exclude non-linear terms, i.e. terms of order α_m^2 and higher but we include the coupling between the modes on vortex 1 and those of the expansion (4.17). The coupling terms have coefficients $\eta_1^{j/2}$, but only terms of order $\eta_1^{m/2}$ or less are included for a mode m. By collecting all terms with the common factor e^{imp} we find the resulting equation for α_m :

$m > 1$

$$\frac{d\alpha_m}{dt} + i\omega_m\alpha_m = i\,\frac{1}{4}\,\zeta_2\,\frac{\eta_2}{\eta_1}\Big[2\,\eta_1^{m/2}\,e^{-im\phi}q_1 + m\sum_{j=1}^{m-2}\eta_1^{\frac{m-j}{2}}\,\alpha_j e^{-i(m-j)\phi} - (m-2)\,\eta_1^{\frac{1}{2}}\,e^{-i\phi}\,\alpha_{m-1}\Big]$$

$m < -1$ (4.21)

$$\frac{d\alpha_m}{dt} + i\omega_m\alpha_m = -i\,\frac{1}{4}\,\zeta_2\,\frac{\eta_2}{\eta_1}\Big[2\,\eta_1^{m/2}\,e^{-im\phi}q_1 - m\sum_{j=-1}^{m+2}\eta_1^{\frac{j-m}{2}}\,\alpha_j e^{-i(m-j)\phi} + (m+2)\,\eta_1^{\frac{1}{2}}\,e^{i\phi}\,\alpha_{m+1}\Big] .$$

For $m = \pm 1$ we simply get

$$\frac{d\alpha_{\pm 1}}{dt} \approx 0\ (\eta_1,\ \eta_1^{3/2}\ \ \eta_1^{2}\ \ldots.)$$

which by our earlier assumptions is equivalent to $\alpha_{\pm 1} = 0$. The frequency ω_m is given by equation (4.7) for $m > 1$. When $m < -1$ we have

$\omega_m = \frac{1}{2}\zeta_1(m+1)$.

The solutions $\alpha_m(t)$ of equation (4.21) can be shown to be oscillatory, that is with respect to the local coordinate system. In a rest frame α_m would grow as well as oscillate with time, simply because the vortex centre is moving. In the special case $\Gamma_1 = -\Gamma_2$ (vortex pair) equation (4.21) still holds provided we set $\phi = \Omega t = 0$. For small amplitudes, i.e. $\eta_1 \ll 1$, we can therefore describe the interaction from vortex 2 in terms of the oscillatory solutions of equation (4.21) and as mentioned earlier we can by interchanging indices 1 and 2 obtain the similar equations for β_m with respect to to a local coordinate system whose origin is C_2'. The solutions α_m or β_m can be obtained recursively starting with $m = \pm 1, \pm 2$ etc. by virtue of our assumption about the coupling. Indeed it can be seen from (4.21) that without the coupling we get $\alpha_m \sim \eta_1^{|m/2|}$ so that the assumption is <u>consistent</u>.

The $|m| = 1$ mode remains zero to lowest order in η_1. For strong interactions we can get a significant coupling between modes of higher m thereby producing an $m = 1$ contribution in the local coordinate system and this will be dealt with later. The $|m| = 2$ mode is found from equation (4.21) :

$$\alpha_2 = \alpha_2 e^{i2p} + \alpha_{-2} e^{-i2p} = \zeta_2 \eta_2 \frac{q_1}{\omega_2 - 2\Omega} (\cos 2(p-\Omega t) - \cos(2p-\omega_2 t)) \quad (4.22)$$

i.e. a combination of the natural mode of frequency $\omega_2 = \frac{1}{2}\zeta_1$ and a "tidal" type mode arising from the precessing motion of the two vortices. There is a type of resonance effect present when $\omega_2 = 2\Omega$, or approximately $\zeta_1 = 2\eta_2\zeta_2$, since then a_2 becomes zero. (Similarly $b_2 \to 0$ when $\zeta_2 = 2\eta_1\zeta_1$). For this resonance case the $|m| = 3$ mode becomes ($\eta_1, \eta_2 \ll 1$)

$$a_3 = \alpha_3 e^{i3p} + \alpha_{-3} e^{-i3p} \approx \frac{1}{2} \eta_1^{\frac{1}{2}} q_1 (\cos 3(p-\Omega t) - \cos(3p-\omega_3 t)), \quad (4.23)$$

since no coupling with $|m| = 1$ or $|m| = 2$ takes place; the amplitude α_3 is virtually independent of the size of vortex 2.

It appears reasonable to neglect the deformation of vortex arising from weak interactions with other vortices and this has been done by several authors. The modes of higher m have amplitudes of the order $\eta_1^{m/2}$ and in the local coordinate system only the $m = 2$ and perhaps the $m = 3$ contributions can become important as they result in a slight elliptic or triangular shape respectively. The interest must lie in assessing the strength of interaction for which the above results are no longer valid. This can conveniently be done by studying numerical solutions, and in the second part of this chapter we discuss the interaction between vortices for larger values of η_1 and η_2.

4.5 The energy balance

In section 4.3 we expressed the total energy as a sum of four terms E_1, E_2, E_{12}, and $\bar{E}$. At any instant during the precessing motion of two vortices (Figure 4.3) the quantities E_1, E_2, E_{12} and E_{21} are changed by amounts δE_1, δE_2, δE_{12} and δE_{21} respectively because of the presence of the surface waves. The barred quantity $\bar{E}$ is constant. Suppose now that at time t we know all modes α_m and β_m on vortex 1 and 2 respectively. Let

$$\alpha_m = c_m + i\, d_m \quad \text{and} \quad \beta_m = f_m + i g_m$$

such that $\alpha_m = \alpha^*_{-m}$ and $\beta_m = \beta^*_{-m}$, because $\alpha_m e^{imp} + \alpha_{-m} e^{-imp}$ is a real quantity and similarly for β_m. From equation (4.9) we find the changes

$$\delta E_1 = -\frac{\pi}{4}\rho\,\zeta_1^2 \sum_1^\infty (c_m^2 + d_m^2)(1 - 2/m)$$

$$\delta E_2 = -\frac{\pi}{4}\rho\,\zeta_2^2 \sum_1^\infty (f_m^2 + g_m^2)(1 - 2/m)$$

To work out δE_{12} and δE_{21} for vortex 1 and 2 respectively we shall assume that δE_{12} is due only to the distortion of vortex 1 coupled with ψ^* (equation 4.17), i.e. δE_{12} does <u>not</u> include the change arising from the coupling between the distortion of vortex 1 and that of vortex 2. A similar assumption is made for δE_{21}, since in both cases the coupling between the distortions will involve higher order terms in η_1 and η_2. (This assumption is consistent with the expansions (4.17), (4.18) and (4.19)). By inserting for ψ^* and using G_1 and G_2 in the energy integral (equation 1.18) we find

$$\delta E_{12} = \frac{\pi}{4}\rho\,\zeta_1\zeta_2 \sum_1^\infty \frac{2}{m}\, q_2\, \eta_1^{m/2}\, c_m \quad ,$$

$$\delta E_{21} = \frac{\pi}{4}\rho\,\zeta_1\zeta_2 \sum_1^\infty \frac{2}{m}\, q_1\, \eta_2^{m/2}\, f_m \quad .$$

The conservation of energy requires

$$\Delta E = \delta E_1 + \delta E_2 + \delta E_{12} + \delta E_{21} = 0 \quad .$$

An estimate of α_m and β_m from equation (4.21) shows that the above condition cannot be met as $\Delta E < 0$. The surface waves therefore release energy which is made available for some other mechanism. From equation (4.14) we see that the only possible way of consuming energy is by increasing or decreasing η_1 and η_2 depending on whether $\Gamma_1\Gamma_2 > 0$ or $\Gamma_1\Gamma_2 < 0$ respectively. The amounts $\delta\eta_1$ and $\delta\eta_2$ by which η_1 and η_2 are changed correspond approximately to $m = 1$ modes for vortex 1 and vortex 2, that is $\alpha_{\pm 1}$ and $\beta_{\pm 1}$ will be of the order $\delta\eta_1$, $\delta\eta_2$ respectively. Since all the coefficients c_m, d_m, f_m and g_m oscillate

with time, $\delta\eta_1$ and $\delta\eta_2$ will oscillate with time. The instantaneous value of η oscillates between η and $\eta - \delta\eta$ ($\Gamma_1\Gamma_2 > 0$) or between η and $\eta - \delta\eta$ ($\Gamma_1\Gamma_2 < 0$). The approximate expression for α_1 with similar expressions for α_{-1}, β_1 and β_{-1} can be obtained from equation (4.21) taking into account higher order terms in η_1 :

$$\frac{d\alpha_1}{dt} = i\,\frac{1}{4}\,\zeta_2\,\frac{\eta_2}{\eta_1}\sum_j \eta_1^{\left|\frac{1-j}{2}\right|}\, e^{i(j-1)\phi}\,\alpha_j \ ,$$

that is all modes $|m| > 1$ contribute through the release of energy to the oscillatory motion of the centres C_1 and C_2 along the line C_1C_2 .

When two finite-sized vortices interact weakly they perform the classical motion as depicted in Figure 4.3, but in addition we have surface waves developing due to their finite size. These surface waves accounting for the deformations of the vortices behave as negative energy waves (section 4.2). They alter the classical motion by a finite amount $\delta\eta$ in the interaction parameter. When $\Gamma_1\Gamma_2 > 0$ we have $\phi \neq 0$ and this leads to a set of incommensurable frequencies ω_m of the surface waves. The motion of two like-signed vortices is ergodic since all surface waves will never reach zero amplitude at the same time thereby producing a circular vortex. The shape of each vortex changes continually from its initial circular shape as the vortex undergoes the processing motion around the other vortex. When $\Gamma_1\Gamma_2 < 0$ we have $\phi = 0$; all frequencies ω_m correspond to those given by equation (4.7). However, through the coupling with other modes, a given mode m will have several oscillation frequencies. The behaviour can then be much the same as described above.

4.6 A brief introduction to the numerical experiments

In the previous four sections we studied how initially circular vortices will undergo deformation because of their mutual interactions. In

the following three sections we will discuss the results from a series of numerical experiments made with the VORTEX code (Appendix) on the interaction between two vortices. A table at the end of this section presents the details of each numerical experiment.

In all experiments we place the two vortices as shown in Figure 4.1, but their motion is confined to a square box of dimensions 64 by 64. The boundaries $y = 0$ and $y = 64$ are fixed, e.g. the stream function ψ is a constant along these lines. The boundary conditions with respect to x vary and Table 4.1 shows whether periodicity or fixed x-boundaries are assumed. Point vortices are now distributed as explained in section 2.8 and for <u>all</u> experiments we choose

$$\Gamma_1 = 1501 \quad \text{and} \quad R_1 = 7.2$$

such that $\zeta_1 = \dfrac{\Gamma_1}{\pi R_1^2} = 9.2$ corresponding to a period of rotation for a non-interacting vortex of $T = \dfrac{4\pi}{\zeta_1} = 1.36$. The corresponding parameters for vortex 2 may be $\Gamma_2 = \pm\Gamma_1$ and $R_2 = R_1$ or $R_2 = 0$ (see Table 4.1). Our choice of parameters is not arbitrary, but results from attempts to minimize the effects from the boundaries and the mesh. We shall not elaborate this point further.

Section 4.7 describes two experiments (I and II) on the interaction between a Rankine vortex and a point vortex of the same strength ($\Gamma_2 = t\,\Gamma_1$, $R_2 = 0$). These experiments were made to study the deformation of vortex 1 in the time independent velocity field induced by vortex 2. The experiments represent the situation examined in sections 4.2-4.5 and we find good agreement between theory and experiment.

Next we discuss results from experiments made to study the interaction between two equal-sized vortices with $\Gamma_2 = \pm\Gamma_1$. Four experiments (II-VI) were made with relatively small values of η ($= \eta_1 = \eta_2$). We

find some agreement between theory and experiment. The vortices undergo the classic motion as would arise from two interacting point vortices. We also have large amplitude oscillations on the surface of the vortices. The amplitudes are measured and compared with the theoretical predictions.

In section 4.8 six further experiments (VII-XII) on the interaction between two identical vortices ($\Gamma_1 = \Gamma_2$, $R_1 = R_2$) are described. Two experiments (see VII and VIII) demonstrate how like-signed vortices will fuse or coalesce provided the initial value of η is above a certain critical value η_c. When η is approximately equal to η_c initially the two vortices approach, touch to form a 'figure 8'-shaped vortex, retract, approach again etc. Experiments IX-XII were carried out partly to show this behaviour, partly to determine η_c. By a simple argument we attempt to find the value η_c for two interacting vortices in an infinite medium. At the end of this chapter we sum up the results from experiments I-XII.

In the table below we give data for the experiments. The value of η is worked out as $\eta = \frac{R_1^2}{D^2}$ where D is the distance C_1C_2 (Figure 4.1).

Expt. No.	Γ_2/Γ_1	R_2/R_1	η	Elapsed time T_E	Timesteps	T_E/T_1	x-boundaries
I	+1	0	0.109	1.534	576	1.125	F
II	-1	0	0.1176	2.046	768	1.50	P
III	+1	1	0.0778	8.186	768	6.0	F
IV	+1	1	0.067	2.046	192	1.50	F
V	-1	1	0.1176	10.23	960	7.50	P
VI	0	1	0.1176	4.093	768	1.50	P
VII	1	1	0.132	4.093	384	3.0	F
VIII	1	1	0.109	4.093	384	3.0	F
IX	1	1	0.0915	2.046	192	1.5	F
X	1	1	0.0843	2.046	192	1.5	F
XI	1	1	0.0871	6.14	576	4.5	F
XII	1	1	0.0885	8.18	1536	6.0	F

TABLE 4.1. Experiments on Vortex Interaction

Two columns indicate the duration T_E of each experiment and number of timesteps. In the following column the duration is expressed in terms of the rotation period T_1 for a non-interacting vortex of density ζ_1 and radius R_1. F or P in the last column means that the x-boundaries are fixed (stream lines) or that the stream function is assumed periodic in x. The flow fields are visualised by the method described in chapter 3.

In section 4.4 we described the boundary (and thus the distortion) of vortex 1 by equation (4.10). The amplitudes μ_m of the surface waves are worked by an analyser program (chapter 3) which uses r,θ rather than $\frac{1}{2}r^2,\theta$. Hence

$$\mu_m = \sum_{j=1}^{n_1} R\,(j\Delta\theta)\; e^{-1} \quad , \tag{4.24}$$

where $R\,(j\Delta\theta)$ represents the (r,θ) coordinates of the n_1 point vortices initially placed at $r = R_1$. Because the area πR_1^2 is conserved we have no $m = 0$ mode (expansion mode), and since $R\,(j\Delta\theta)$ is with respect to the moving centre C_1 we have no $m = 1$ mode either. If we express equation (4.10) by (r,θ) we get

$$\frac{R(\theta)}{R_1} \approx 1 + \sum_m \frac{\alpha_m}{R_1^2}\, e^{im\rho} - \frac{1}{2}\Big(\sum_\ell \frac{\alpha_\ell}{R_1^2}\, e^{i\ell\rho} \sum_k \frac{\alpha_k}{R_1^2}\, e^{ik\rho}\Big) + \ldots . \tag{4.25}$$

whereas the inverse expansion of (4.24) gives

$$R(j\Delta\theta) = R_1 + \sum_m \mu_m\, e^{imj\Delta\theta} \quad . \tag{4.26}$$

Taking into account the linear term only we find

$$\mu_m = \frac{\alpha_m}{R_1} \quad , \tag{4.27}$$

and this relation will be assumed to apply in the following.

4.7 The interaction between a Rankine vortex and a point vortex

In Figure 4.5 we show two stages of the distortion of an initially circular vortex interacting with a positive or negative point vortex respectively. In experiment I we have a precessing motion around P_o with an angular velocity of 1.09 (based on the first quarter period), e.g. slightly more than the theoretical value $\Omega = \zeta_o \eta = 1.04$. The vortex is continuously being stretched and the second frame of Figure 4.5 shows a shape like a "drop with a spike", closely resembling one half of the separatrix in the streamline configuration (Figure 4.2a). As time progresses the spike will be wound round the point vortex (compare with experiment VIII).

A completely different behaviour is seen in experiment II. Since the two vortices travel in the negative x-direction the line adjoining C_1 and C_2 is always perpendicular to the x-axis (conservation of momentum). In Figure 4.6 we show the time variation of the amplitudes μ_2, μ_3 and μ_4 of the surface waves. After one period of rotation T_o' we have to a good approximation a circular vortex, e.g. $\mu_m(T_o') \approx 0$ for most m. The period T_o' is found to be 1.57, that is longer than the theoretical period $T_o = 1.363$. Because of the finite values of μ_m the coupling between these produces a small but finite $m = 1$ mode as explained in section 4.5. In Figure 4.7 we show the motion of the centre C_1 and also its resulting x-velocity. Both oscillate with a period T_o'. The mean velocity of advance u_x' is found to be -7.05 as opposed to the velocity induced by the point vortex $u_x = -\frac{\Gamma}{2\pi D} = 11.3$, where D is the distance C_1C_2.

These deviations found for experiment II are naturally caused by the presence of the fixed boundaries and to a smaller extent numerical errors. The general velocity of advance for the situation in experiment II will

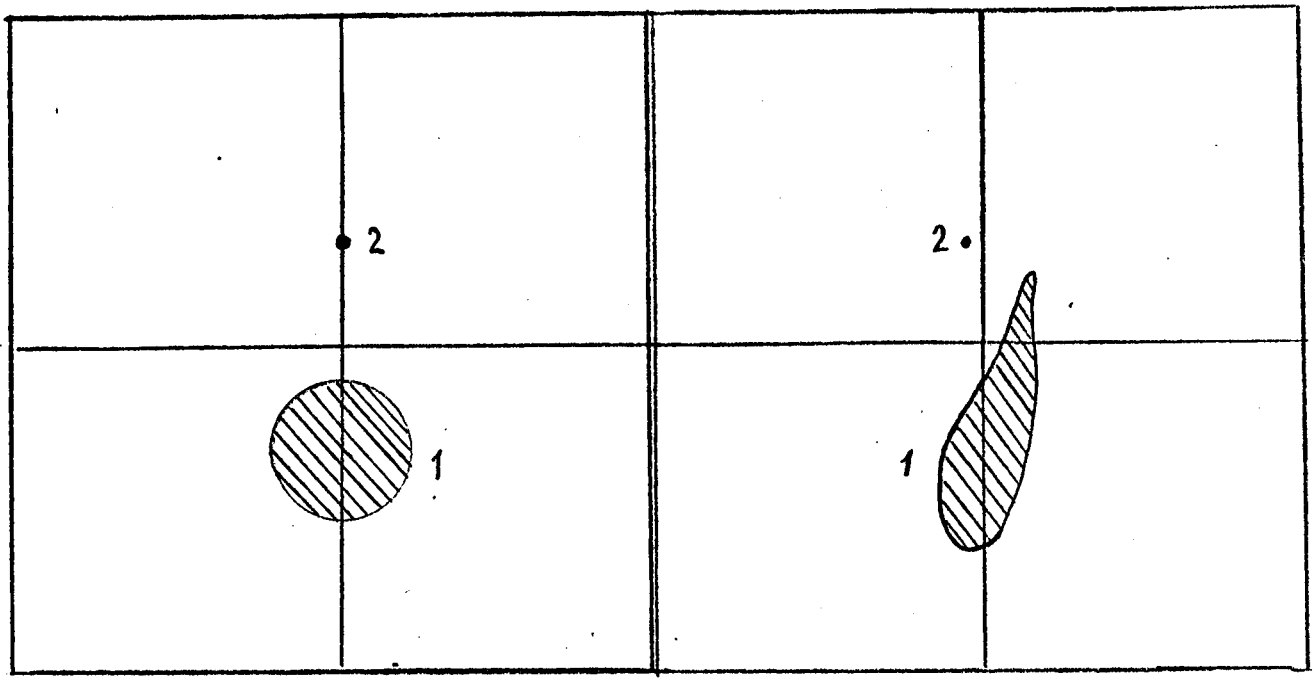

Time = 0.0 Time = 1.4

Experiment I

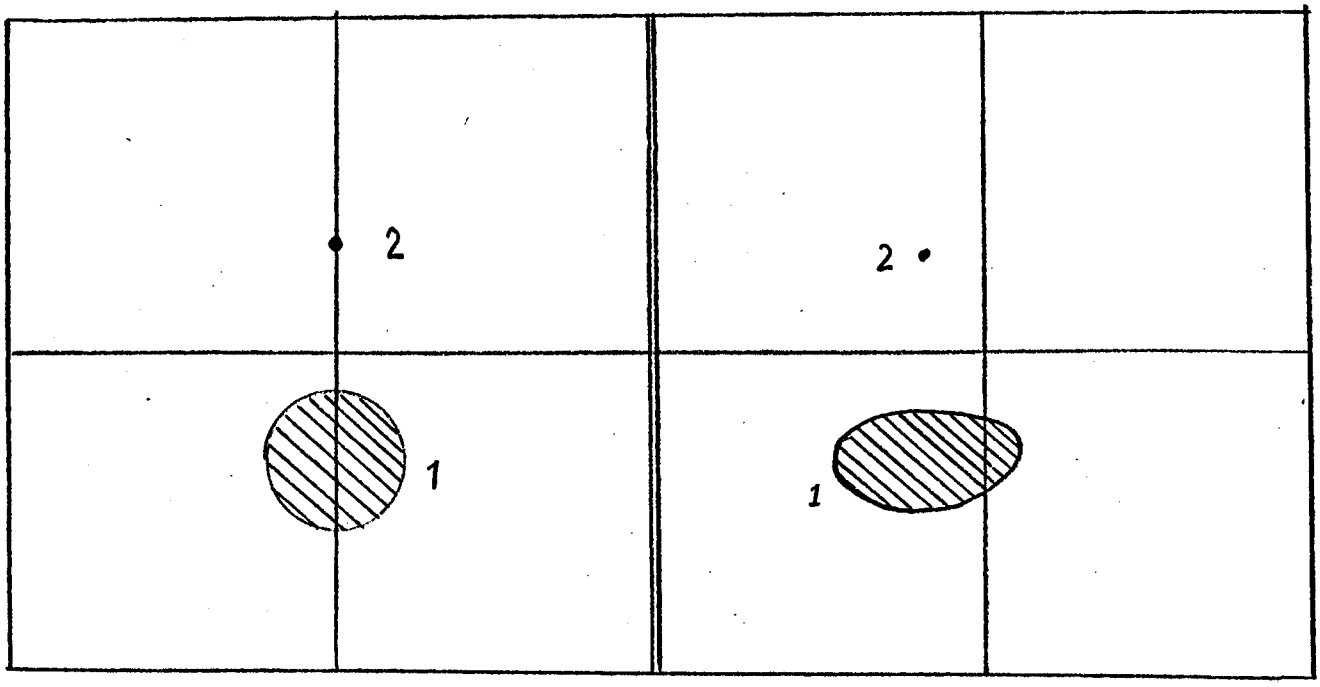

Time = 0.0 Time = 0.8

Experiment II

Figure 4.5. Two stages of the distortion of an initially circular vortex.

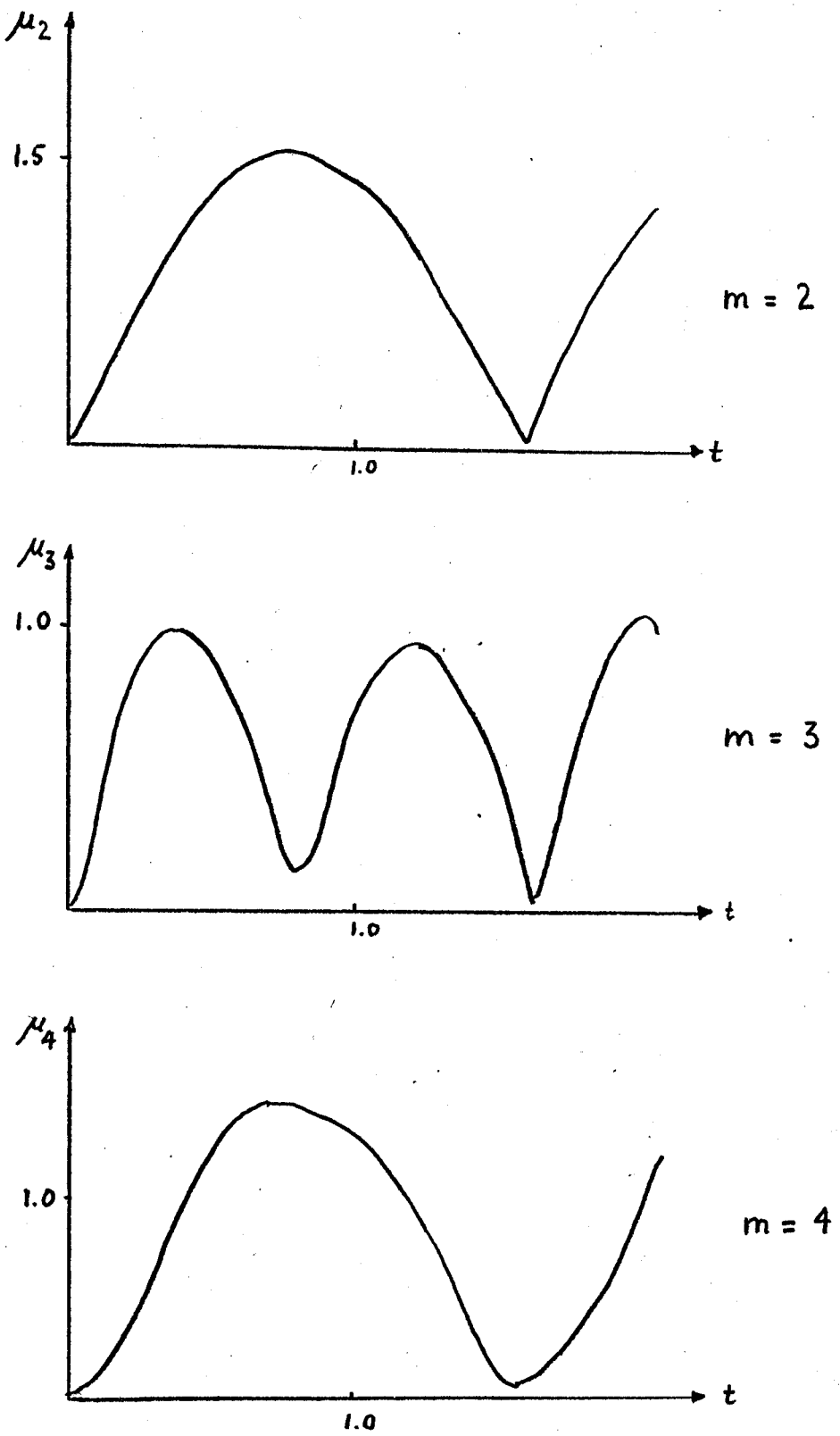

Figure 4.6. The amplitudes μ_m vs time. Experiment II.

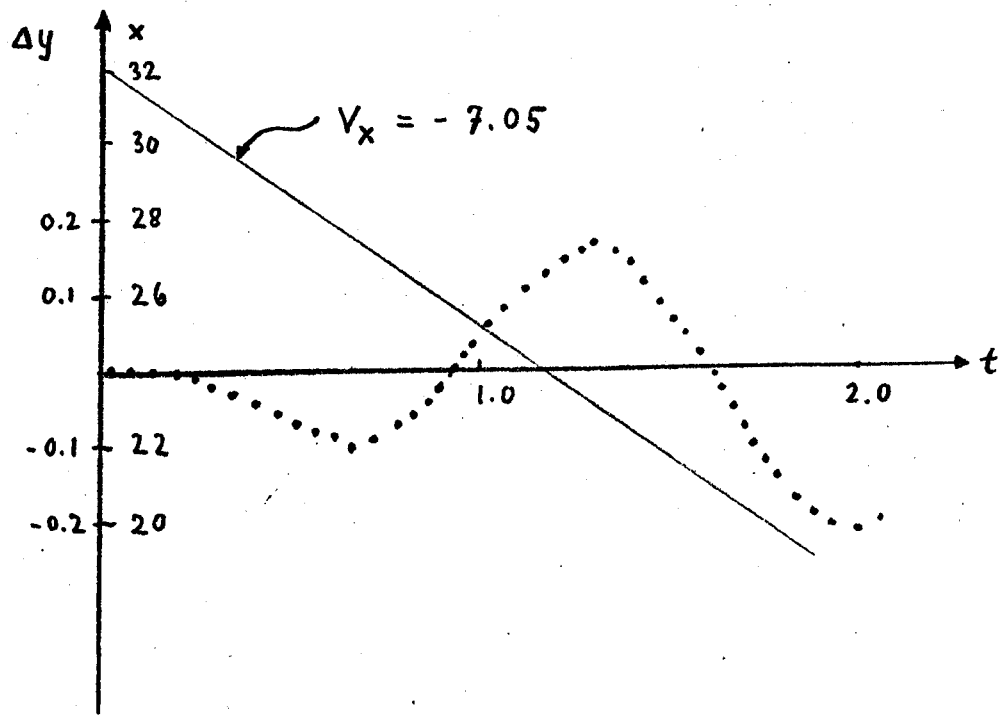

Figure 4.7. The motion of vortex centre C_1 in Experiment II. Δy is the difference $y(t=0) - y(t)$.

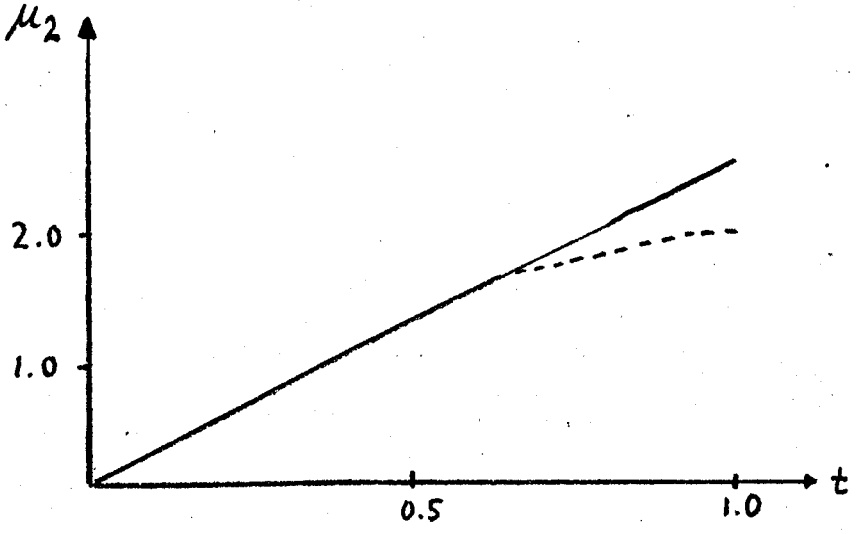

Figure 4.8. The amplitude μ_2 of the m=2 mode vs time. Experiment I.

be given as a sum of contributions from an infinite set of images (in the y-direction) of alternatively point vortices and Rankine vortices. It can be shown that

$$u_x = \frac{\Gamma}{2\pi} \sum_{j=0}^{\infty} \left[\frac{1}{j\delta+(\delta-D)} - \frac{1}{j\delta+D} \right] = 7.03 \quad .$$

For experiment I with fixed x and y boundaries it is more difficult to assess the effect from the images since these now move in a precessing motion. However a comparison can be made with the amplitude of the surface modes calculated in section 4.4. From equation (4.21) we find the amplitude of the $m = 2$ mode for experiments I and II taking $\zeta_1 = \zeta_2 = \pm\zeta_o$

$$\begin{aligned} &\text{(I)} \quad \alpha_2(t) = \frac{1}{2}\,\zeta_o\,\eta\,\frac{q_1}{\omega_2-2\Omega}\,(e^{-i2\Omega t} - e^{-i\omega_2 t}) \,, \\ &\text{(II)} \quad \alpha_2(t) = \frac{1}{2}\,\zeta_o\,\eta\,\frac{q_1}{\omega_2}\,(1 - e^{-i\omega_2 t}) \,, \end{aligned} \tag{4.28}$$

where $\alpha_2 = C_2 + id_2$ and similarly $\alpha_{-2} = C_2 - id_2$ (equation 4.22). Inserting for ζ, q, η ω_2 and Ω we get

$$\begin{aligned} &\text{(I)}: \quad |\alpha_2| = 14.16\,\left|\sin\frac{\pi t}{2.42}\right| \\ &\text{(II)}: \quad |\alpha_2| = 11.3\,\left|\sin\frac{\pi}{1.363}\right| \quad . \end{aligned} \tag{4.29}$$

From equation (4.27) we derive the amplitudes: $\mu_2 = 1.97$ (experiment I) and $\mu_2 = 1.57$ (experiment II). The agreement with the curve $\mu_2(t)$ (experiment II) in Figure 4.6 is quite good considering the effect from the boundaries. The curve $\mu_2(t)$ for experiment I is shown in Figure 4.8 with the curve given by equation (4.29) for comparison. We see that after $t = 0.5$, approximately, the mode continues to grow above the theoretical curve. This of course is due to non-linear effects as well as the coupling with other modes μ_3, μ_4 etc. Experiment I reflects a

situation in which the time evolution agrees with linear theory over a short time interval of the order half a rotation period T_o. In the subsequent non-linear stage the $m = 2$ mode continues to grow rather than oscillate as the spike on vortex 1 gets closer to the point vortex. In experiment II we have on the other hand large oscillations whose amplitudes and periods are those given by the linear theory. The two vortices can never move closer together than they were initially (conservation of energy) and the maximum amount by which they separate (Δy in Figure 4.7) is a function only of the initial η. The y-motion of vortex 1 is necessarily in phase with the modes $m = 2,3, \ldots$, otherwise energy would change. The interaction between a positive and a negative vortex is indeed a peculiar dynamical situation since the linear approximation apparently holds for even large values of η provided the vortices do not overlap.

4.8 Numerical experiments on weaker interactions

Of the four experiments carried out, V and VI are essentially repeats of experiment II. In experiment V the negative point vortex is replaced by a negative Rankine vortex and in experiment VI we have only one vortex placed close to the upper y-boundary, thereby interacting with its image.

The motion of the vortices in experiment III is shown in Figure 4.9. (Experiment IV, being very similar to III, is not illustrated). The two vortices rotate around the individual centres C_1 and C_2 whilst these perform one rotation around the point at rest P_o during a period T' which is found to be 8.05. Compared with the period of precession $T = \frac{2\pi}{\Omega} = \frac{T_o}{2\eta} = 8.85$ for two vortices in an infinite medium we have here a more significant reduction than in experiment I. This must result from a larger influence of the boundaries since vortex 2 is now of finite size.

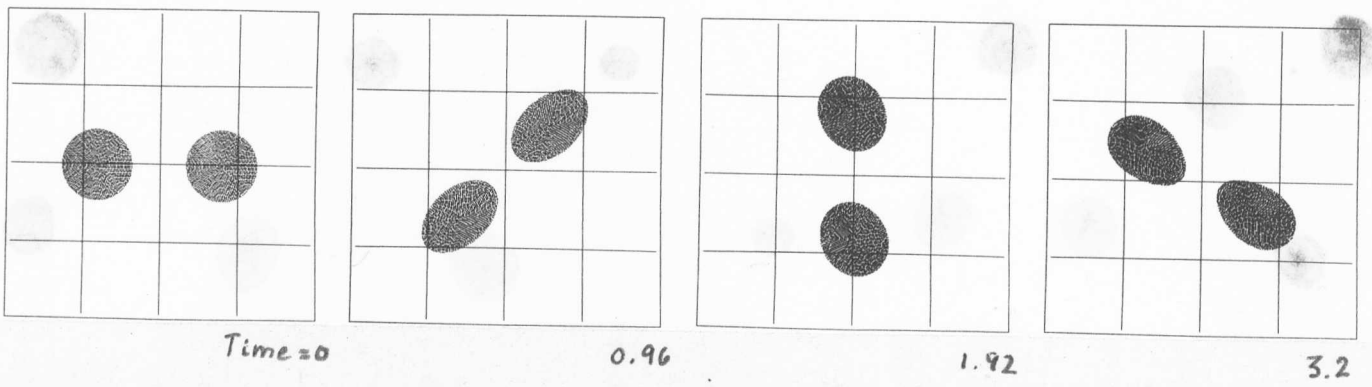

Figure 4.9. Two vortices precessing around each other. Large amplitude oscillations on their surfaces. Experiment III.

The experiments of section 4.9 on larger η values will exhibit even larger reductions in T.

We compare the measured surface modes with the theory of section 4.4. Inserting for η in equation (4.28) we find

$$\text{(III)} \qquad |a_2| = 8.25 \left| \sin \frac{\pi t}{1.98} \right| ,$$

giving $\mu_2 = 1.25$ and the quarter period of oscillation is 1.15 rather than 0.99. All modes with $m > 2$ exhibit oscillatory behaviour, e.g. a superposition of several oscillations whose frequencies are combinations of Ω, ω_m, ω_{m-1} etc., because of the coupling with modes of lower m. The reduction in the period T of the precessing motion and the increase in the period T_2 of the $m = 2$ mode can be interpreted as a net increase in η during the time T_E, since we have $T = \frac{T_o}{2\eta}$ and $T_2 = \frac{1}{2} \frac{T_o}{1-4\eta}$. As discussed in section 4.5 this net increase in η corresponds to a small but finite $m = 1$ mode. From Figure 4.10 showing $a_1(t)$ we see that a_1 consists of approximately two oscillations with amplitudes ~ 0.5 and 0.75, that is of the order $\eta^{3/2} a_1$; these presumably arise as a result of coupling with the larger $m = 2$ and $m = 3$ modes.

Experiments V and VI both have the same values for η as experiment II. The $m = 2$ mode in experiments V and VI is virtually the same as that

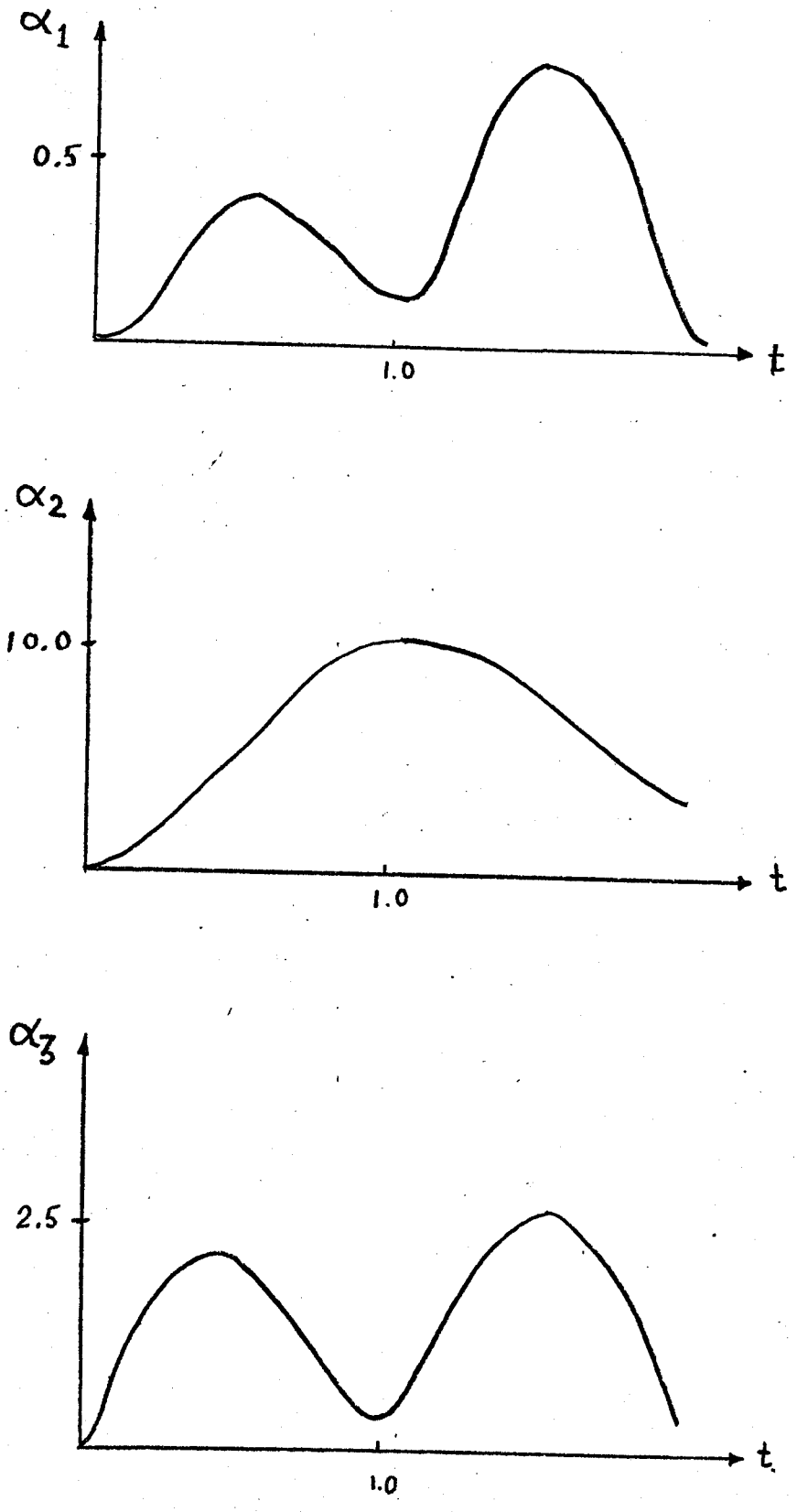

Figure 4.10. Amplitudes α_m vs time. Experiment III.

in II. (See Figure 4.6). For modes with $m > 2$ up to $m = 8$ we find an oscillatory behaviour just like that of experiment II, but with amplitudes that are enhanced increasingly as m increases. We find however a return to the circular shape of both vortices after each has completed one period of rotation. The check on this approximate recurrence for experiments II, V and VI is made by phase plane diagrams (μ_{real} versus $\mu_{imaginary}$). In Figure 4.11 we show such diagrams for $m = 2$, 3 and 4. The amplitudes are for convenience normalized to 1. The curves nearly close up after one period of rotation. (Accumulation of numerical errors is likely to leave the curves with a gap that increases as m increases). The configuration in Figure 4.12 shows the vortices travelling to the left with a velocity that oscillates around the same mean value as in experiment II ($u_x = -7.03$). The situation is much the same as that of experiment II; each vortex has a y-motion that oscillates in phase with the $m = 2$ mode.

4.9 Numerical experiments on strong interactions

Experiments VII and VIII carried out with large values of η both show fusion or coalescence of the two vortices before these have completed a quarter of the period of precession. Experiment VIII is given the same value of η as experiment I, and Figure 4.8 demonstrates the difference in the surface modes. Comparing I and VIII we find that the amplitudes are enhanced increasingly as m increases when the point vortex is replaced by a Rankine vortex, e.g. a difference similar to that between experiments II and V. The difference arises because both vortices become distorted such that the stream function ψ^* (equation 4.17) is no longer time-independent. The modes of its expanded form will now initially oscillate with time thereby introducing solutions different from those of section 4.4.

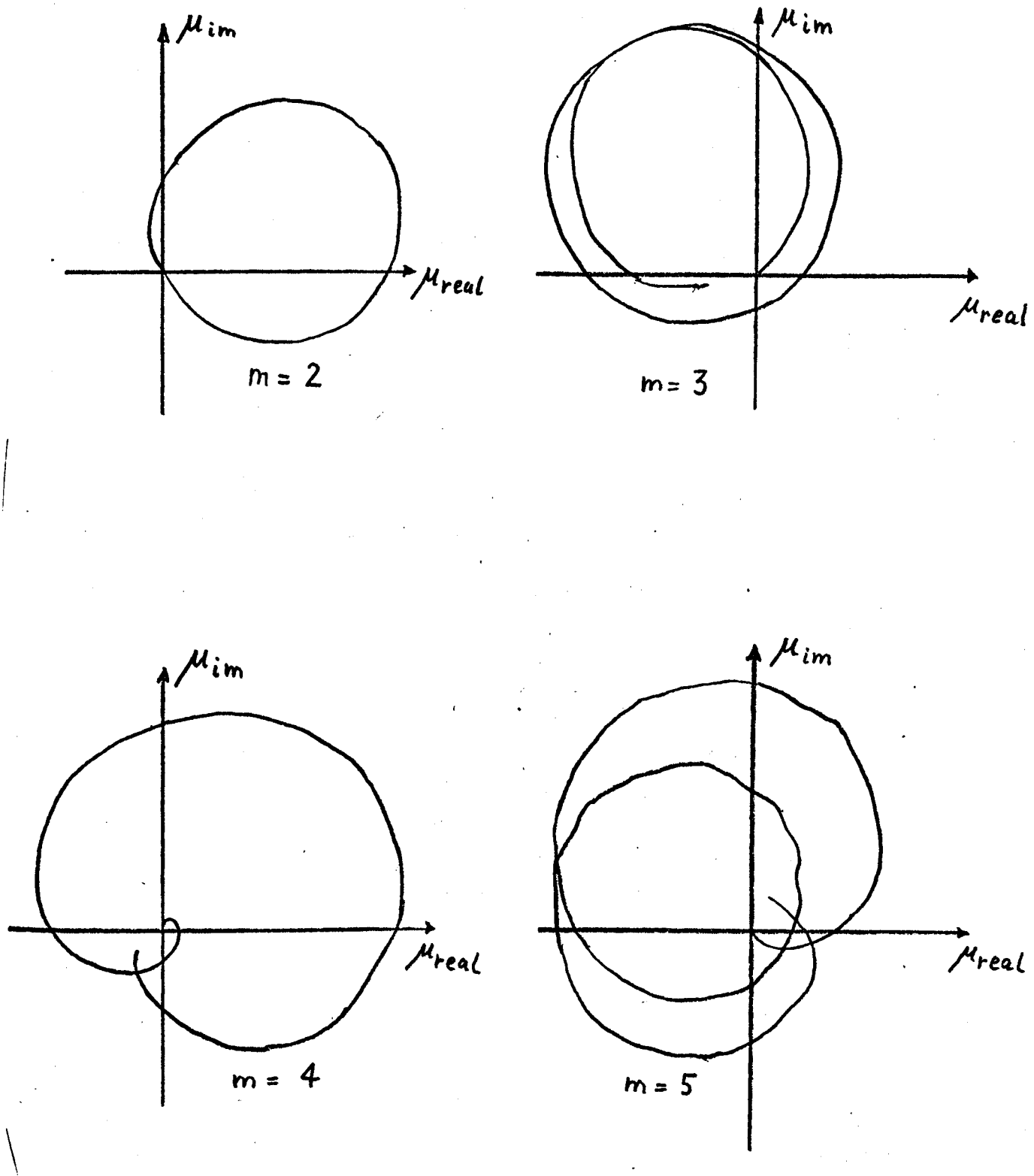

Figure 4.11. Phase plane diagrams for Experiment V. (The imaginary part μ_{im} is plotted versus the real part μ_{real} for a time period t = 0 - 1.57.)

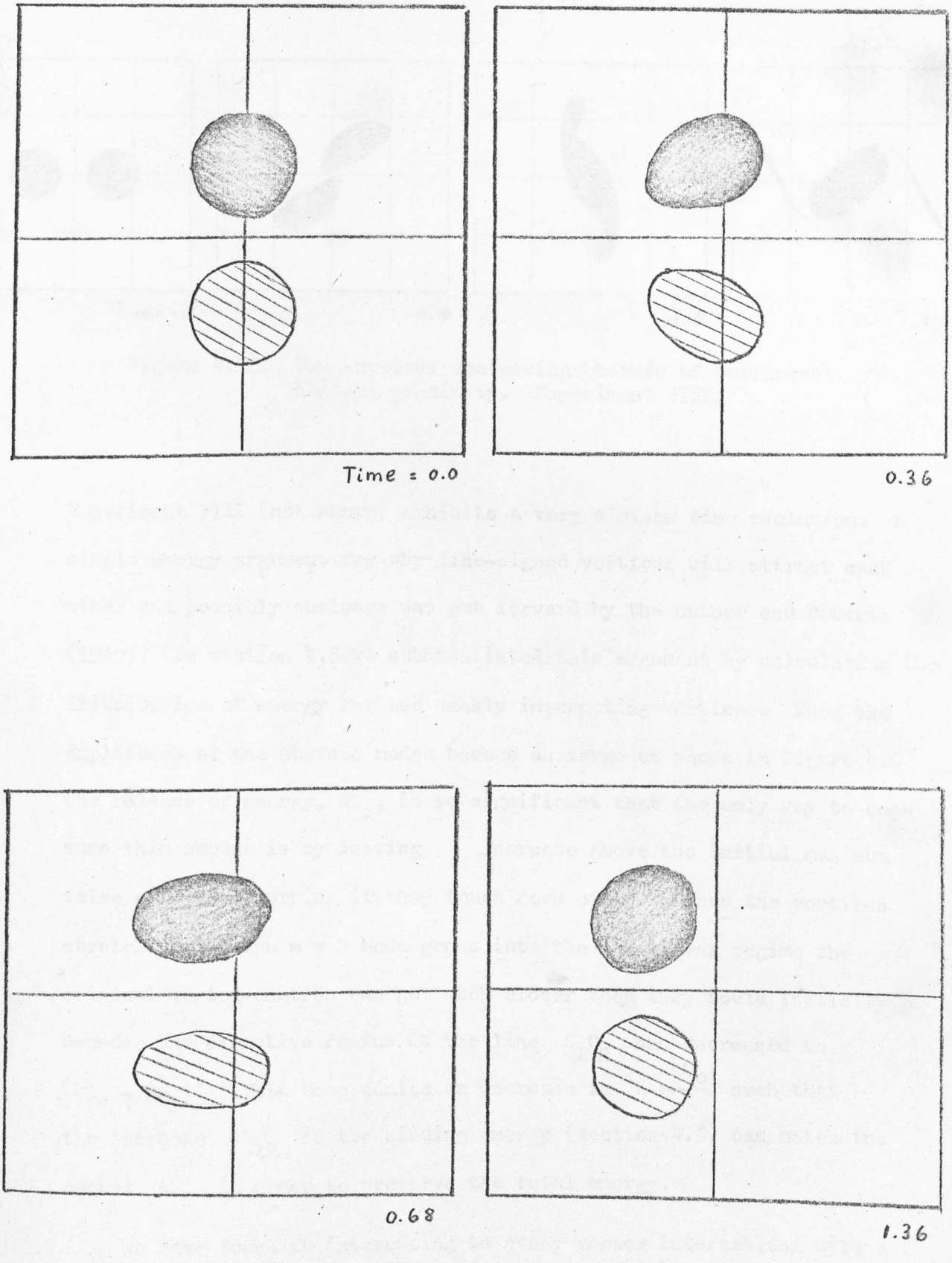

Figure 4.12. Two oppositely-signed vortices. Experiment V.

In Figure 4.13 we show how the vortices in experiment VIII fuse together to form an oval-shaped single vortex with spiral arms.

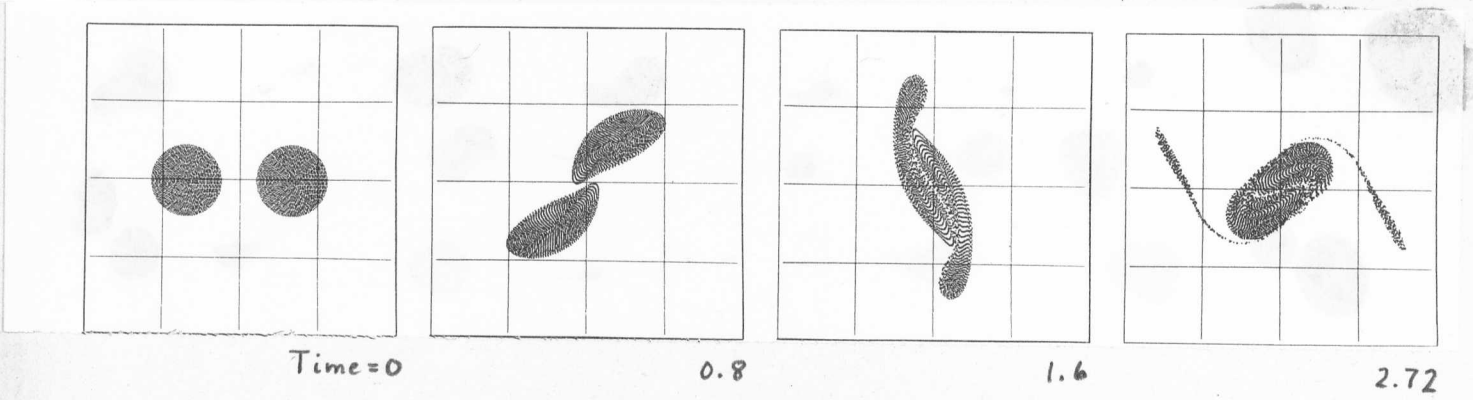

Figure 4.13. Two vortices coalescing because of sufficient initial proximity. Experiment VIII.

Experiment VIII (not shown) exhibits a very similar time evolution. A simple energy argument for why like-signed vortices will attract each other and possibly coalesce was put forward by the author and Roberts (1969). In section 4.5 we substantiated this argument by calculating the distribution of energy for two weakly interacting vortices. When the amplitudes of the surface modes become as large as shown in Figure 4.8 the release of energy, δE_1, is so significant that the only way to consume this amount is by letting η increase above the initial maximum value of 0.25 occurring if they touch each other. Since the vortices stretch whilst the $m = 2$ mode grows into the non-linear regime the original vortex centres can get much closer than they could initially because the effective radius at the line C_1C_2 has decreased to $(2q_o - 2\alpha_2)^{\frac{1}{2}}$. This then admits an increase in $\eta = \frac{q_o}{q}$ such that the increase δE_{12} in the binding energy (section 4.5) can match the amount δE_1 in order to preserve the total energy.

We have found it interesting to study vortex interactions with a

range of values of η lying between the value of experiment III and that of experiment VIII. Some value, η_c, lying in this range will separate interactions that lead to fusion ($\eta > \eta_c$) and interactions that produce the classical precessing motion with surface modes distorting the vortices. We have carried out four experiments, IX-XII, (Table 4.1) in order to investigate the time development of the interaction around $\eta = \eta_c$. Experiment IX shows fusion after about half a period T, whilst X-XII follow the pattern of evolution depicted in Figure 4.14. The $m = 2$ mode oscillates with a period $T_2 = \frac{T_o}{1-4\eta} = 4.18$. At times $t = 2, 6, 10$ etc. we have the vortices touching in a "figure 8" configuration corresponding to a maximum value of α_2. Figure 4.14 for experiment XI shows how point vortices are exchanged at each encounter.

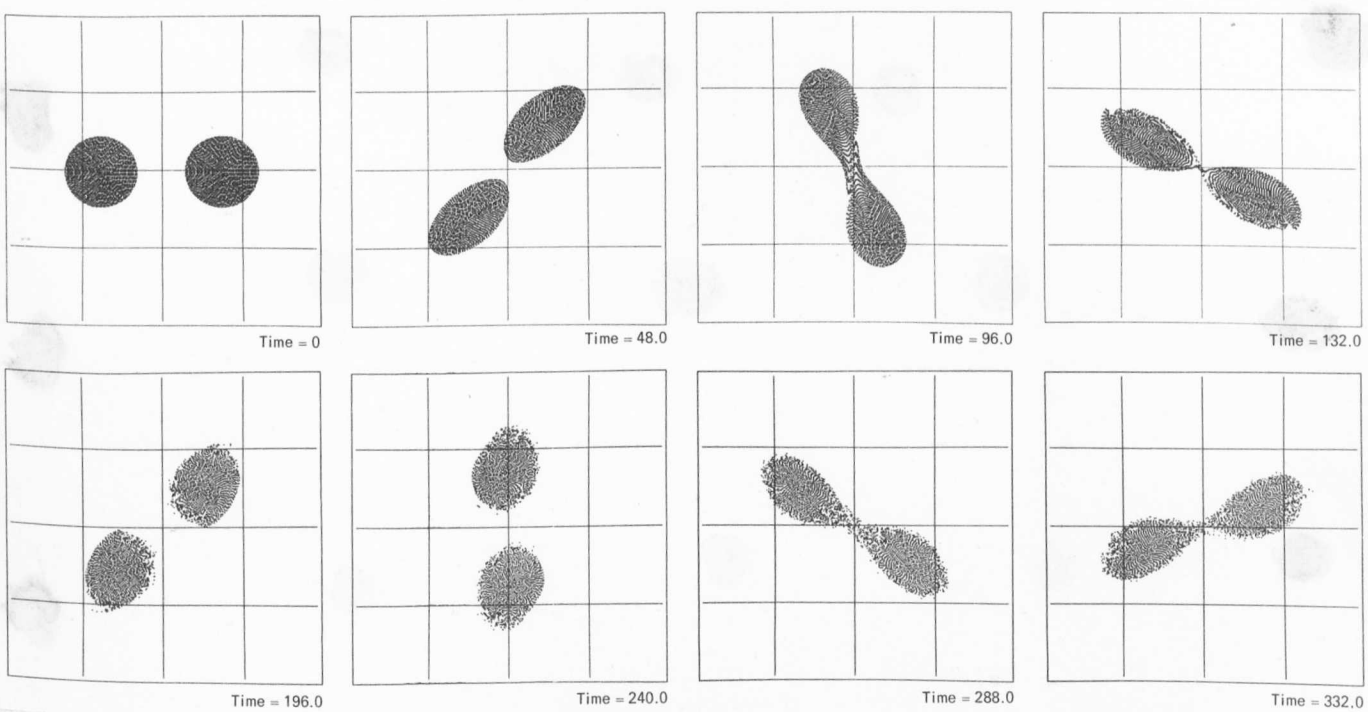

Figure 4.14. Two vortices with a critical initial proximity. At the approach they exchange vortex fluid. Experiment XI.
(N.B. the times given should be divided by 50 as explained in chapter 3).

This of course is meant to represent the winding up of thin slivers of vorticity, such that after $t = 2.0$ approximately the vortices have effectively fused together, only the resulting vortex structure differs from that of experiment VIII. The "figure 8" shape of the resulting vortex closely resembles the separatrix of the streamline configuration. It could therefore be interpreted as a final stationary state since we have ζ = constant inside the separatrix, e.g. $\zeta = \zeta(\psi)$.

By a simple argument we can calculate the initial value η_c above which two circular vortices in an infinite medium will fuse together. When $\eta < \eta_c$ initially both vortices are contained within the separatrix and although the surface modes oscillate no part of each vortex can cross the separatrix (the flux across a streamline is zero). For $\eta > \eta_c$ the separatrix cuts through the vortices and the amount of vorticity outside it can now become convected along the separatrix and merge with the other "outside" part. Thus the vortices fuse. For $\eta = \eta_c$ the separatrix touches the far ends of each vortex. As the $n = 2$ mode grows the part of the vortex touching the separatrix moves up during half a vortex rotation $(\frac{1}{2} T_o = \frac{1}{4} T_2)$ to touch the symmetric part. The value η_c is found from equation (4.12) by equating ψ_3 evaluated at P_o and ψ_1 evaluated at $(\varsigma,p) = (\varsigma_o,\pi)$. A calculation gives

$$\eta_c = \frac{\sqrt{2}-1}{4} \approx 0.103 \quad .$$

This is higher than our value 0.087 estimated from experiments IX-XII. To get a better agreement one would have to make a more sophisticated calculation of η_c incorporating the images that are caused by the square boundaries.

4.10 Short summary

The numerical experiments presented in this chapter demonstrate that

the interaction between vortices which are initially circular can be one of three types depending on η_1 and η_2 (we have used $\eta_1 = \eta_2 = \eta$ for simplicity).

1) $\eta < \eta_c$. The vortices perform their classical motion as if they were point vortices. However because they are of finite size surface waves will develop such that the vortices undergo deformation. For oppositely-signed vortices we conclude that $\eta_c = 0.25$, corresponding to the point at which they overlap; even for large values of η we find for this case a surprisingly good agreement between theory and experimental results.

2) $\eta = \eta_c$. Like-signed vortices approach and "touch", forming a "figure 8"-shaped vortex; subsequently they retract, approach and touch again.

3) $\eta > \eta_c$. Like-signed vortices approach and fuse to form a single vortex of oval shape and with spiral arms.

The cases $\eta \geq \eta_c$ represent interesting phase transitions from 2-vortex systems to 1-vortex systems, phase transitions such as we encounter in Thermodynamics or Quantum Mechanics. The reverse transition: the fission of a vortex into 2 or more fragments is also possible. Such fission can be caused by other vortices as we shall see in chapter 5. We believe that fission of a single non-interacting vortex can also take place provided it is brought to the "right" state initially. Numerical experiments (Table A.3) on Kirchoff's elliptic vortex (Lamb,1930,p.230) have shown that an elliptic vortex of eccentricity close to 1 will collapse to form a "figure 8"-shaped vortex (compare with experiment XI). These experiments are however not included in this thesis.

CHAPTER 5

STABILITY PROPERTIES OF VORTEX CONFIGURATIONS MODELLING LAMINAR WAKES AND NOZZLE FLOWS

In this chapter we study the stability and long-time evolution of two-dimensional wakes, asymmetric vortex streets and vortex rings. The vorticity distributions considered are meant to approximate situations occurring in laminar flows and nozzle flows. Previously obtained analytical results in the linear regime are discussed first. The subsequent description of results from a series of computational experiments covers the non-linear regime of evolution. Attempts are made to interpret results from tunnel experiments in which three-dimensional effects have been minimized. The computational experiments demonstrate how the dynamics of the flows is governed by the interaction between nearby vortex regions, a process studied in detail in the previous chapter. It is shown how vortices can form from initially stratified flows, how vortices can fuse (or coalesce), how they can undergo fission and how they can persist for longer times.

5.1 Introduction and epitome of numerical experiments

In recent years there have been renewed efforts to understand the non-linear dynamics of interacting vortex structures in high Reynolds number (high-R) two-dimensional jets and wakes. Carefully controlled experiments (Taneda 1959 and 1965), that minimize three-dimensional effects in low noise wind tunnels have shown that asymmetric vortex structures have a finite life time, i.e. they become unstable. At variable distances downstream (many wavelengths of the fundamental vortex structure), the observed pattern abruptly loses its coherence and degenerates or "breaks down into a less ordered pattern". From this visually chaotic state evolves a secondary asymmetric vortex structure, more diffuse than the primary structure and of longer wavelength. This hierarchy of two-dimensional vortex structures is sufficiently simple that a deterministic, non-statistical approach should elucidate the basic mechanisms involved. As exemplified below, numerical simulations with a two-dimensional zero-viscosity model can provide such insights.

In flat-plate wake experiments, Sato and Kuriki (1961) have also measured the properties of high-R wakes at moderate distances behind flat plates. Their high-quality hot-wire data was interpreted by Zabusky and Deem (1971) in a computational/experimental study as consistent with the motion of an asymmetric wake of elliptical nutating vortices. Zdravkovich (1968 and 1969) also found elliptical and other distorted vortex structures to be a common occurrence in wakes of cylinders. The elliptical shape of the vortex is a non-viscous effect due to the mutual interaction of nearby vortex regions; this was observed in chapter 4 for the case of two interacting vortices.

To clarify the qualitative features of ideal high-R laminar flows

downstream of flat plates, it is convenient to describe phenomena in contiguous spatial regions:

(1) At very short distances one finds nearly laminar flows with a Gaussian type velocity profile. For $R > 10^4$ the inviscid Rayleigh equation provides eigenfunctions and unstable eigenvalues. R is based on the length of the plate. The Reynolds number based on the boundary layer thickness (or radius of a cylinder) is > 500.

(2) At short distances, induced perturbations (via acoustically driven loudspeakers, vibrating ribbons etc.) grow in accordance with linear stability theory. For $R > 10^4$, Sato and Kuriki (1961) and Zabusky and Deem (1971) showed that the Rayleigh equation provides unstable eigenvalues that agree with observations.

(3) At moderate distances, the fastest growing modes have the most energy and saturate when a regular asymmetric street of elliptical vortices form. The finite-sized elliptical vortices undergo a slow pitching or nutating motion in the laboratory frame of reference. This phenomenon was also observed in the wake of cylinders and in two-dimensional jets by Beavers and Wilson (1970).

(4) At large distances, the vortex structure may break down (collapse or undergo a transition) to another asymmetric street, where the longitudinal distance between nearby vortices in the same row can increase by a factor of 2 to 10 depending on the Reynolds number (Taneda 1959).

(5) At very large distances the breakdown and reformation of the vortex structure may be repeated several times. However, at very high-R the turbulent or chaotic structure may persist.

In wakes beyond cylinders and other bluff bodies, regions (1) and (2) are inseparable and pockets of vorticity aggregate alternatively on either

side. When the vortex concentrations are sufficiently large they are convected away to form an asymmetric street. The rate of convection of vortex aggregations determines the Strouhal number.

For real rather than ideal high-R flows, the above regions may not be clearly separated. The flow configuration at moderate to large distances (particularly at very high-R) is very sensitive to the precise operating conditions and excitation mechanisms, that is the predictability of the flow decreases at large distances or long times. The suppression of 3-dimensional disturbances; the rigidity of the mounting; the smoothness of the construction and excitation mechanisms; the quietness of the wind tunnel; and a finite viscosity all contribute to a more predictable result.

We have made a series of computer simulation studies of the stability of wake-like configurations because the literature of analytical non-linear treatments is an empty set. However we have linear stability theories for symmetric and asymmetric configurations of point vortices begun by von Kármán and elaborated by Kochin, Kibel and Roze (1964). For two oppositely signed streets of point vortex filaments the symmetric configuration is unconditionally unstable. The asymmetric configuration on the other hand is only stable if the transverse to longitudinal separation $(\frac{b}{a})$ is 0.281. However, as emphasized by Kochin, Kibel and Roze (p.226-234) this is a necessary condition: "A first order perturbation theory shows that the positions of vortices in a street with $(\frac{b}{a}) = 0.281$ will separate by a finite amount". Rosenhead (1930) examined the linear stability of the $(\frac{b}{a}) = 0.281$ asymmetric street for small-but-finite area circular vortex regions. However this calculation is not applicable to strictly 2-dimensional finite area vortex streets, as described later.

Most past analytical and computational work has concentrated on studying point vortex configurations, that is vortex deformations are

excluded from the dynamics. The reasons for excluding deformations of finite area vortices can be summarized by quoting Bassett (1888, p.42, vol.II): "If more than one vortex exists in a fluid, the effect of any one of the vortices upon the others will be to produce a motion of translation combined with a deformation of their cross sections. The mathematical difficulties of solving this problem when the initial distribution of the vortices and the initial forms of their cross-sections are given, are very great; and it seems impossible in the present state of analysis to do more than obtain approximate solutions in certain cases".

Our study generalizes and considers finite-area constant density vortices (Rankine vortices) whose interaction properties were studied in chapter 4. Each vortex is confined by a contour which is represented by an equation of the type (1.28), i.e.

$$r2\ (\theta) = R_o^2 + \sum_m \alpha_m e^{im\theta} + cc\ ,$$

where r is measured from the vortex centre. For $\alpha/R_o^2 << 1$ a translation with no distortion corresponds to an $m = 1$ disturbance and an $m = 2$ disturbance results in an elliptic shape. Generally high-m disturbances can arise through close non-linear interactions as we showed in chapter 4.

There has been work on wake-like configurations ($v_y = 0$, $v_x = v_x(y)$. The shape of $v_x(y)$ is referred to as the profile). Solving a finite-difference representation of the Navier-Stokes equation, Deem, Hardin and Zabusky (1971) initially perturbed a laminar Gaussian profile with a second-harmonic plus small-random perturbation and observed the growth of four elliptically-shaped vortices of unequal strength. There follows a period of quasi-stationary evolution of the vortex configuration and finally a rapid coalescence of pairs of like-signed vortex regions. Similar phenomena are described below in the simulations of a triangular

velocity profile and the evolution of two pairs of oppositely signed asymmetrically placed vortex regions.

The numerical experiments summarized in this section and outlined in Table 5.1 are all related to our abstraction of high-R wakes of flat plates or bluff bodies. The calculations start from uniform vorticity distributions and periodicity with x is assumed.

In section 5.3 we discuss the laminar triangular longitudinal velocity profile with random perturbations (experiment I) and show that the linearly unstable profile transforms into an asymmetric (staggered) array of unequal strength vortex regions which coalesce or fuse.

For comparison section 5.4 studies the trapezoidal longitudinal velocity distribution with widely separated flanks and also subject to random perturbation (experiment XI). The flanks roll up and form an asymmetric array of four elliptic vortices.

In section 5.5 we begin the study of the stability of four finite area vortex regions, with periodic boundary conditions in the longitudinal (x) direction. The parameters of the study are:

(i) The area of the vortex regions

(ii) The initial shape of the regions

(iii) The transverse boundary conditions (fixed or periodic)

(iv) The nature of the perturbation to one or more vortex regions (lateral or longitudinal displacement of the centroid of a vortex region, shape or size charge, etc.).

(v) The transverse-to-longitudinal separation $\frac{b}{a}$ of the vortex centres.

Section 5.5 studies the case where $\frac{b}{a} = 0.281$ (experiments II to V) which is known to be "marginally" stable for point vortices. For runs of duration 19 rotation periods, we find stability.

In section 5.6 we treat the case $\frac{b}{a} = 0.6$ known to be unstable for point vortices and we find instability followed by fusion of like-signed vortices. See experiments VI to IX.

In section 5.7 the standing wave case $\frac{b}{a} = 0$ is treated and we find instability and a peculiar strong dynamical interaction that finally leads to a rapid fission of one vortex followed by fusion of vortex regions on a longer time scale. See experiment X.

Expt. No.	$\frac{b}{a}$	Eccentricity of vortices	π^{-1} (Area) of typical vortex	y-boundaries	Elapsed time T_E	No. of time-steps	ζ_o	T_E/T_o
I	Laminar wake		-	F	10.5	1344	6.25	
II	0.281	0.0	9	F	9.0	576	27.0	19.4
III	0.281	0.0	35	P	9.0	576	7.0	5.0
IV	0.281	0.85	26	F	3.0	192	9.4	2.24
V	0.281	0.85	26	F	3.0	192	9.4	2.24
VI	0.6	0.7	35	F	24.0	768	7.0	13.3
VII	0.6	0.7	35	P	6.0	192	7.0	3.3
VIII	0.6	0.0	35	P	6.0	192	7.0	3.3
IX	0.6	0.0	9	P	9.0	1152	27.0	19.4
X	0.0	0.0	35	P	17.0	576	7.0	9.45
XI	Trapezoidal wake		-	F	8.5	768	6.25	

TABLE 5.1 Experiments on vortex streets

Column 5: F and P mean fixed or periodic y-boundaries. In column 9, $T_o = 4\pi/\zeta_o$ is the rotation period of the vortex.

5.2 Comments on previous analytical work

The original calculation by von Kármán for an asymmetric point vortex system has been repeated by Lamb (1932, Section 155, p.228) and somewhat generalized by Kochin, Kibel and Roze (1964, Section 5.21). If nearest neighbour vortex filaments on the same line (separated by a) are given the same displacement, $x_m = \alpha e^{im\phi}$, $y_m = \beta e^{im\phi}$, the solution of the linearized perturbation equations yields the dispersion relation (solutions varying as $e^{\lambda t}$)

$$\lambda = (\Gamma_o/2\pi a^2)(\pm iD \pm \sqrt{A^2-C^2}) \quad , \tag{5.1}$$

where

$$A = \frac{1}{2}\phi(2\pi-\phi) - \pi^2/\cosh^2(\pi b/a) \quad , \tag{5.2}$$

$$B = iD = i\{\frac{\pi\phi\sinh(\pi-\phi)b/a}{\cosh(\pi b/a)} + \frac{\pi^2\sinh\phi b/a}{\cosh^2(\pi b/a)}\} \quad , \tag{5.3}$$

$$C = \frac{\pi^2\cosh(\phi b/a)}{\cosh^2(\pi b/a)} - \frac{\pi\phi\cosh(\pi-\phi)b/a}{\cosh(\pi b/a)} \quad . \tag{5.4}$$

The condition $\phi = \pi$ is most unstable as it makes $C = 0$ and

$$A = \frac{1}{2}\pi^2[1-2\cosh^{-2}(\pi b/a)] \tag{5.5}$$

$$B = iD = i\pi^2[\sinh(\pi b/a)\cosh^{-2}(\pi b/a)] \, . \tag{5.6}$$

The condition $A = 0$ is necessary for stability and this yields the well-known condition

$$\cosh(\pi b/a) = 1 \quad \text{or} \quad b/a = 0.281 \, . \tag{5.7}$$

The oscillation frequency is

$$\text{Im}\,\lambda = \pm \frac{1}{4}\pi\Gamma_o/a^2 = \pm 0.5895 \tag{5.8}$$

where the numerical value corresponds to our case, $a = 32$ and $\Gamma_o = \pi R_o^2 \zeta_o = 766$ (the number of filaments in each vortex region).

The growth rates at two values of b/a are

$$b/a = 0.6 \; ; \qquad \lambda = 0.481 \tag{5.9}$$

$$b/a = 0 \; ; \qquad \lambda = \tfrac{1}{4}\pi\Gamma_o/a^2 = 0.590 \; . \tag{5.10}$$

Three additional analytical calculations bear on the results below. Kochin, Kibel and Roze (1964, pp.226-234) applied a higher-order perturbation calculation to the asymmetric point vortex street with $b/a = 0.281$. They have shown that the street is always unstable, i.e. arbitrary small displacements will cause vortices to ".... separate by a finite amount". This is not surprising as the Kármán street is unstable for $b/a \neq 0.281$. If odd vortices on the upper street are displaced upward by ε a configuration results identical to that obtained by increasing the separation to $0.281 + \varepsilon/2$ and then displacing positive vortices upwards by $\varepsilon/2$ and negative vortices downward by $\varepsilon/2$. Since the latter system is linearly unstable, it would be reasonable to assume that the former system is unstable to finite amplitude disturbances.

Rosenhead (1929, 1930) has extended the von Kármán linear analysis by examining the effects of transverse free-slip boundaries (1929) and the effects of 3-dimensional/small-area regions (1930). In the first study Rosenhead shows for point vortices that if fixed y-boundaries are introduced at a distance $\pm h/2$ from the centre of the street, the b/a ratio for "stability" decreases from 0.281 to 0.256 as a/h increases from 0 to 0.815. As a/h is increased further, the b/a line becomes a region or area of stability. Rosenhead gives a formula for the modified stability line as

$$b/a = 0.281 - 0.090(a/h)^6 = .280 \quad ,$$

where we have used our ratio $a/h = 0.5$. (See Rosenhead, Equation (5), p.321. N.B. Rosenhead uses: 2b for the longitudinal distance between vortices; 2a for the transverse distance between vortices and 2c for

the distance between fixed walls). In comparison with finite area the transverse boundaries play a negligible role.

In the second study (1930), Rosenhead purports to treat finite-area effects but in fact mixes 3-dimensional considerations with small-area 2-dimensional considerations. He states "The problem in its initial stages can no longer be treated as one in two dimensions because the "self-induction" [effect of a vortex on itself] of a vortex only enters when we deal with a 3-dimensional disturbance, and it is the self-induction that produces the difference between this and the original treatment [i.e. von Kármán's treatment] of the subject".

Rosenhead begins his study with a consideration of the behaviour of small circular vortices of radius ε that have $m = 1$ self-interactions resulting from 3-dimensional perturbations of wavelength $2\pi\ell^{-1}$ in the z-direction. Rosenhead defines a parameter

$$\eta = -\frac{1}{2} a^2 \ell^2 \log(\ell\varepsilon), \qquad (\ell\varepsilon) < 1$$

which is claimed to be a measure of the self-induction. This parameter is introduced inconsistently into the von Kármán equations. The result becomes a set of four first-order ordinary differential equations for the (x,y) velocities of the upper and lower streets. His paper goes on to discuss the dispersion relation which is now a function of η, and concludes (p.608) that there is "a distinct domain of instability in the neighbourhood of $\phi = \pi/2$", where ϕ determines the initial perturbation.

We find Rosenhead's statement about the "self-induction" misleading, especially since η is a function of a and also applicable only when either $\ell \to 0$ or $\varepsilon \to 0$. Rosenhead's claim (p.599) that for $\eta \to 0$ the stability investigations reduce to those of von Kármán is misdirected since our 2D calculations clearly show self- and mutual-induction effects. From this analytical work we conclude that there is scope for a further exten-

sion through numerical calculations in order to illuminate the mechanisms that control the transitions between the five different states discussed in section 5.1.

5.3 Laminar wake with a triangular velocity profile

To simulate a laminar triangular velocity profile with a random perturbation, we distribute uniformly 1600 positive and 1600 negative point vortex filaments over an area of 8 x 64 as shown in Figure 5.1.

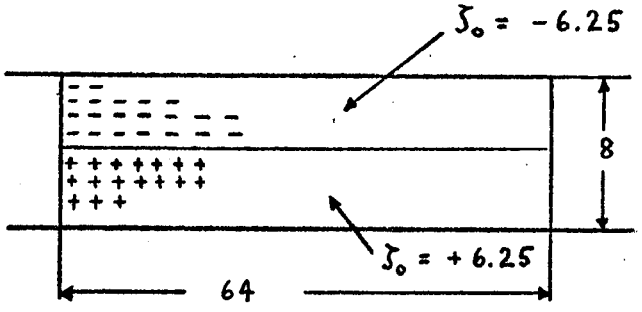

Figure 5.1. Initial distribution of vorticity in experiment I.

This results in two strips of vorticity density $\zeta_0 = \pm 6.25$. The laminar state is perturbed by displacing each filament less than one lattice interval in a random and incompressible velocity field (section 3.6).

Figure 5.2 shows the longitudinal velocity profile obtained by integrating the resultant ζ and choosing the constant of integration to result in zero x-momentum. The initial departure from the triangular profile is caused by the random perturbation as well as by the area-weighting method mentioned in the Appendix.

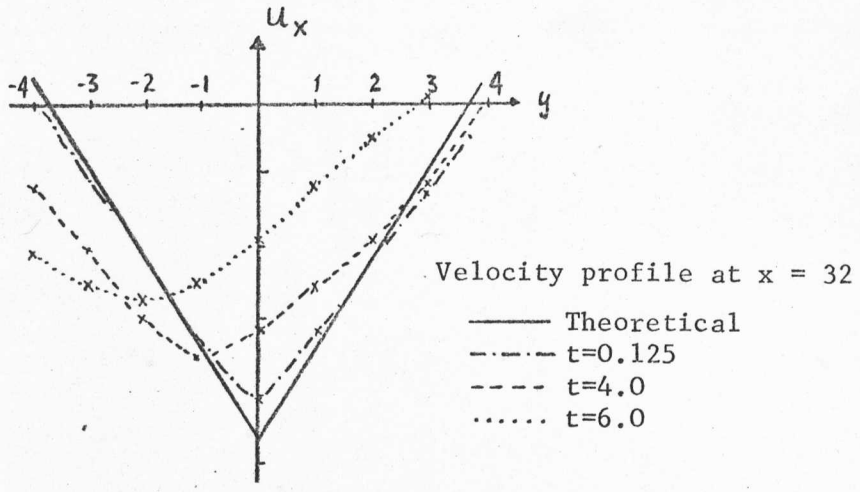

Figure 5.2. Initial velocity profiles for experiment I.

The evolution of the perturbed triangular profile is shown in Figure 5.3. We will not discuss the linear phase of evolution as this and closely related problems have been well treated elsewhere (Zabusky and Deem, 1971; Drazin, 1958; Chandrasekhar, 1961).

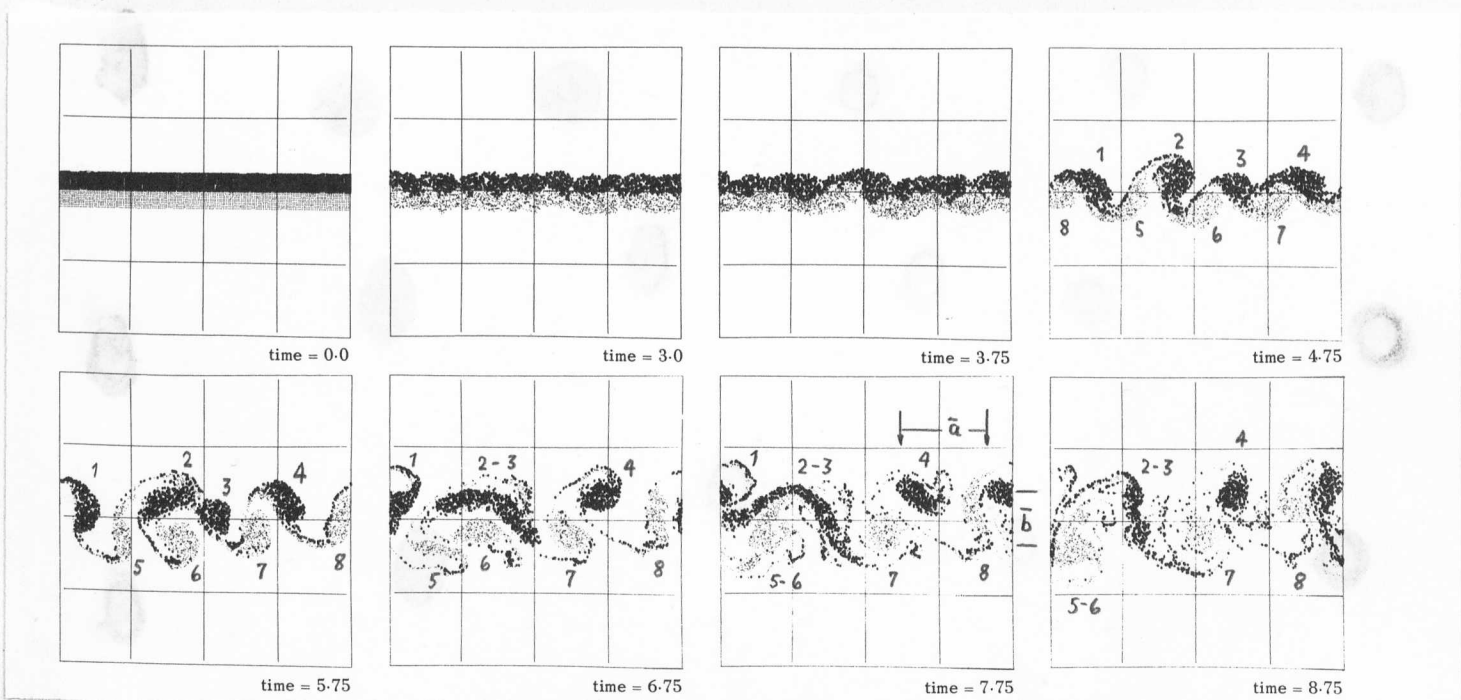

Figure 5.3. Experiment I. Instability of a laminar wake subject to a small random perturbation. Fixed y-boundaries.

After approximately t = 4.2 the perturbation has grown and saturated because of non-linear effects. At t = 4.75 we see that 4 negative and 4 positive elongated vortex regions of varying area have formed into an asymmetric pattern. Note that at this stage small areas of positive or negative vorticity become "trapped" within or behind the larger vortex of opposite polarity. Between t = 5.0 and 6.75 two negative vortex regions (Nos.2 and 3) fuse into an elongated structure. At t = 6.75 we see positive vortex regions (Nos.5 and 6) begin to fuse. At t = 7.75 vortex region 1 is beginning to fuse with region 2-3, but the process is inhibited by region 5-6. Note that at t = 7.75 the approximate transverse-to-longitudinal separation ratio is $\bar{b}/\bar{a} = 0.42$, that is, the wake width has increased by a factor of three due to the fusion, elongation, rotation and jetting of vortex "streams" or "arms", that is by convective processes. After t = 8.0 we have an irregular structure of 3 negative and 3 positive vortices per period with some mixing of positive and negative vortex filaments between the larger vortex regions. The situation corresponds roughly to an array of vortices staggered with respect to each other and moving in a weakly turbulent flow caused by "dispersion" of vortex filaments. This situation still prevails at t = 10.5 (not shown in Figure 5.3) with more filaments dispersed away from the main regions. Numerical finite-difference effects contribute to this dispersion and mixing of filaments and can be observed at t = 7.0. However for a short time the intermixing of the small-scale chaotic motion does not affect the mean behaviour of the large-scale vortex structures.

In Figure 5.3 at t = 4.75 we see that negative vortex No.4 is elongated and its major axis rotates clockwise at a non-uniform rate whose average period is 4.7 (measured over the range $4.75<t<10.25$). A non-interacting ellipse (Kirchoff vortex, Lamb p.230) has a period $T_2 = \frac{4\pi}{\zeta_o}(\mu+1)$ where

$\mu = \frac{2 - \varepsilon^2}{2\sqrt{1 - \varepsilon^2}}$, ε being the eccentricity of the ellipse. A rough estimate of vortex No.4 gives $\varepsilon^2 = 0.75$ so that $T_2 = 4.52$, close to that of the deformed strongly interacting elongated vortex region. Note that all vortex regions are drifting slowly to the left, whereas the distant irrotational fluid is streaming uniformly to the right.

In Figure 5.3 we observe that small trapped regions are convected around at the rotational frequency of the oppositely signed host vortex. This phenomenon was also observed and noted by Zabusky and Deem (1971) and they designated these small regions as "secondary" vortices (see their Figure 8, p.368). Due to vortex rotation (in an appropriate frame) or "nutation" in the laboratory frame of reference, tracer particles, smoke, or single vortex filaments will be transported to the opposite side of the vortex street, a phenomenon observed by Zdravkovich (1969, Section 3 and Figure 3). Thus, we have an enhanced transport of material across a flow due to convection by vortex states formed as a result of a linear instability of the system.

5.4 Laminar wake with a trapezoidal velocity profile

In order to simulate the evolution of a laminar trapezoidal velocity profile we again distribute point vortices as shown in Figure 5.1 but separate the two strips by an amount 8 in the y-direction. The same random perturbation (section 3.6) is then applied as before.

The evolution of the trapezoidal velocity profile is shown in Figure 5.4. Again we shall not describe the linear phase of evolution since the stability analysis is almost identical to that of the triangular profile and both classes of profile have received attention by many authors (Chandrasekhar, Chapter XI, 1961).

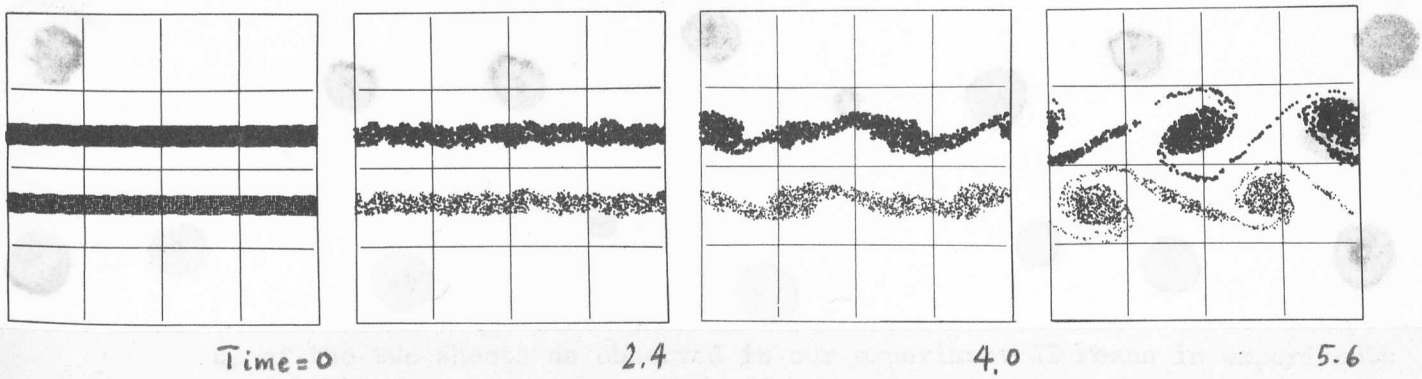

Figure 5.4. Evolution of a trapezoidal velocity profile

The four frames of Figure 5.4 depict the situation qualitatively. As before we have a tendency to form 4 positive and 4 negative elongated vortex regions when the evolution has advanced well into the non-linear regime of time. At time t = 4.0 we see how alternate vortices (both positive and negative) stretch to form sheets of vorticity linking the larger elliptic vortices. The effect of separating the flanks initially by an amount 8 is to reduce the influence of the negative vortex on the positive vortex sheet and vice versa. The type of perturbation applied to this system is less important in determining the final state (last frame of Figure 5.4). It can at most determine the phases of the elliptic vortices. The number of surviving vortices (2 negative and 2 positive per period) is determined solely by the initial separation of the flanks. The final state represents an asymmetric von Kármán vortex street but the trapezoidal profile results in much less mixing of vorticity and the wake width does not increase as significantly as before. This increase is partially suppressed by the fixed y-boundaries now being closer to the wake. We do not see any crossflow transport of vorticity as we did in the case of the triangular profile (section 5.3); the wake is too wide for this process to be stimulated by the initial linear instability.

The trapezoidal wake is of interest in many laboratory experiments where we encounter flows from large nozzles. With three-dimensional

effects minimized, the flow pattern in the nearby region of the nozzle is approximately that shown in Figure 5.4 (first frame); the two strips of vorticity correspond to the boundary vorticity layers escaping out of the nozzle at its walls. It would be interesting to examine what the rolling up of the two sheets as observed in our experiment XI means in experiments that enjoy a cylindrical geometry. Possibly the final state of Figure 5.4 may be interpreted as a cross-section through a helical vortex tube advancing in the x-direction by its self-induced velocity field. However in section 5.8 we shall illuminate the situation further by a different approximation to the nozzle flow.

To summarize sections 5.3 and 5.4, in the early stages the linear instability driven by a particular random perturbation yields eight large vortices staggered with respect to each other. At t = 5.75 (experiment I) all vortices are elongated and nearly elliptical in shape but with different phases. The magnitude of the phases as well as the transverse separation between the vortices depends on the initial conditions. This structure is unstable and like vortices attract and fuse in an attempt to find a more stable configuration (experiment I), or alternating vortices stretch and are wound up by the surviving vortices. This transition from one vortex state to a more enduring state provides a heuristic explanation for the observations of Taneda (1959, Section 3, P.847). At intermediate ($100 < R_e < 150$) and high ($R_e > 150$) Reynolds numbers the vortex streets in the wakes of cylinders (and flat plates) break down and re-form such that the ratio of the effective wavelength of the secondary street to the primary street is two for intermediate-R and " ... of order 10". for high-R. The intermediate-R result could be explained as merely the fusion of nearest neighbour like-signed vortex regions as observed above or as more clearly observed in section 5.6. That is, viscous dissipation plays

only a small role in comparison to the convective dynamical rearrangement of vortex filaments. Taneda observes this rearrangement or breakdown to occur again further downstream, a phenomenon consistent with our calculations. Taneda's high-R result is phenomenologically different for ".... after the primary Kármán vortex street breaks down the wake becomes turbulent, ... [a result already noted by Roshko in 1953] .... . The turbulent wake continues to exist for a considerable distance, then there appears again a new Kármán vortex street". In the laboratory, the wake may develop small three-dimensional destabilizing fluctuations that enhance the fusion of larger vortex regions over a moderate distance. The enhancement process will cease when the three-dimensional fluctuations undergo viscous decay and we are left with a new two-dimensional quasi-equilibrium state.

5.5 Stable asymmetric vortex configurations

We now study the stability and dynamics of two pairs of Rankine vortices of radius R_o and density $\pm\zeta_o$. As shown in Figure 5.5, they are placed in a staggered fashion in a box with periodic boundary conditions in x, simulating states encountered in laboratory and computational experiments as described above.

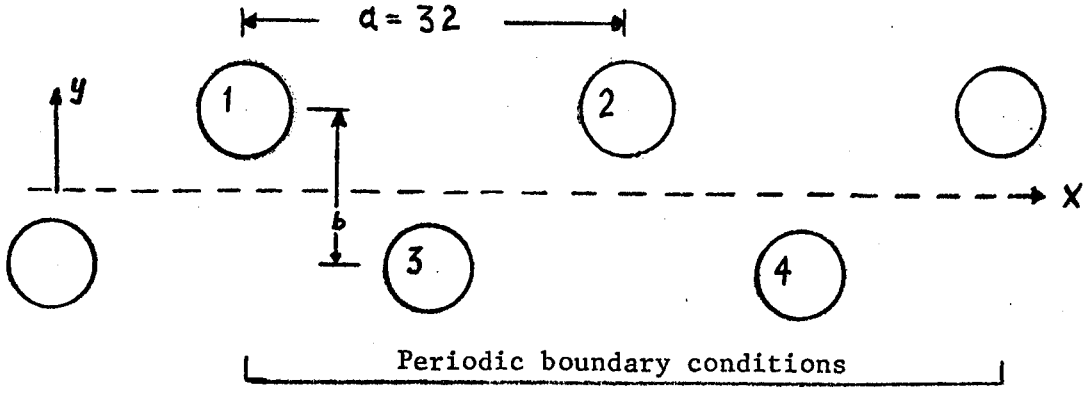

Figure 5.5. Arrangement of vortices

In our model we consider finite-sized vortices. If initially circular, their radius R_o is less than

$$R_M = \frac{a}{4}\sqrt{1 + 4\frac{b^2}{a^2}} = 9.17 \qquad \text{for } a = 32,\ \frac{b}{a} = 0.281\ ,$$

if they are to be non-overlapping. The radius function of a vortex during subsequent dynamics can be written (Equation 1.28)

$$r^2 = R_o^2 + \Sigma\ \alpha_m e^{im\theta}\ , \tag{5.11}$$

where r is measured from the initial centre of the vortex

$$r_c = \frac{1}{2\pi}\int_o^{2\pi} \tilde{r}(\theta)\, d\theta\ .$$

For incompressible fluids there is no $m = 0$ mode and expression (5.11) conserves area ($= \frac{1}{2}\int_o^{2\pi} r^2(\theta)\, d\theta = \pi R_o^2$). It is natural to ask: How does the finite area of vortex regions affect the von Kármán stability conditions? The instability that leads to a rearrangement of the street results from a growth of the $m = 1$ mode for one or more vortices (equation 5.11).

We have performed 4 different numerical experiments all using $\frac{b}{a} = 0.281$ in order to examine the stability properties of the arrangement sketched in Figure 5.5. Experiments II and III have initially 4 circular vortices of radius 3.0 and radius $\sqrt{35}$, respectively. In experiment II we introduce fixed y-boundaries, whilst III employs a doubly periodic geometry. The perturbation is in both cases a displacement of 1.0 in the y-direction of vortex 4, that is an $m = 1$ disturbance. Both experiments last for a time interval of 9.0 corresponding to 576 discrete timesteps (see Table 5.1). In experiments IV and V we introduce very strong non-symmetric perturbations: in experiment IV the major axes of positive vortices are inclined at 0.2 radian, whereas the major axes of negative vortices 3 and 4 are inclined at - 0.2 and 0 radian. Experiment V has

vortex 1 with the major axis reduced from 7 to 4 so that the resulting density becomes $\frac{7}{4}$ times that of the other 3 vortices. In both experiments vortex 4 is given a longitudinal displacement (also an m = 1 disturbance) of - 6.0 . Experiments IV and V last only for a time interval of 3.0 .

From Figures 5.6 and 5.7 displaying the time evolution of experiments II and III it can be seen that both flow fields are apparently stable, with respect to a small transverse perturbation. For all four

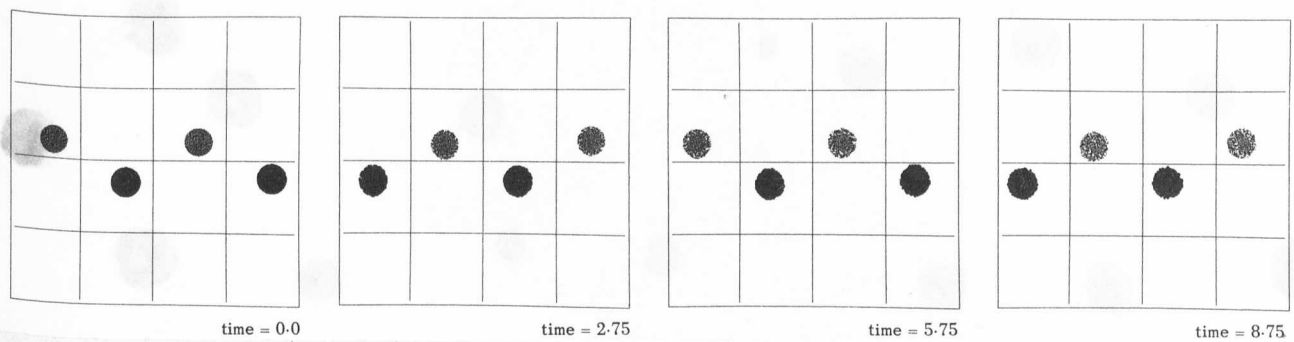

Figure 5.6. Experiment II. Small vortices. b/a = 0.281. Fixed y-boundaries.

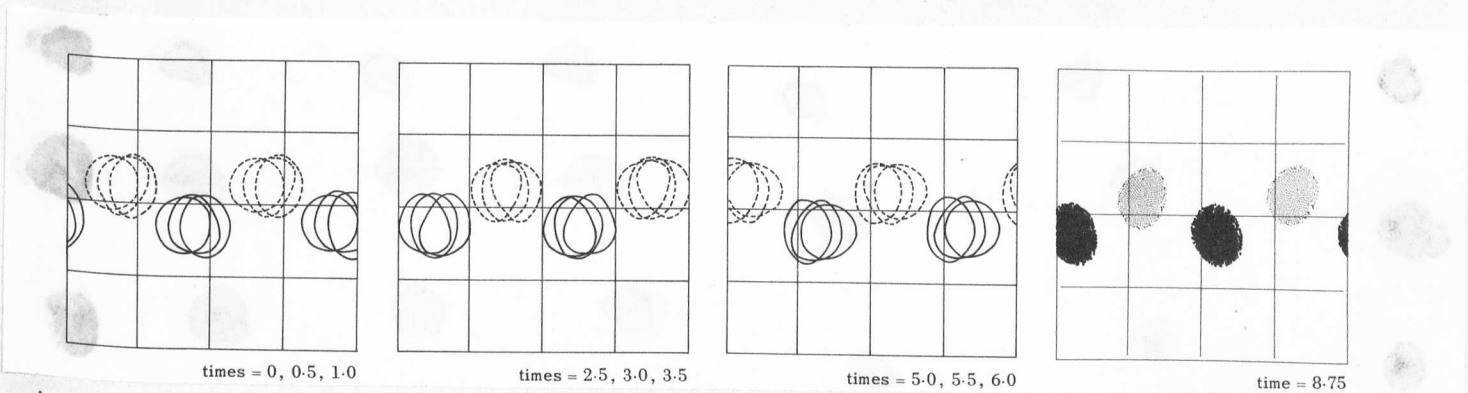

Figure 5.7. Experiment III. Large vortices. b/a = 0.281. Periodic y-boundaries.

(The first three frames show only the vortex boundaries. The leftmost contour is the smallest time indicated)

vortices in both experiments the amplitude of the perturbation (say the position of the lowest point on the boundary) is found to be 1.0 (the same as the initial amplitude) and the period is 11.0 . This is in good agreement with the result given by equation (5.8), $T = 2\pi/\mathrm{Im}(\lambda) = 10.7$.

In both experiments the vortices rotate, deform and drift to the right with velocities nearly independent of their areas. Surface modes $m = 2$, 3 and higher develop from the mutual interactions of vortices. This is illustrated in Figure 5.7, where the first three frames each show only the boundaries of the vortex regions at three close times (left-most contour is the smallest time indicated). The amplitudes of the surface modes oscillate with time, such that after one period of rotation T_o the circular form is reached again. The period T_o is 1.9. For a non-interacting vortex in an infinite medium the period is 1.8 (Table 5.1). The difference is due to non-linear effects as well as coupling between modes of different m as we saw in chapter 4.

The fine scale structure and surface corrugations that develop (as exhibited at $t = 8.75$) are due to numerical effects and do not disturb the large-scale dynamics. These structures were already observed and given an interpretation in chapter 2.

Experiments IV and V (figures not shown) with different initial conditions and strong perturbations show similar effects, namely rotation, deformation and translation. In these short runs we observe an oscillation period of 8.0 (instead of 11.0) and no sign of a growing perturbation. This may be a finite amplitude effect, however, the run duration is too small to make a definitive statement. The difference in periods could also be a measurement error since we have less than 1/4 period of interaction.

The effect of the finite-difference algorithm on the small growth rates of a marginally stable system must be assessed. The variety of

results presented here and the fact that parts of the vortex regions obviously extend into regions that are unstable for the point vortex system leads us to conclude that the observed stability is a property of the continuum, namely equation (1.16). The existence of negative energy modes resulting from area-conserving surface deformations contributes to this stability if the initial finite amplitude disturbance is not too large. We conclude that high-R finite area vortex streets have a small domain of stability around b/a = 0.281 .

5.6 Unstable asymmetric vortex street

We have performed 4 experiments with b/a = 0.6 as summarized in Table 5.2 :

Experiment	Figure	Area	Boundary Condition	Perturbation	Measured Growth Rate λ_m	Approx. Fusion Time
VI	7	large	fixed	large	0.62	5.5
VII	8	large	periodic	small	-	5.8
VIII	8	large	periodic	small	0.67	5.8
IX	9	small	periodic	small	0.67	6.9

TABLE 5.2

In Figure 5.8 we display the time evolution of experiment VI, whilst Figure 5.9 shows both experiments VII and VIII. Experiment IX employing small vortices is shown in Figure 5.10.

Experiments VI, VII and VIII for the large-area vortices all show fusion of positive regions at about t = 5.5 (fixed boundary condition) and t = 5.75 (periodic boundary condition). Experiment IX for the small-area vortices shows fusion at about t = 6.87 (15 vortex rotations). The initial positive vertical perturbation of the centre of vortex 4 is rapidly communicated to vortex 2 which while being ejected from the flow,

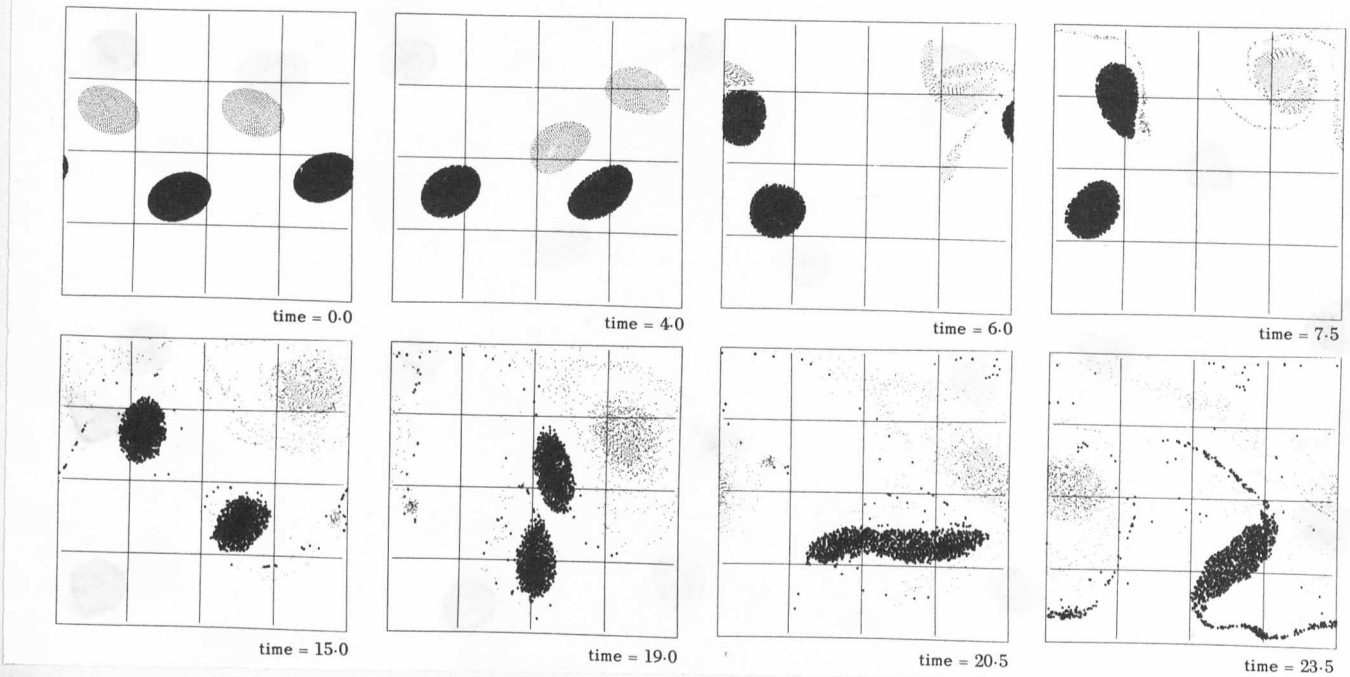

Figure 5.8. Experiment VI. Large vortices. b/a = 0.6. Fixed y-boundaries.

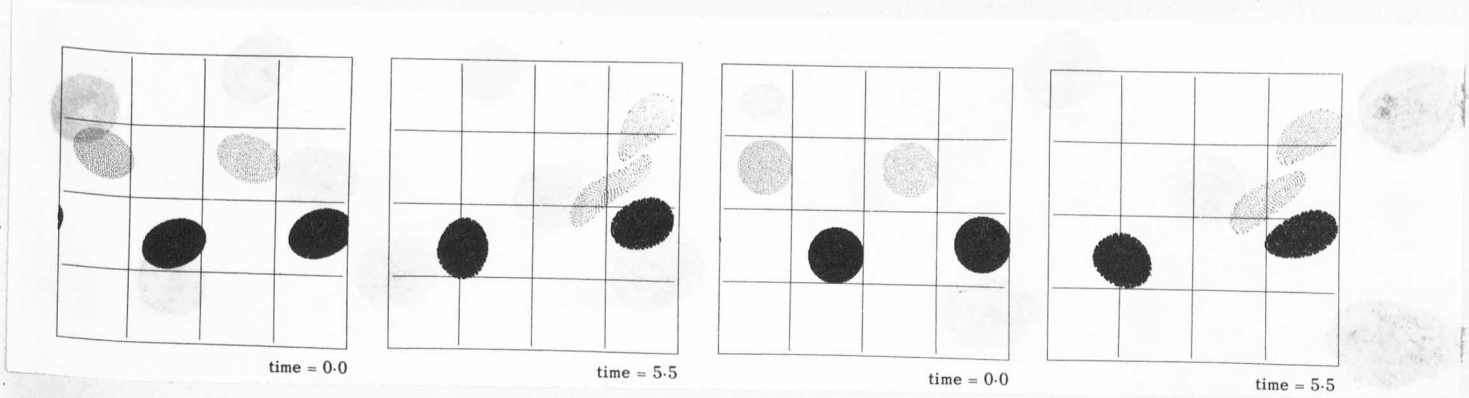

Experiment VII Experiment VIII

Figure 5.9. Two initially different unstable configurations. b/a = 0.6. Periodic y-boundaries.

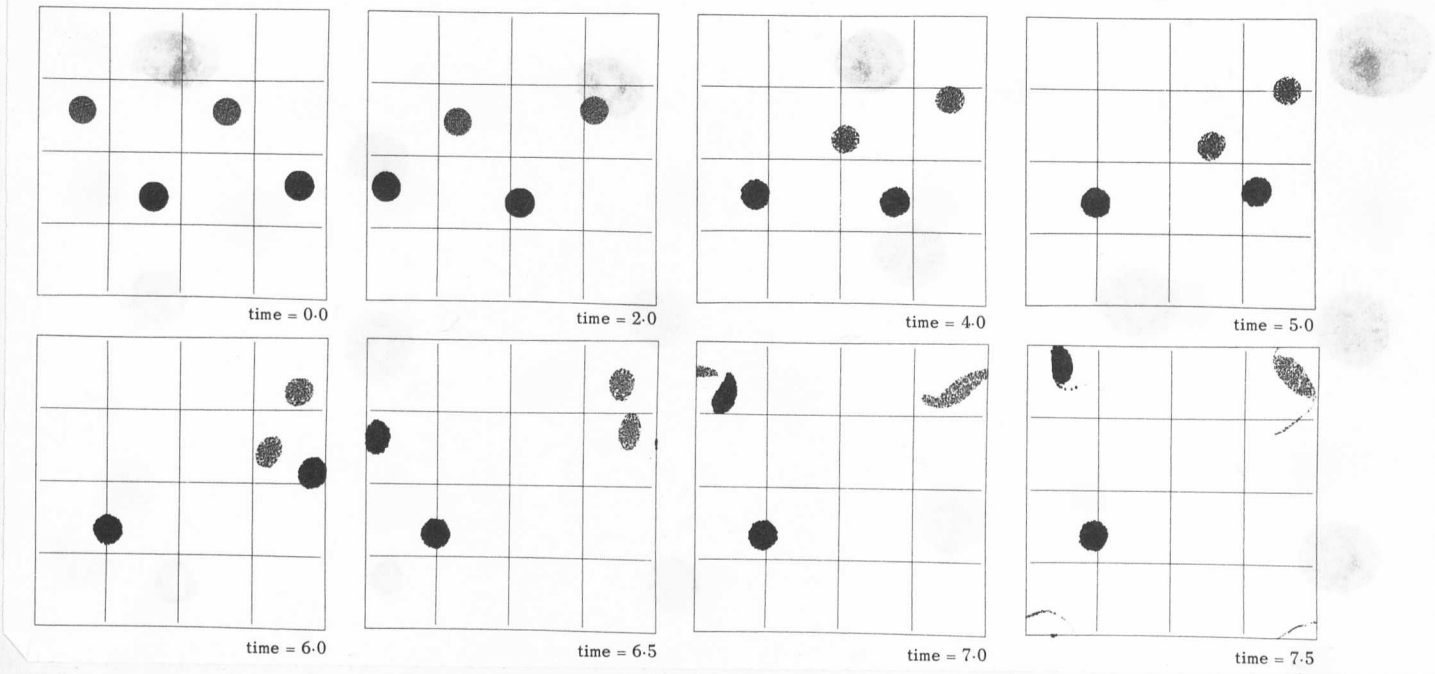

Figure 5.10. Experiment IX. Small vortices. b/a = 0.6. Periodic y-boundaries.

attracts vortex 1. In experiment VI, although vortices 3 and 4 are close together at t = 6.0, the dynamics does not allow fusion until t = 19.5 .

In Figure 5.11 we show the Δy_c of vortex 1 (moving downwards) for

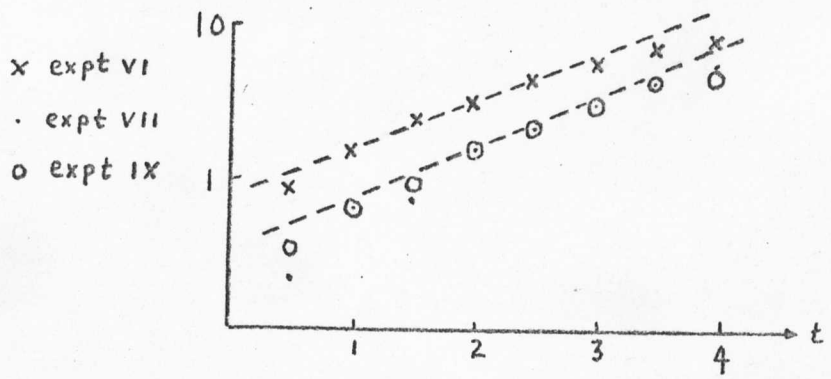

Figure 5.11. Growth of vortex centre deviations, Δy_c, and measured growth rates for systems with (b/a) = 0.6 .

experiments VI, VIII and IX. Δy_c is the difference of the ordinates of the centre of the vortices

$$\Delta y_c = y_c(t) - y_c(o)$$

as measured from enlarged figures similar to those given in this thesis and

has an accuracy of ± 0.3 units. The motion of lower vortices 3 and 4 is initially oscillatory. The measured growth rate given in Table 5.2 shows a larger value for the larger area vortex and both are about 30% larger than the 0.481 for the point vortex system. This increase is undoubtedly due to the facts that: the vortex extends into "more unstable" regions, that is where the "effective" growth rate experienced by a point vortex is larger than that experienced by a point vortex at the centre of the finite area region; and finite-amplitude effects are important early in the dynamics. (note that at $t = 2$, $\Delta y_c = 2.5$ units).

At later times when the dynamics are non-linear and there are large distortions to the vortex surface ($m = 2, 3, \ldots$), the rate of approach of like-signed large vortices is enhanced leading to a smaller fusion time. We find no significant change in the growth rate when the area is changed by a factor of $\frac{35}{9}$.

Beyond fusion, in the interval $t = 7 - 19$ (see Figure 5.8) the centroid of the fusion vortex is nearly stationary at the upper right and the two remaining vortices undergo precession. When they approach after $t = 7.5$, the vortex nearest to the fusion vortex is perturbed by the latter, i.e. a large $m = 2$ mode develops. At $t = 18.5$ the two negative vortices have completed a full precession around their mutual centre and have also moved $\frac{1}{3}$ of the period in the + x-direction. The upper vortex and the fusion vortex now form a binary system which travels downward. The lower vortex cannot move further downward (fixed boundary condition), hence the two negative vortices fuse. The elongated shape of the resulting vortex at $t = 20.5$ is a result of the lower y-boundary being fixed, since a circular or slightly elliptic shape would give rise to a net motion towards the lower boundary. At $t = 23.5$ we note that the elongated vortex has contracted and thrown off spiral arms. The final result

is then a "secondary" vortex street, with larger regions of positive and negative vorticity in asymmetric or staggered positions.

The dispersion and mixing of small-scale positive and negative vortex filaments between the larger vortex regions are strongly affected by numerical truncation errors, but play an insignificant role. This is analogous to real finite but high-R systems where small scales are dissipated. Two-dimensional fluid dynamic systems are known to seek states with larger scales (energy flowing to longer modes). This represents a kind of condensation phenomenon.

5.7 Collinear asymmetric vortex street - a standing wave

The collinear (b/a = 0) asymmetric vortex street (see Figure 5.12) is initially a standing wave with zero velocity

$$V_o = \Gamma_o/2a) \tanh(\pi b/a) = 0 \ .$$

Koopman (1967, p.508) has shown that such a configuration can be generated in the laboratory by oscillating the cylinder transverse to the direction of flow. (In essence, packets of vorticity are detached from the cylinder at times that correspond to the transverse motion of the packet across the axis of the flow). The results obtained in our experiment X show linear instability regions followed by a strikingly new phenomenon - the fission of one vortex.

A transverse perturbation is given to vortex 4 (the fourth on the line) and it grows during $0 < t < 6.0$, while the centre of vortex 3 is slightly displaced downwards. The measured initial growth rate is

$$\lambda_m = 0.41 \ ,$$

smaller than the point vortex value of 0.59.

Qualitatively, one may explain this reduction by noting that the

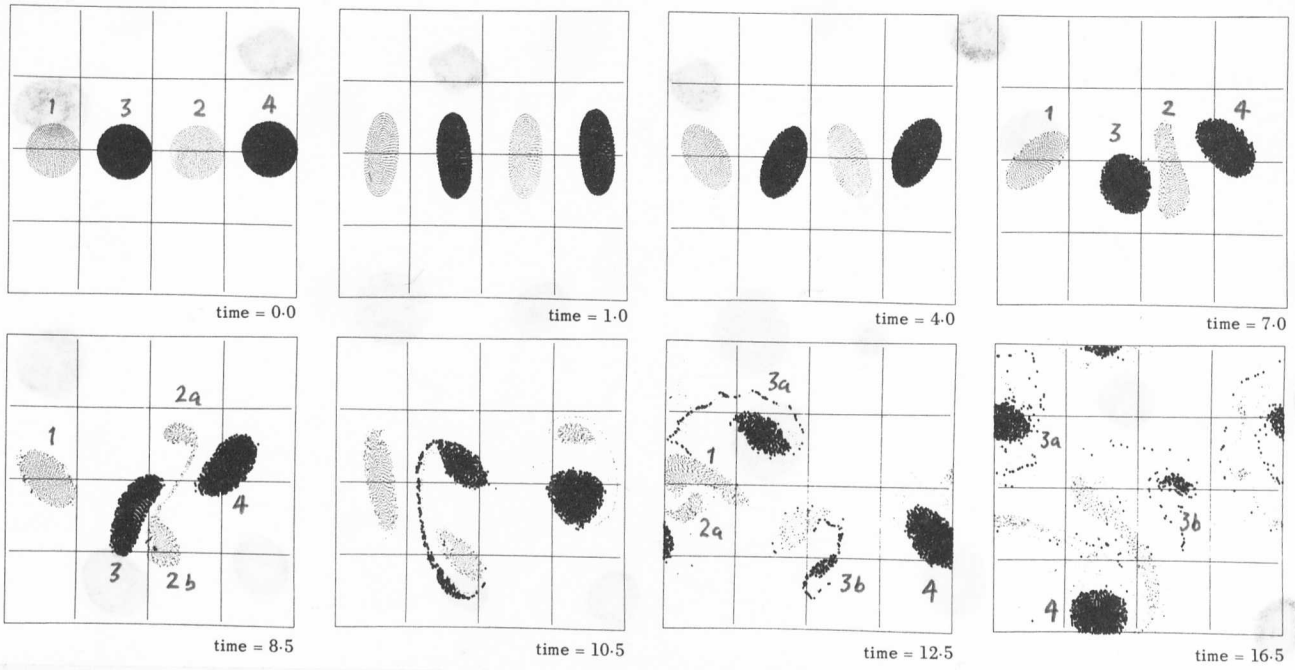

Figure 5.12. Experiment X. Large vortices. b/a = 0.0. Periodic y-boundaries.

outer areas of the collinear vortices are in spatial regions where the growth rate of a point vortex is smaller. That is, a first approximation to the growth rate of a finite-area system may be obtained by weighting the vorticity distribution with the growth rate due to that vorticity treated as a point-vortex system.

Strong m = 2 perturbances develop immediately because of the mutual interaction between vortices. Their period (measured during $0 < t < 4.0$) is about $4.0 - 4.5$. The increase over the period of small amplitude m = 2 modes on a non-interacting vortex ($T_{m=2} = 3.6 = 2\ T_o$) arises because of the close interaction with nearby vortices, i.e. a non-linear effect. At $5.0 < t < 7.0$ we see that oscillations of the high m-modes (mainly m = 2) are no longer in phase because the applied disturbance has become large. At $t = 7.0$ there is an explosive growth of the m = 2 mode on vortex 2 causing it to undergo a fission process. The upper fission product is left nearly free while the lower fission product is trapped below vortex 3. At $t = 12.5$ the upper fission product fuses with vortex 1 and much later at $t = 16.5$ the lower fission product fuses with vortex 1. At this time

we still have a fission product from vortex 3 in the centre of the frame.

The fission of large-area regions may be a common feature for collinear asymmetric streets and is the result of strong self-consistent vortex interactions. For smaller values of the interaction parameter $\eta = \frac{2R}{a}$ we get only the predicted m = 1 instability, followed by fusion as in experiments VI to IX. The initial amplitude of the standing wave is a function of η, e.g. $\psi_m \sim (\eta)^m e^{im\theta}$, where ψ_m is the stream function associated with mode m (we saw this in section 4.4 for the case of two interacting vortices). This means that the standing wave represents a physical system whose stability properties strongly depend on the amplitude of the wave; indeed a truly non-linear situation.

An obvious question can be posed: How does the slightly perturbed system evolve if $0 < b/a < .281$? If the perturbation to both upper vortices is small then both upper vortex regions will rise at a rate which decreases in time as they approach a "stable band" around 0.281. The assumption of a decreasing rate is consistent with the observed lower growth rate of the collinear finite-area street described above. It also accounts for the experimental observation shown by Wille (1960) in his Figure 3. There he presents a graph of the growth of a "corrected" ratio, $(b/a)_c$, versus distance behind a circular cylinder in water. The separation ratio begins at $(b/a)_c \approx 0.1$ and slowly grows to an asymptote $(b/a)_c = 0.37$. The $(b/a)_c$ ratio then seems to oscillate around the asymptote (we see a slight decrease followed by an increase). According to section 5.6, we conclude that the vortex regions are oscillating in a quasi-stable region. We are not sure if $(b/a)_c = 0.37$ is an estimate of the upper boundary of the "stable band" or whether there is a systematic error in reducing the data to $(b/a)_c$. Furthermore, if the perturbation is sufficiently non-uniform and/or strong, the rising vortex regions may

"pass through" the stable band and undergo fusion as described in section 5.6.

In sections 5.5 - 5.7 we have shown that the measured growth rates of finite-area vortex streets differ from those of corresponding point vortex systems (von Karman systems). For small and moderate areas the difference is weakly dependent upon area and shape, but strongly dependent upon $(b/a)_c$ as illustrated in Figure 5.13. In this figure we

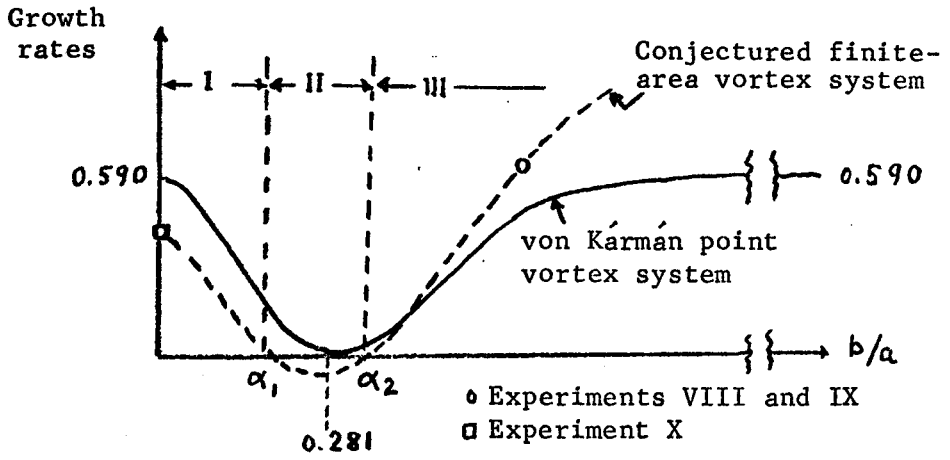

Figure 5.13. Perturbation theory growth rates: von Karman dispersion relation for asymmetric point vortex system compared with a corresponding moderate area system.

conjecture that there exists a region (α_1 , α_2) on the (b/a) axis

$$\alpha_1 < 0.281 < \alpha_2 \quad ,$$

where the growth rate is negative, that is, the presence of negative-energy modes on the surface of finite-area vortex systems is stabilizing. Furthermore, because the vorticity is distributed the growth rate is reduced in regions I and II and increased in region III.

In the initial phases of evolution of an unstable laminar shear profile we have also observed an enhanced transport of vorticity across the

dominant flow direction. This results from large-scale convection produced by vortex rotation (or "nutation"). As the vortex street is forming, small oppositely-signed ("secondary") vortices appear across the flow, as illustrated in Figure 5.3. Smoke or other contaminant particles will also undergo convective transport. These results are also consistent with experiment.

At long times, systems with b/a > 0.281 are unstable. Like-signed regions of vorticity attract and finally fuse (coalesce or "condense"). For a collinear asymmetric vortex street, we observed a linear growth phase followed by a rapid fission of one vortex, undoubtedly due to the high-shear field produced by the nearest-neighbour oppositely-signed vortex regions. This symmetry breakdown permits a rapid fusion of like-signed vortex regions at later time. These are strictly inviscid phenomena for they are in good agreement with those obtained previously by Zabusky, Deem et al, who solved the primitive Navier-Stokes equation with a high Reynolds number.

5.8 Approximated vortex flows arising from jets

We finish this chapter by studying a model that approximates the flows arising from jets which escape nozzles. In section 5.4 we saw how the vortex sheet generated at the nozzle wall rolls up to form vortices. In experiments I and XI we were primarily studying processes whose scale length was of the order or larger than the radius of the vortices formed. In Figure 5.14 we illustrate how the rolling-up process can be approximated by a simple vortex model that will elucidate the short scale length behaviour. The model is useful because linear stability theory of rotating fluids is applicable.

Laboratory experiments investigating the stability of free laminar boundary layers have been made by Wille (1952), Sato (1960), Michalke and

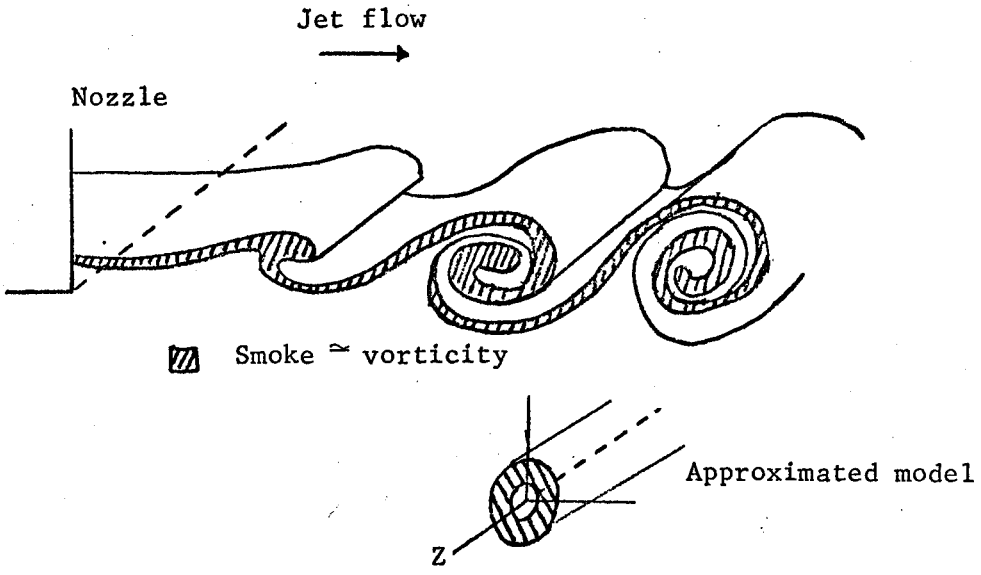

Figure 5.14. The rolling-up process of a free boundary layer and the approximated vortex model.
(Copy of Figure 1, Michalke and Timme, 1967)

Wille (1966) and Freymuth (1966). Experiments that are typically two-dimensional demonstrate how disturbed free boundary layers roll up into vortices. Analytical work by Michalke (1965) and Freymuth (1966) concludes that the formation of vortices (e.g. the rolling-up of the vortex sheet) is not essentially influenced by viscosity (high-R approximation). In the work of Michalke and Timme (1967) the approximated model of Figure 5.14 has been exposed to linear stability theory. Four types of vorticity distribution are considered (refer to Figure 5.14) (the fourth omitted here)

(1) Infinitely thin circular vortex sheet $(R_1 = R_2)$

(2) $\zeta_o = \zeta_1$ for $r \leq R_1$ $\quad \zeta_1 = \zeta_2$ for $R_1 < r \leq R_2$

(3) $\zeta = 0$ for $r \leq R_1$ $\quad \zeta = \zeta_o$ for $R_1 < r \leq R_2$.

The disturbance applied to these systems consists of polar harmonics (chapter 4) and it is found that case (1) is always unstable for $|m| \geq 1$. (2) and (3) are found to exhibit regimes of stability for each mode, that

is the growth rates (positive or negative) depend on $\gamma = \frac{R_1}{R_2}$ and $\xi = \frac{\zeta_1}{\zeta_2}$. (N.B. Michalke and Timme use (δ,γ) for our (ζ,ξ)). Their Figure 7 (p.660) shows the linear growth rates versus the mode number for the $\xi = 0$ case of interest to us. The smaller γ is (thin vortex ring) the more unstable the flow becomes (in the limit of course case (1)).

We have performed 4 numerical experiments on case (3), all with fixed y and x boundaries. 3002 positive point vortices are distributed in two different ways as described in chapter 3. The centre of the ring is placed in the centre of the square such that initially the effects from the images are highly reduced. In section 2.4 we estimated the contributions to the amplitudes a_m (m = 4, 8, 12 ... etc.) arising from the square boundary and found (section 2.9)

$$a_m = \frac{2m}{\zeta_o} b_m \qquad (5.12)$$

where

$$b_m = \frac{\Gamma}{4\pi} \frac{1}{2m} \left(\frac{r}{2L}\right)^{4m} .$$

Γ is the circulation (total vorticity) and 2L in this formula is the box length. Inserting for $\Gamma = \pi(R_2^2 - R_1^2)\zeta_o$ and setting $r = R_2$ thereby looking for the maximum amplitude we get

$$a_m = \frac{R_2^2 - R_1^2}{4} \left(\frac{R_2}{64}\right)^{4m} . \qquad (5.13)$$

An estimate for $R_2 = 12$ and $R_1 = 8$ gives $a_4 = 0.025$, that is a <u>finite</u> but small contribution (see later in this section).

The perturbation applied is random (section 3.6). In Table 5.3 we summarize the details of experiments XII to XV. T_o is the period of rotation occurring at $r = R_2$, i.e.

$$T_o = \frac{2\pi R_2}{v_\theta(R_2)} = \frac{4\pi}{\zeta_o} \frac{R_2^2}{R_2^2 - R_1^2} .$$

Expt. No.	R_1	R_2	Elapsed time T_E	No.of timesteps	T_E/T_o	ζ_o
XII	8	12	5.6	576	3.25	13.1
XIII	8	12	2.00	192	1.08	12.25
XIV	8	12	12.00	1152	6.48	12.25
XV	8	10	13.75	880	10.7	27.2

TABLE 5.3. Experiments on vortex ring distributions.

Experiments XII-XIV have the same geometrical dimensions, but XII has point vortices distributed at random inside the ring, whereas in experiments XIII and XIV we use the quiet start procedure (section 3.6). All 4 experiments are subject to the same random perturbation but in XII its amplitude is raised by a factor 5. In Figure 5.15 we display the time evolution of experiment XIV. Experiment XII evolves like XIV in the linear regime of time only with larger amplitudes. We shall not discuss the linear phase of evolution as it has been well described by Michalke and Timme (1967). For comparison with theory we evaluate the surface modes in experiment XIII by the method described in chapter 3.

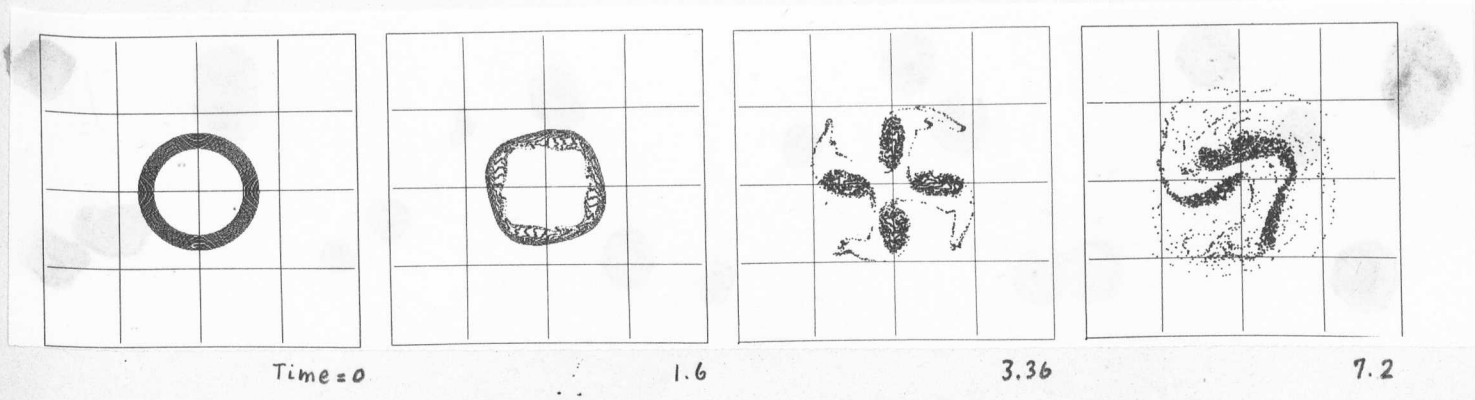

Figure 5.15. The vortex ring. Formation of 4 vortices. Experiment XIV.

The modes are measured at $r = R_2$ and in Figure 5.16 we show the time evolution of these modes for $m = 2,3,4$ and 5. The stability analysis by Michalke and Timme, which formally is the same as that of the laminar wakes (sections 5.3 and 5.4), yields the following expression for the exponential growth rates (perturbations are assumed to vary as $e^{im\theta+\sigma_m t}$)

$$\sigma_m = \frac{1}{4}\zeta_o\left[4\gamma^{2m} - (m(1-\gamma^2)^2\right]^{\frac{1}{2}} . \qquad (5.14)$$

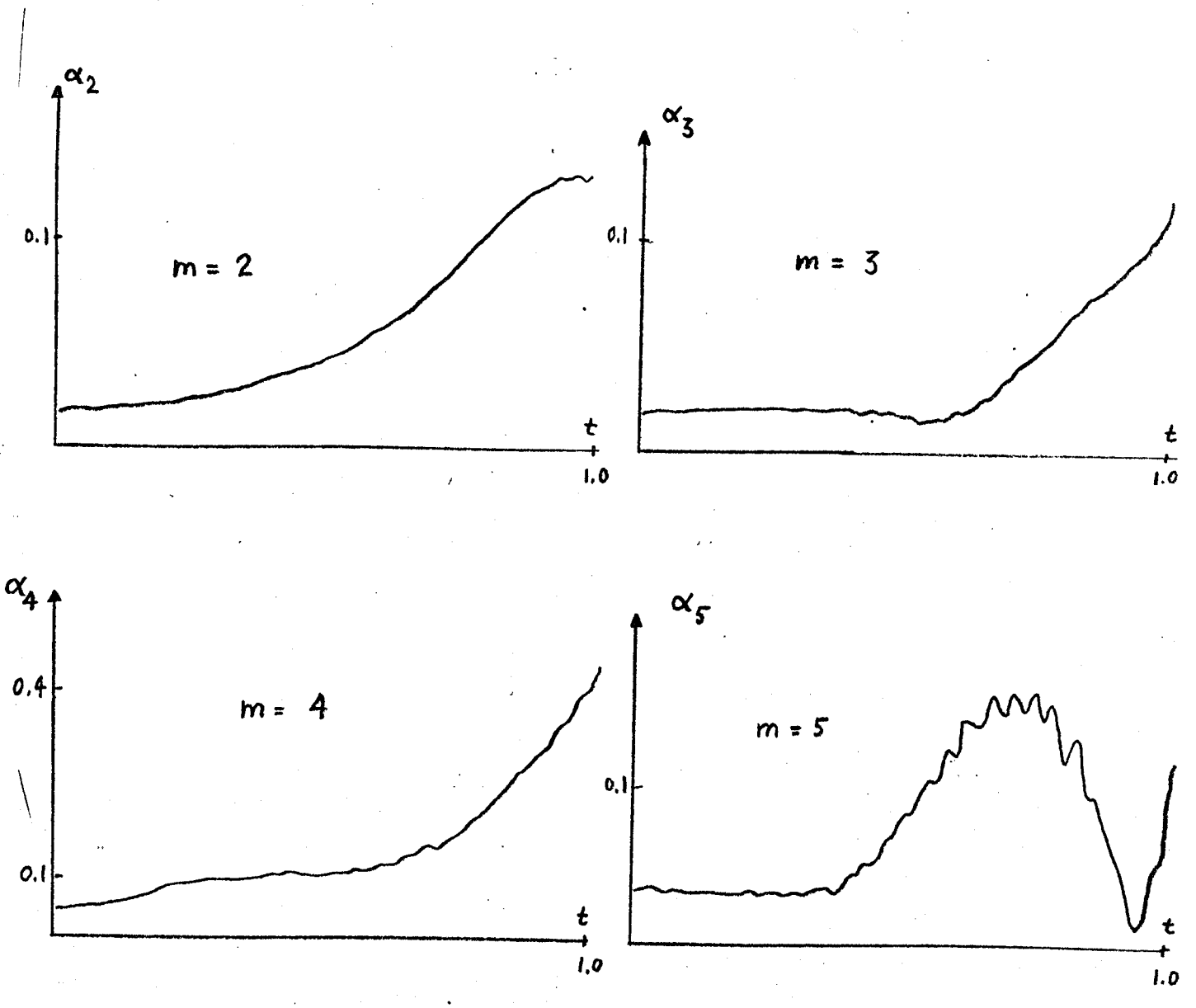

Figure 5.16. Growth of azimuthal modes in experiment XIII. The amplitude $|a_m|$ plotted versus time.

For $\gamma = \frac{8}{12}$, $\zeta_o = 12.25$ (experiment XIII) only $m = 3$ and $m = 4$ are unstable with $\sigma_3 = 1.45$ and $\sigma_4 = 1.00$. A comparison with Figure 5.16 reveals some discrepancy between theory and experiment. The initial growth rate of the $m = 4$ up to $t = 0.25$ is much larger than the theoretical value. On the other hand the $m = 3$ does not grow appreciably over the same time interval, whereas the $m = 2$ grows at the rate $\sigma_2 \approx 1.4$. We have no complete and satisfactory explanation for this disagreement. In deriving equation (5.14) no account has been taken of a finite-sized system or coupling between modes of different m. However the contribution to the $m = 4$ mode from the square boundary (equation 5.13) turns out to be of the same order as the initial value α_4 of the perturbation, probably enhancing the growth of the $m = 4$ mode. The coupling between the finite amplitude modes may also make the dynamics more complex, e.g. notice how all modes suddenly grow at a very high rate after $t = 0.5$.

When the perturbations have grown well into the non-linear regime it is eventually the growth of the $m = 4$ mode that causes 4 vortices to form. This happens at approximately $t = 2.0$ for experiment XII and $t = 2.5$ for experiment XIV. In both these experiments the vortex formation takes place after one and a half rotation periods T_o . For experiment XV with the thinner ring the growth is so fast that we have 4 vortices formed at $t = 1.0$, i.e. less than one rotation period ($T_o = 1.28$) of the ring. We have found a prominent lack of symmetry (4-fold) in experiment XII whereas both experiment XIV and XV show a 4-fold symmetry for long times. The difference occurs because of the different initial distributions of point vortices. In the experiments XII and XIV on thick rings we see how vortices fuse or coalesce to form elongated structures. In the final stage we have the core of the ring, which initially was at

rest, filled up with vorticity. To some approximation this core is undergoing a solid body rotation like a Rankine vortex. In experiments XII and XIV there is a fair amount of scattered point vortices whose motions are not adequately represented by the numerical scheme (see section 5.3).

In experiment XV the 4 vortices formed remain in a stable configuration for the whole of the run. These 4 finite-sized Rankine vortices persist despite the small-scale perturbations induced by the scattered point vortices. There are two different explanations for this result. In chapter 4 we learned that like-signed vortices will fuse if the interaction parameter η exceeds a certain value and the experiments of section 5.6 also demonstrated this. The area of the vortices formed depend on the ring thickness and in experiment XV the ring is so thin that the resultant η is not large enough for fusion to occur even in the presence of the small-scale perturbations. Experiments XII and XIV however yield η values that allow fusion to occur as a result of small-scale asymmetries.

A second explanation originates from the study by Morikawa and Swenson (1971) of a rotationally symmetric arrangement of N point vortices forming a polygon. Linear stability of this arrangement against random perturbations is found for the case $N \leq 5$. Their results could explain the behaviour observed in experiment XV especially since in the small value regions of η we have a better approximation to a point vortex configuration. We did actually carry out an experiment (code no.22 in Table A.3) starting with 4 like-signed Rankine vortices placed in azimuthally symmetric positions. The experiment was motivated by the final stage of experiment XV and the value of η was raised slightly. Apart from the development of surface modes $m = 2, 3, \ldots$ which oscillate we found stability with respect to the $m = 1$ mode forcing the

4 vortices round their mutual centre at a constant rate.

We can interpret experiments XII to XV as the collapse of a cylindrical vortex sheet or blanket such that downstream in flows from nozzles we encounter a break-up of the cylindrical vortex sheet. In the initial stages more fine-scaled structures (4 vortices) can be formed. Depending on the thickness of the sheet we see in the following stages a collapse of the fine-scaled structures which evolve into more coarse-grained structures. For thin sheets subject to small amplitude disturbances (experiment XV) the vortices arising from the linear instability persist, that is the advective motion admits their existence. Only viscous effects can change the pattern, so that much further downstream we may see the regular pattern of 4 vortices being disrupted by vorticity diffusing away from the core.

In summary, we have an interesting analogy between the evolution of the vortex ring distribution and the laminar distributions of sections 5.3 and 5.4. Both flows are linearly unstable and evolve into symmetric/asymmetric vortex structures respectively. The parameter γ of the vortex ring problem is analogous to the $(\frac{b}{a})$ parameter in that it determines whether the resulting vortex structure is stable against small-scale perturbations.

CONCLUSION

The impetus to work on establishing a general theory for two-dimensional phase fluids has arisen from observations made in numerical experiments performed by several authors in the field of Computational Physics. Numerical studies of non-linear phenomena in electrostatic and magnetized plasmas have demonstrated that it is often advantageous to base the interpretation of the results on the behaviour of the appropriate phase fluid. In a paper by Berk, Nielsen and Roberts (1970) attempts are made to generalize on the behaviour of 2-D classical phase fluids. We have pursued their investigations by choosing to study the behaviour of a 2-D ideal fluid, because its motion can be interpreted via that of a 2-D phase fluid, as we saw in chapter 1.

Two-dimensional phase fluids are idealized systems, but of interest to study in their own right. It has however not been possible to obtain a complete picture of this classical system although it was our main concern originally. Rather than presenting an incomplete theory we have chosen to describe numerical experiments and give the interpretation of these some relevance to reality.

The numerical model described in chapter 2 has been examined carefully in order to establish its limitations. We have chosen to work with this new model since any existing numerical model could not have produced the results presented in chapters 4 and 5. We feel confident that the model is capable of dealing with even more complex situations than those considered. Apart from being applied to the hydrodynamic studies presented in this thesis, the numerical model has been used by Taylor and McNamara (1971) and the Author and Taylor (1973) for studies of 2-D

guiding centre plasmas. Our experience and knowledge about this numerical model is thus based on a variety of situations. Although the numerical model is quite simple compared to many other models in use, we have nevertheless learned that it requires a substantial effort to employ the model on a computer and analyse the results. The account given in chapter 3 is deliberately made as short as possible and it is our hope that future work can be implemented with far less computational effort.

The non-linear dynamics of hydrodynamic flows cannot be described by existing analytical methods. In chapters 4 and 5 we have seen that a relatively simple numerical model can produce results which may explain many perplexing fluid flows. In order to understand such results it has been useful to work with Rankine vortices. The deformation of these vortices due to interactions with other vortices can conveniently be thought of in terms of negative energy waves, because both theory and numerical experiments can determine the time evolution of these waves. Agreement between the theory and the numerical experiments has been obtained within the linear regime of the time evolution of these waves. In the non-linear regime the numerical experiments have revealed new features of vortex flows: break-down or fission; coalescence or fusion of vortex regions; vortex streets arising from laminar flows; the rearrangement of vortices in vortex streets. These features are observed in laboratory experiments and we have attempted to draw comparisons between the numerical results and the experimental observations.

Our results indicate that further studies can be made with the existing combination of the numerical model and the methods for analysing the results. We believe that the work presented can evolve into two areas:

(a) The general study of 2-D phase fluids based on several different types of vorticity distribution. Some numerical experiment may produce the clues which can complete the understanding of the behaviour of 2-D phase fluids.

(b) The study of vortex flows with attempts to account for real effects such as viscosity or non-uniform vorticity distributions.

Both areas belong to Computational Physics and we hope that this thesis has indicated some of the benefits that can be derived from Computational Physics studies, thereby stimulating further research.

BIBLIOGRAPHY

The layout of references to literature follows the rules set by Journal of Fluid Mechanics. Publications of the 18th and 19th centuries are given in a comprehensive list by

> TRUESDELL, C, 1954. The kinematics of vorticity. Indiana University Press.

Three such references are included explicitly in the list given below.

ABERNATHY, F H and KRONAUER, R E, 1962. J.Fluid Mech. 13, 1.

BASSETT, A B, 1888. A treatise on hydrodynamics. Dover Publications Inc. (Corrected republication 1961).

BEAVERS, G S and WILSON, T A, 1970. Vortex growth in jets. J.Fluid Mech. 44, 97.

BERK, H L, NIELSEN, C E and ROBERTS, K V, 1970. Phys.Fluids 13, 980.

BORIS, J P and ROBERTS, K V, 1969. J.Comp.Phys. 4, 552.

BYERS, J A, 1969. Vol.II, paper 45 in the Proceedings of the Computational Physics Conference at Culham Laboratory, July 1969.

CHANDRASEKHAR, S, 1969. Hydrodynamics and hydrodynamic stability. Oxford University Press.

CHRISTIANSEN, J P and TAYLOR, J B, 1972. Numerical simulation of guiding-centre plasmas. To appear in Plasma Physics.

DEEM, G S, HARDIN, R and ZABUSKY, N J, 1971. Computer-generated film on instability and turbulence of two-dimensional incompressible fluids. Bell Laboratories (unpublished).

DE PACK, D C, 1962. J.Electronics Control 13, 417.

DORY, R A, 1964. J.Nuclear Energy (Pt.C) 6, 511.

DRAZIN, P G, 1958. J.Fluid Mech. 4, 214.

EMMONS, H W, 1970. Critique of Numerical Modelling in Fluid Dynamics Phenomena, Annual Review of Fluid Mechanics, vol.2, p.15. Editors M van Dyke, W G Vincenti and J V Wehausen. Annual Reviews Inc., Palo Alto, California.

FREYMUTH, P, 1966. J.Fluid Mech. 25, 683.

FROMM, J E and HARLOW, F H, 1963. Phys.Fluids 6, 975.

HADAMARD, J, 1901. Sur la propagation des ondes, Bull.Soc.Math.France, 29, 50.

HARLOW, F H, 1964. The particle-in-cell computing method for fluid dynamics. Methods in Computational Physics, 3, Fundamental Methods in Hydrodynamics. Editors B Alder, S Fernbach and M Rotenberg. Academic Press, New York, pp.319-343.

HARLOW, F H, 1970. Numerical methods for fluid dynamics, an annotated bibliography. Los Alamos Report LA-4821.

HELMHOLTZ, H , 1858. On integrals of the hydrodynamic equations, which express vortex motion. (Translation by P G Tait, 1867). Phil.Mag. 33, 485.

HOCKNEY, R W, 1965. J.A.C.M. 12, 95.

KADOMTSEV, B B and KOSTOMAROV, D P, 1972. Phys.Fluids 15, 1.

KELVIN, LORD, 1849. Notes on hydrodynamics (5), On the vis-viva of a liquid in motion. Cambr.Dubl.Math.J. 4, Papers 1, 107

KOCHIN, N E, KIBEL, I A and ROZE, N V, 1964. Theoretical hydromechanics, Interscience Publishers, John Wiley & Sons,Inc. New York.

KOOPMAN, G H, 1967. The vortex wake of vibrating cylinders at low Reynolds numbers. J.Fluid Mech. 28, 501.

KRAICHNAN, R, 1967. Phys.Fluids, 10, 1417.

LAGRANGE, J L, 1783. Mémoire sur la théorie du mouvement des fluides, Nouv.Mem.Acad. Berlin, 4, 695.

LAMB, H, 1932. Hydrodynamics. 6th edition. Cambridge University Press.

LEITH, C E, 1969. Numerical simulation of turbulent flow in properties of matter under unusual conditions. Editors H Mark and S Fernbach. Interscience, New York.

LIGHTHILL, M J, 1963. Introduction, Boundary layer theory in laminar boundary layers. Editor L Rosenhead. Clarendon Press, Oxford.

LIN, C C, 1943. On the motion of vortices in two dimensions. The University of Toronto Press.

LYNDEL-BELL, D, 1967. M.N.R.A.S. 136, 101.

METHODS OF COMPUTATIONAL PHYSICS, VOL.9, 1970. Editors Alder, Fernbach and Rotenberg. Articles by Dawson, Berk and Roberts, Byers and Killeen, Birdsall, Langdon and Okuda. Academic Press.

MICHALKE, A, 1965. J.Fluid Mech. 22, 371.

MICHALKE, A and WILLE, R, 1966. Applied Mechanics, Proceedings of the 11th Congress on Applied Mechanics, Munich 1964, pp.962. Editor H Görtler. Springer Verlag, Berlin.

MICHALKE, A and TIMME, A, 1967. F.Fluid Mech. 29, 647.

MORIKAWA, G, 1960. Journal of Meteorology, 17.

MORIKAWA, G and SWENSON, E V, 1971. Phys.Fluids 14, 1058.

ONSAGER, L, 1949. Nuovo Cimento, Suppl.VI, 279.

RICHTMEYER, R D and MORTON, K W, 1964. Difference methods for initial value problems. 2nd Ed. Interscience, New York.

ROSENHEAD, L, 1930. The spread of vorticity in the wake behind a cylinder. Proc.Roy.Soc. A. 127, 590.

ROSENHEAD, L, 1929. The Kármán street of vortices in a channel of finite breadth. Phil.Trans.A. 208, 275.

SATO, H and KURIKI, K, 1961. The mechanism of transition in the wake of a thin flat plate placed parallel to a uniform flow. J.Fluid Mech. 11, 321.

TAMEDA, S, 1959. Downstream development of wakes behind cylinders. J.Phys.Soc.Japan, 14, 843.

TAMEDA, S, 1965. Experimental investigation of vortex streets. J.Phys.Soc.Japan, 20, 1714.

TAYLOR, J B and McNAMARA, B, 1971. Phys.Fluids 14, 1492.

TING, L and TUNG, C, 1965. Phys.Fluids 8, 1039.

VON KÁRMÁN, T, 1911. Flüssigkeits u. Luftwiderstand. Phys.Zeitschr.XIII, 49.

WILLE, R, 1952. Jb.Schiffbautechn.Ges. 46, 174.

WILLE, R, 1960. Kármán vortex street. Advances in Applied Mechanics, VI, p.273. Editors H L Dryden and Th.von Kármán, Academic Press, New York.

ZABUSKY, N J and DEEM, G S, 1971. Dynamical evolution of two-dimensional unstable shear flows. J.Fluid Mech. 47, 353.

ZAROODNY, S J and GREENBERG, M D, 1972. On a vortex sheet approach to the numerical calculation of water waves. Submitted for publication in Journal of Computational Physics.

ZDRAVKOVICH, M M, 1968. Smoke observations of the wake of a group of three cylinders at low Reynolds number, J.Fluid Mech. 32, 339.

ZDRAVKOVICH, M M, 1969. Smoke observations of the formation of a Kármán vortex street, J.Fluid Mech. 37, 491.

APPENDIX

This appendix contains three tables listing computer codes and computer runs. A Culham Laboratory Research report is also included. This report presents the design and operation of the VORTEX computer code.

TABLE A.1.

The History of the VORTEX Code

Version	Design Period	Period of Operation	Special Features
Mk 0	Dec.68-Feb.69	March 69	Test of machine coding
Mk I	Mar.69-June 69	June 69-Apr.70	Clarified for documentation
Mk II	Apr.70-May 70	May 70-Jan.71	Mainly hydrodynamic runs
Mk III	Jan.71	Jan.71-Feb.72	Mainly runs on guding centre plasmas
Mk IV	June 71-Oct.71	Not used	Written in FORTRAN

TABLE A.2.

The Analyser Codes and their purpose

Name	Design Period	Ver-sions	Purpose
MARKER	May 69	2	Fluid motion by dummy particles
FERMI	June 69	2	Evaluates $\zeta = \zeta(\psi)$
SS-3D	June 69	1	3D plots of $\zeta(x,y)$ or $\psi(x,y)$
MODANA	Feb.70	2	Mode analyser
TELESCOPE	Feb.70	2	Magnifies pictures of $\zeta(x,y)$
CONTOURS	May 70	1	Plots the contours of constant ψ
SPECTRUM	June 70	1	Area function of the first kind $A_1(\zeta)$
TURBO 2	Feb.71	3	Correlation integral of charge fluctuations
SHOW	Apr.71	1	Displays the motion of an interface
LONG	Apr.71	1	Evaluates the length of an interface
TURBO 2	Dec.71	3	Correlation integral of charge fluctuations

TABLE A.3.

Complete list of Numerical Experiments carried out with the VORTEX code in the period Feb.69 - Jan.72

Project No.	No.of Experiments	No.of Simulations	No. of Analysis runs	Time Period	Category of expmt	Short description
0	3	4	5	July 70	N	Rankine's vortex tested
1	1	1	-	Apr. 69	T	Single vortex. TEST OF CODE
2	1	1	-	Feb. 69	T	Coalescing vortices. TEST OF CODE
3	3	7	5	Jan. 70	N	Kelvin-Helmholtz instability
* 4	4	11	2	Oct. 70	N	Vortex ring
* 5	12	20	31	June 69	N	Interaction between two like vortices
6	1	3	-	July 69	N	Chessboard distribution. Turbulence simulation
7	2	5	-	July 69	N	" " " "
* 8	3	13	4	Jan. 70	N	Formation of von Kármán vortex street
* 9	7	24	13	Dec. 69	N	Interaction between positive and negative vortex
10	4	12	4	Mar. 70	N	Kirchoff's elliptic vortex
12	1	1	3	Apr. 70	N	Attempt to find equilibrium from 9 (5)
13	2	2	2	Sept.70	N	Single vortex with large m = 2, m = 3 modes
*14	3	3	3	Sept.70	N	Rankine's vortex tested. dt varies
*15	3	3	2	Oct. 70	N	" " " Matching varied
*16	7	7	4	Oct. 70	N	" " " No time dependence
17	5	6	9	Mar. 71	F	Penetration of a slug
18	1	1	-	May 71	F	Random motion of blobs in open system
19	2	3	4	May 71	F	Motion of droplet
20	1	1	-	Apr. 71	F	NSFR Injection experiment
22	1	3	-	Oct. 71	N	Interaction between four vortices

23	1	4	-	Oct. 71	H	Interaction between vortex and a box
*24	5	10	-	Jan. 72	H	Vortex streets in closed systems
*25	5	14	-	Jan. 72	H	Vortex streets in open systems. Standing wave expmt.
P1	1	1	5	Feb. 71	P	Guiding centre plasma. Mesh 64 dt = 1
S1	7	7	53	Feb. 71	P	" " " " dt = 0.5
T1	4	16	33	Mar. 71	P	" " " " dt = 0.25
Q1	1	8	7	Apr. 71	P	" " " dt = 0.125
S2	1	2	6	Aug. 71	P	" " " Mesh 32 dt = 0.5
T2	1	4	6	Aug. 71	P	" " " Mesh 32 dt = 0.25
SME	12	72	72	Nov. 71	P	Single mode experiments for thermal start
THERMAL	5	7	4	Jan. 72	P	Guiding centre plasma in thermal equilibrium

N ~ Numerical analysis experiment
T ~ Test experiment
H ~ Hydrodynamic experiment
F ~ Fluid mechanics experiment
P ~ Guiding centre plasma experiment
* ~ Project described in this thesis

VORTEX

A 2-DIMENSIONAL HYDRODYNAMICS SIMULATION CODE

by

J.P. CHRISTIANSEN

A B S T R A C T

Program VORTEX is a computer code which simulates the behaviour of an incompressible, inviscid homogeneous fluid in two dimensions by following the motion of a large number of point vortices. A clarified, documented listing of the program is available in the Culham Library. The 1st edition of the program was completed in November, 1969, whilst the 2nd edition used at present was completed in May, 1970.

This report is written in two parts. Part I describes the theory behind the program and Part II describes the program itself. Part II could conveniently be read in conjunction with the clarified listing.

U.K.A.E.A., Research Group,
Culham Laboratory,
Abingdon,
Berks.

July, 1970.

C O N T E N T S

INTRODUCTION

Although the basic equations of hydrodynamics have been studied for many years[1,2], their complexity sets a limit to the types of problems that can be solved analytically. In some cases relatively simple non-linear stationary flow patterns can be realized, in which the parameters that describe the physical systems are independent of time. In other cases the interest lies in the stability properties of such a stationary flow pattern, that is, whether or not it is able to sustain itself against small variations in certain of the characteristics parameters. To solve this type of problem one normally applies perturbation theory, in order to predict whether or not the original equilibrium is linearly stable. A theoretical analysis of this kind can follow the history of a fluid system in the linear regime, when the perturbation amplitudes are small, but because the equations of hydrodynamics are non-linear it is of considerable interest to study its history in the subsequent large amplitude regime. One way of doing this is to simulate the time behaviour of a mathematical model of the fluid on a computer. This report describes one of the various alternative methods by which a computer simulation can be carried out.

PART I: HYDRODYNAMIC MODEL

1. HAMILTONIAN EQUATIONS OF MOTION

The basic equations governing the time behaviour of an incompressible, inviscid, homogeneous fluid in purely 2-dimensional motion are

$$\underline{\nabla} \cdot \underline{u} = 0 \tag{1.1}$$

$$\frac{\partial \underline{u}}{\partial t} + \underline{u} \cdot \nabla \underline{u} = - \frac{1}{\rho_o} \nabla P \tag{1.2}$$

where $\underline{u}$ is the fluid velocity, ρ_o is the density and P the pressure. It has been pointed out by Onzager[10], and more recently by Morikawa[16], that these equations can be expressed in Hamiltonian form, with the spatial coordinates x, y playing the part of conjugate coordinates and momenta q, p. To see this we write

$$\underline{u} = \underline{\nabla} \times H \tag{1.3}$$

$$f = \underline{\nabla} \times \underline{u} \tag{1.4}$$

where the Hamiltonian H is the usual stream function, and f is the vorticity. Then eqs.(1.2) and (1.3) combined with (1.4) give

$$\nabla^2 H = - f \tag{1.5}$$

$$\frac{\partial f}{\partial t} + \underline{u} \cdot \nabla f \equiv \frac{\partial f}{\partial t} + [f, H] = 0 \tag{1.6}$$

Eq.(1.6) is Liouville's equation in Poisson-bracket form*, and the Hamiltonian H is to be obtained by solving Poisson's equation (1.5).

---

* For any two functions A, B, the Poisson bracket is defined by

$$[A, B] = \frac{\partial A}{\partial q} \frac{\partial B}{\partial p} - \frac{\partial B}{\partial q} \frac{\partial A}{\partial p}$$

2. INVARIANTS OF THE MOTION

Because the fluid system we are considering is not interacting with any other physical system there are no dissipative phenomena. Hence the total energy E is an invariant of the motion and this energy is purely kinetic

$$E = \tfrac{1}{2} \rho_o \int_R \underline{u} \cdot \underline{u} \, dS \tag{2.1}$$

or if we integrate by parts using (1.3 and (1.4)

$$E = - \tfrac{1}{2} \rho_o \int_R f \, H \, dS \tag{2.2}$$

The expression (2.2) is valid provided that

$$\int_C H \frac{\partial H}{\partial h} \, ds = 0 \tag{2.3}$$

where C is a contour bounding the region of integration R.
Because the scalar vorticity f is convected with the moving incompressible fluid, there is an infinite number of other invariants

$$A(f) \, df \tag{2.4}$$

expressing the area between moving contours of constant f, $f + df$. In most of the cases which we study, only part of the fluid has vorticity different from zero, and then this fluid has constant total area.

$$= \int_{f_{min}}^{\infty} A(f) \, df \tag{2.5}$$

Real space acts as a phase space for the system with the coordinates (x, y) or (q, p) conjugated through

$$\dot{x} = \dot{q} = \frac{\partial H}{\partial p} = \frac{\partial H}{\partial y} \quad , \quad \dot{y} = \dot{p} = - \frac{\partial H}{\partial q} = - \frac{\partial H}{\partial x} \tag{2.6}$$

Hamiltonian notation will be used throughout this report to emphasize the true structure of the equations, but another simplication that should be pointed out is that the Hamiltonian is invariant under rotations and translations of the (q, p) plane, which are of course just rotations and translations of the real 2-dimensional space. This degree of symmetry is unusual in Hamiltonian mechanics, and should introduce simplification, (as compared to Vlasov's equation in plasma physics, for example).

Our present understanding of the significance of this Hamiltonian formulation of 2D fluid dynamics may be explained in the following way. There are two great independent classical formalisms which involve the motion of incompressible fluids:

I. Hamiltonian theory, (phase fluids)

II. Vortex theory, [1,18] (real fluids).

Hamiltonian theory is intimately related to statistical mechanics, (both Maxwell-Boltzmann and Lynden-Bell[15]), vortex theory is related to the theory of fluid turbulence. Any connection between the two theories would be of great interest, however, and while the ideas of turbulence theory are currently being applied to phase fluids (e.g. in plasma physics), those of statistical mechanics are being applied to hydrodynamic turbulence.

(a) In the case of Vlasov's equation for particles interacting in n-dimensional configuration space, it is useful to study the incompressible motion of a self-interacting phase fluid[18] in an $m = 2n$-dimensional phase space, $n = 1, 2, 3$. The distribution function f is always a <u>scalar</u>, and m must be <u>even</u>. Classical statistical mechanics can be applied to the particles, and Lynden-Bell theory[15] to the phase fluid.

(b) In fluid dynamics, one can have incompressible inviscid motion in any number of dimensions $m = 1, 2, 3$, and the <u>vorticity</u> plays a significant role.

(c) For the particular case $m = 2$, the two types of formalism are in close correspondence, with the scalar vorticity f playing the part of the distribution function. Lynden-Bell theory can be applied to continuous distributions of vorticity, and Maxwell-Boltzmann theory to collections of point vortices.

(d) For the physically more significant case $m = 3$, ordinary Hamiltonian theory cannot be applied, because the number of dimensions is <u>odd</u> and the vorticity is a <u>vector</u>; one is studying the interaction of a collection of vortex tubes, rather than point vortices. Nevertheless it would be interesting to look for some generalization of Hamiltonian dynamics to this case, and the rewards might be great if statistical mechanics could also be successfully generalized.

3. POINT VORTICES

One way of following the motion of the fluid is to compute the time behaviour of two functions, the vorticity $f(q, p, t)$ and the Hamiltonian $H(q, p, t)$. These can be represented on a discrete mesh, as in the method of Fromm and Harlow[5]. Another technique is to calculate the motion of a limited number of point vortices, interacting with each other via their individual 2-body velocity potentials. This was done by Abernathy and Kronauer[6] in their study of the formation of a von Karman Vortex Street. A third possibility is to follow the motion of contours f = constant. This has been done successfully in plasma physics for the analogous case of the 1-dimensional Vlasov equation by Roberts and Berk[7], who used the 'waterbag' model earlier adopted by de Pack[8] and Dory[9], in which f is everywhere either a constant f_0, or zero. An assumption of a similar type, (vorticity constant or zero), has been made by many workers in hydrodynamics. Extensions of the Roberts-Berk method in the vortex case would involve changes in their program, but would be an interesting problem to try.

The method used in the VORTEX program, and reported briefly by Christiansen and Roberts[11,12] is more analogous to the particle methods used in plasma physics. It approximates f by a large number of point vortices:

$$f = \sum_{i=1}^{N} f_i \, \delta(q - q_i) \, \delta(p - p_i) \qquad (3.1)$$

where $f_i = +1$ or -1, interacting via a self-consistent velocity field. Each set of coordinates (q_i, p_i) is called a point vortex and satisfies the equations of motion

$$\dot{q}_i = \frac{\partial H}{\partial p_i} \qquad \dot{p}_i = -\frac{\partial H}{\partial q_i} \tag{3.2}$$

where H is the solution of Poissons equation (1.5) with f obtained from eq.(3.1);

$$H = -\sum_{\substack{i=1 \\ i\neq j}}^{N} \sum_{j=1}^{N} f_i f_j \log r_{ij} \tag{3.3}$$

with

$$r_{ij}^2 = (q_i - q_j)^2 + (p_i - p_j)^2 \,. \tag{3.4}$$

The infinite 'self energy' of a point vortex is excluded. The problem is thus reduced to solving eqs.(3.1), (3.2) and (3.3).

4. THE REGION OF CALCULATION AND ITS BOUNDARY CONDITIONS

For practical reasons we shall restrict ourselves to considering a square region in (q, p) or (x, y) space. Three types of boundary conditions are of interest:

A. H constant along a boundary, i.e. the boundary is a streamline.

B. $\frac{\partial H}{\partial n} = 0$ along a boundary, i.e. the boundary is perpendicular to all streamlines.

C. H is a periodic function.

These three conditions can be imposed separately on the x and y boundaries and therefore combine to give 9 possible sets of boundary conditions. The square region is covered by a square mesh of size 64×64.

A hydrodynamic fluid which is incompressible, inviscid and homogeneous is not entirely realistic in a physical sense, but it is mathematically convenient for two reasons; firstly because it provides a model for turbulent flows in the limit of infinite Reynolds number, and secondly because (in 2 dimensions) the system obeys classical Hamiltonian dynamics, so that a good deal of existing dynamical theory is likely to be applicable.

The basic hydrodynamic system, which obeys the partially differential equations (1.5) and (1.6), is a classical Hamiltonian system with an infinite number of degrees of freedom because of the continuous nature of the fluid. Such systems are well known, (the most familiar example being the classical electromagnetic field), and when interacting with systems with a finite number of degrees of freedom they give rise to interesting phenomena such as the ultra-violet catastrophe. By itself, however, a classical system with an infinite number of degrees of freedom behaves in a self-consistent way.

Compared to the exact physical system, the numerical model which is used to approximate it has three principal limitations:

I. The finite number of point vortices used to approximate f (eq.3.1).

II. The use of a discrete mesh.

III. The choice of boundary conditions.

I and II are of a practical nature and can be improved upon by increasing N (the number of point vortices) and M (the number of meshpoints). The simplified boundary conditions which are used facilitate the coding and speed up the program, but because of the square region of calculation, small m = 4 perturbations are produced in rotationally symmetric problems. A physically more realistic choice of boundary conditions would be problem dependence, more difficult to code and more time-consuming in execution.
The computer model described in this note has been used at Culham to simulate some 10 different problems, and there seems to be no reason why many other interesting hydrodynamic problems could not be solved in this way.

5. DIFFERENCE FORMULATION OF THE EQUATIONS

Since the calculation takes place on a mesh we approximate all space derivatives by finite differences.

Suppose that f is given at all the meshpoints (section 7). Instead of solving eq.(3.3) we solve Poisson's equation according to:

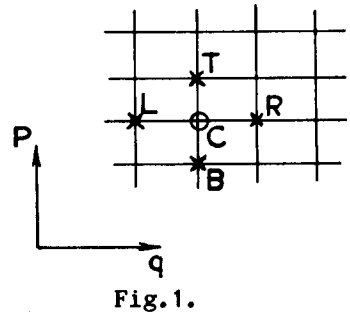

Fig.1.

$$\frac{H_T + H_B - 2H_C}{(\Delta p)^2} + \frac{H_R + H_L - 2H_C}{(\Delta q)^2} = - f_C \qquad (5.1)$$

where the suffices are explained in Fig.1. Equations (5.1) is solved by the "Hockney-Poisson solver" program[13,14] using a fast Fourier transform and recursive cyclic reduction technique and will not be dealt with further here.

Equation (3.2) becomes

$$\dot{q}_C = \frac{H_T - H_B}{2\Delta p} \qquad \dot{p}_C = \frac{H_L - H_R}{2\Delta q} \qquad (5.2)$$

6. LEAPFROG TIME INTEGRATION SCHEME

In order to integrate eq.(5.2) in time we simply write

$$\frac{q(t+\Delta t) - q(t-\Delta t)}{2\Delta t} = q(t) \qquad (6.1)$$

and similarly for p. (A first-order integration would be too inaccurate, as explained in Section 11A). Thus if f, (and hence the Hamiltonian H and the velocity fields $\frac{\partial H}{\partial p}, -\frac{\partial H}{\partial q}\Big)$, as well as vortex positions q, p are known at time t, we can advance the positions from $t - \Delta t$ to $t + \Delta t$. This is done by introducing 2 sets of point vortices whose positions are defined at even times $t = 2n\Delta t$ and odd times $t = (2n+1)\Delta t$ respectively. Each set of vortices determines the values of f(t), H(t) and hence the velocity fields which are used to move the other set.

Referring to Fig.2, we can write eq.(6.1) for the even coordinates q_e as follows, (and similarly for p_e, and for q_o, p_o):

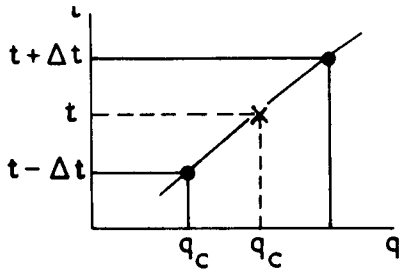

Fig.2.

$$q_e(t+\Delta t) = q_e(t-\Delta t) + \dot{q}_o(q_C, p_C, t) \cdot 2\Delta t \qquad (6.2)$$

where q_C, p_C are the vortex coordinates at the 'central' time t.

However, there are several ways of finding q_C and p_C in order to obtain a time and space - centred approximation.

The most straightforward and best known method is the leapfrog scheme, in which q_C, p_C are simply the coordinates of the odd set of particles, from which the velocity fields q_o, p_o themselves are determined. Another method used in program VORTEX (Section 9) is a Taylor-expansion scheme, in which q_C, p_C are computed from the even particle coordinates at time $t - \Delta t$, by the preliminary calculation

$$q_C(t) = q_e(t-\Delta t) + q_o(q_e(t-\Delta t), p_e(t-\Delta t), t)\ \Delta t \qquad (6.3)$$

The leapfrog method is normally used in VORTEX, but the more elaborate Taylor-expansion scheme can be embedded in the code without difficulty. Both schemes are weakly unstable because the odd and even vortices gradually get out of step. This problem is studied in Section 8, and a 'matching' procedure used to remove incipient instabilities is described in Section 9.

7. AREA-WEIGHTING OR NEAREST-GRID-POINT APPROXIMATIONS

From the vector N_{qp} containing N sets of particle coordinates (q, p) we construct a mesh or grid function f_{ij}. To do this, the 'charge' associated with each point vortex must be allocated to the surrounding grid points in a prescribed way. Two standard methods are mentioned here:

Nearest-grid-point approximation

The region is divided up into square cells (Fig.3). All the charge belonging to a point vortex is allocated to the grid-point at the centre of the cell in which the vortex lies.

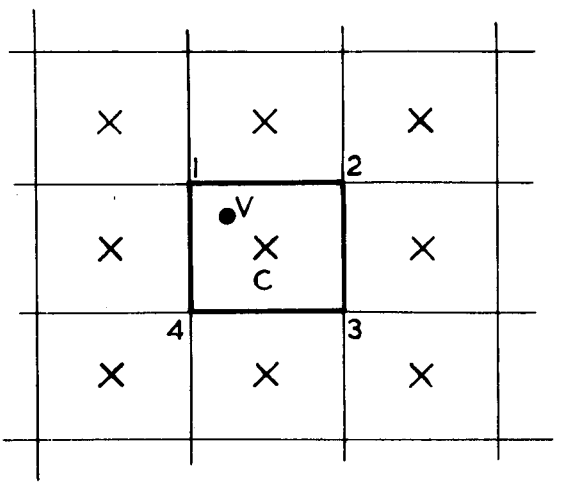

Fig.3. All the charge associated with a vortex V inside the cell 1234 is credited to the grid point C.

Area-weighting approximation

The point vortex is imagined to be replaced by a space vortex of uniform vorticity, whose size and orientation are the same as those if the grid cells. It will then overlap 1, 2, 3, or 4 grid cells. (Fig.4). Its charge is allocated to the centres of the cells which it overlaps, the weighting field being given by the areas of overlap. If the cells have unit dimension and (α,β) are the coordinates of V relative to D, then the weighting factors are:

A	$(1-\alpha)\beta$
B	$\alpha\beta$
C	$\alpha(1-\beta)$
D	$(1-\alpha)(1-\beta)$

(7.1)

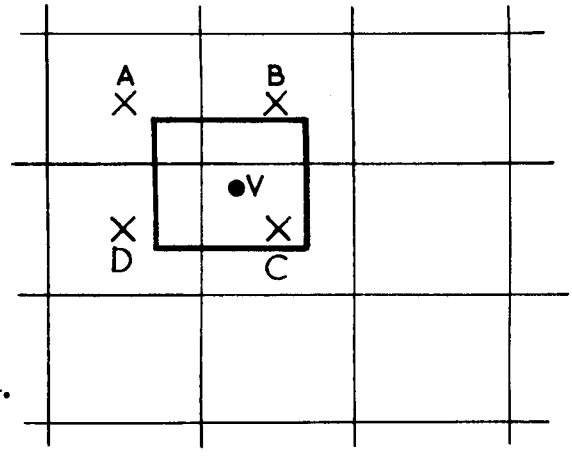

Fig.4.

Program VORTEX uses this second method which provides a higher accuracy, although at an increased cost in computer time.

8. STABILITY OF THE DIFFERENCE SCHEME

Care is needed to prevent the odd and even vortices getting out of step. Fig.5. shows a streamline on which the "correct" position of point vortices are marked. $\underline{\underline{\bullet}}$ is an "even" point, i.e. at a time $t + 2n\Delta t$.
$\underline{\underline{o}}$ is an "odd" point, i.e. at a time $t + (2n+1)\Delta t$.

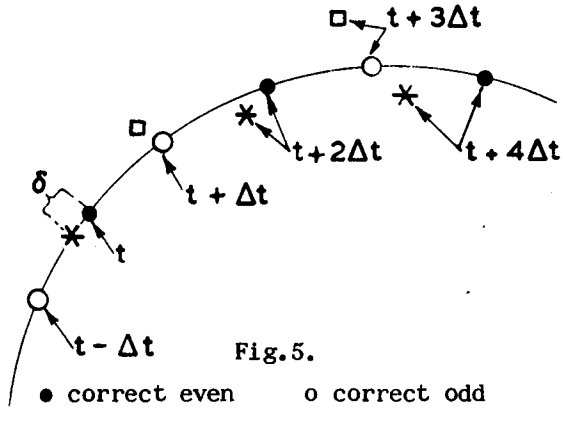

Fig.5.

● correct even o correct odd
□ calculated even * calculated odd

In order to examine the numerical stability of the calculation we write eq.(6.1) for both the odd and even positions and form the limit $\Delta t \to 0$. Setting $\underline{r} = (q, p)$ we get

$$\frac{d\underline{r}_e}{dt} = \dot{\underline{r}}\,(\underline{r}_C) \qquad \frac{d\underline{r}_o}{dt} = \dot{\underline{r}}\,(r_C) \tag{8.1}$$

where $\underline{r}_C$ is the position at which the velocities are evaluated. This $\underline{r}_C$ is assumed to deviate from the correct value R_C.

Leapfrog scheme

$$\text{Suppose} \quad \underline{r}_e = \underline{R}_C + \underline{\delta} \quad \text{and} \quad \underline{r}_o = \underline{R}_C - \underline{\delta} \tag{8.2}$$

and consider the motion in a specified velocity field, independent of the vortex particles.

Inserting (8.2) in eq.(8.1) we have:

$$\frac{d(\underline{R}_C + \underline{\delta})}{dt} = \dot{\underline{r}}\ (\underline{R}_C - \underline{\delta}), \quad \frac{d(\underline{R}_C - \underline{\delta})}{dt} = \dot{\underline{r}}\ (\underline{R}_C + \underline{\delta})\ . \tag{8.3}$$

Subtraction gives

$$\frac{d\underline{\delta}}{dt} = - \frac{\partial \dot{\underline{r}}}{\partial t} \underline{\delta} \ , \tag{8.4}$$

or

$$\left.\begin{aligned} \frac{d\delta_q}{dt} &= - \frac{\partial \dot{q}(\underline{R}_C)}{\partial q} \delta q - \frac{\partial \dot{q}(R_C)}{\partial p} \delta p \ , \\ \frac{d\delta_p}{dt} &= - \frac{\partial \dot{p}(R_C)}{\partial q} \delta q - \frac{\partial \dot{p}(R_C)}{\partial p} \delta p \ . \end{aligned}\right\} \tag{8.5}$$

Setting $u_q = \dot{q}$, $u_p = \dot{p}$, and using eqs.(1.1) and (1.3), eq.(8.5) becomes

$$\left.\begin{aligned} \frac{d\delta_q}{dt} &= - \frac{\partial u_q}{\partial q} \delta q - \frac{\partial u_q}{\partial p} \delta p \ , \\ \frac{d\delta_p}{dt} &= - \left(f + \frac{\partial u_q}{\partial p} \right) \delta q + \frac{\partial u_q}{\partial q} \delta p \ . \end{aligned}\right\} \tag{8.6}$$

At this stage we must specify the kind of velocity field which is being studied. If we assume a stationary state, eqs.(8.6) can be integrated in time. We can set $\delta_p = \delta_q = \delta \, e^{i\delta t}$, the eigenvalues being given by

$$\delta^2 = - \left(\frac{\partial u_q}{\partial q} \right)^2 - \left(\frac{\partial u_q}{\partial p} \right)^2 - f \frac{\partial u_q}{\partial p} \tag{8.7}$$

Numerical stability requires $\delta^2 \geqslant 0$.

As an example we look at a rotational flow where $\underline{u} = (u_q , u_p) = \omega(\underline{r}) \times \underline{r}$, $\omega = (0,0,\omega)$ being the angular frequency of rotation, and $\underline{r}$ the radius vector.

Since $f = 2 \omega(\underline{r}) + |\underline{r}| \frac{d\omega}{dr}$, eq.(8.7) gives

$$\omega^2 \left[1 + \frac{1}{\omega} r \frac{d\omega}{dr} \right] \geqslant 0 \quad \text{or} \quad r \frac{d \, \ell_n \omega}{dr} \geqslant - 1 \tag{8.8}$$

Hence for $\omega(r)$ varying as r^n the stability condition is

$$n \geqslant - 1 \tag{8.9}$$

corresponding to

$$\left.\begin{aligned} \delta &= \pm \omega \sqrt{n+1} \ , \qquad n \geqslant - 1 \ , \\ \delta &= \pm \omega \sqrt{|n| - 1} \ , \quad n \leqslant - 1 \ . \end{aligned}\right\} \tag{8.10}$$

The amplification of δ during one rotation is $\exp(2\pi \sqrt{|n| - 1})$. From this we conclude that since in regions where $f = 0$ ω will very often vary as r^{-2}, whilst in regions where $f \neq 0$ ω will predominently vary as r^2, numerical instabilities will occur at the border between these regions over a time period in which $\frac{\partial u_q}{\partial q}$, $\frac{\partial u_q}{\partial p}$ and f do not change significantly. It is therefore necessary to prevent numerical instabilities from dominating the motion of the point vortices.

9. THE MATCHING PROCEDURE

Figure 6 shows, (in an exaggerated way), how the odd and even positions can "get out of step".
To prevent this from becoming too serious we stop the integration periodically, and readjust the positions of the vortices.

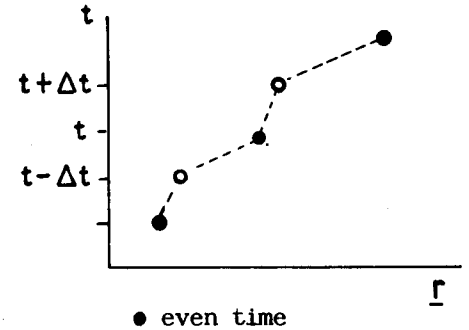

● even time
o odd time Fig.6.

If the calculation is stopped at time t we know $\underline{r}_e(t)$ and $\underline{r}_o(t - \Delta t)$. We form

$$\underline{r}_C(t - \tfrac{\Delta t}{2}) = \tfrac{1}{2}(\underline{r}_e(t) + \underline{r}_o(t - \Delta t)). \tag{9.1}$$

We then calculate $f(t - \frac{\Delta t}{2})$ as explained in Section 7, and solve for $H(t - \frac{\Delta t}{2})$ using the potential-solver. From eqs.(5.2) we find $\underline{u}_C(t - \frac{\Delta t}{2})$ and define a <u>new</u> set of positions at time $t - \Delta t$ and t respectively:

$$\tilde{\underline{r}}_o(t - \Delta t) = \underline{r}_C(t - \tfrac{\Delta t}{2}) - \underline{u}_C(t - \tfrac{\Delta t}{2}, \underline{r}_C)\,\tfrac{\Delta t}{2} \tag{9.2}$$

$$\tilde{\underline{r}}_e(t) \quad = \underline{r}_C(t - \tfrac{\Delta t}{2}) + \underline{u}_C(t - \tfrac{\Delta t}{2}, \underline{r}_C)\,\tfrac{\Delta t}{2} \tag{9.3}$$

So that the positions are displaced symmetrically about $\underline{r}_C$ as shown in Fig.7.

We notice that the procedure is only correct to second order in t, because the chosen central velocity $\underline{u}_C$ is <u>not</u> the space-time averaged value over the interval $\frac{\Delta t}{2}$.

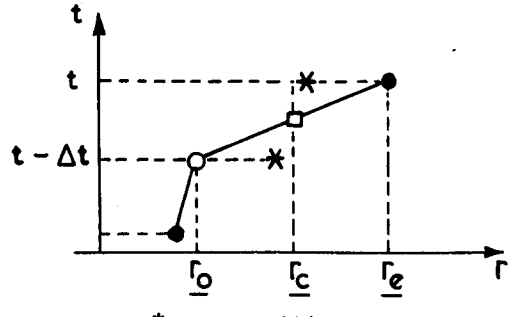

Fig.7. * new positions
□ calculated centre position

We can illustrate the use of this procedure by estimating the number of timesteps M between successive "matching of positions" which will achieve adequate accuracy. We noticed in Section 8 that amplification during one rotation using the leapfrog scheme was

$$\exp(2\pi\sqrt{|n| - 1}) = \exp(2\pi)$$

for $n = -2$. As an example we consider a circular cloud of vorticity of radius R, so that the time for one rotation is $2\pi R/V_R$. For reasons of accuracy we require $\delta M\,\Delta t \approx 1$, so that the time between successive matchings is $\approx R/V_R$. Typically V_R is chosen to be $\lambda/\Delta t$ where $\lambda = \frac{1}{4} - \frac{1}{2}$ the mesh spacing, and R is say 8, so that M is of order

$$M \approx \frac{R}{\lambda} \tag{9.4}$$

or say 16-32.

In the second edition of VORTEX the centring and matching procedures have been improved to reduce the amplitudes of computational modes.

Suppose as before that at time t we know $\underline{r}_C(t)$, $\underline{r}_o(t - \frac{\Delta t}{2})$ and $\underline{u}(t - \frac{\Delta t}{2})$. We then form:

$$\underline{r}'_o(t - \frac{\Delta t}{4}) = \underline{r}_o(t - \frac{\Delta t}{2}) + \underline{u}(t - \frac{\Delta t}{2}\ \ \underline{r}_o)\ \ \frac{\Delta t}{4} \tag{9.5}$$

corresponding to a motion along the tangent at $t = t - \frac{\Delta t}{2}$.

As before we form

$$\underline{r}_C(t - \frac{\Delta t}{4}) = \tfrac{1}{2}(\underline{r}_e(t) + \underline{r}_o(t - \frac{\Delta t}{2})) \tag{9.6}$$

having preserved the set positions $\underline{r}_o(t - \frac{\Delta t}{2})$. As a centre position we then average $\underline{r}'_o$ and $\underline{r}_C$ according to

$$\underline{r}_{CN}(t - \frac{\Delta t}{4}) = \tfrac{1}{2}(\underline{r}_C(t - \frac{\Delta t}{4}) + \underline{r}'_o(t - \frac{\Delta t}{4})) \tag{9.7}$$

From $\underline{r}_{CN}$ we calculate $f_{CN}(t - \frac{\Delta t}{4})$, $H_{CN}(t - \frac{\Delta t}{4})$ and $\underline{u}_{CN}(t - \frac{\Delta t}{4})$. To separate odd and even positions from $\underline{r}_{CN}$ we now use the Taylor-Expansion scheme (eq.6.3), that is we find

$$\underline{r}_1(t - \frac{\Delta t}{8}) = \underline{r}_{CN}(t - \frac{\Delta t}{4}) + \underline{u}_{CN}(t - \frac{\Delta t}{4}, \underline{r}_{CN}) \cdot \frac{\Delta t}{8} \tag{9.8}$$

$$\underline{r}_2(t - \frac{3\Delta t}{8}) = \underline{r}_{CN}(t - \frac{\Delta t}{4}) - \underline{u}_{CN}(t - \frac{\Delta t}{4}, \underline{r}_{CN})\ \frac{\Delta t}{8} \tag{9.9}$$

The new set of positions at $t = t$ (even) and $t = t - \frac{\Delta t}{2}$ (odd) are then in turn found from

$$\tilde{\underline{r}}_e(t) = \underline{r}_{CN}(t - \frac{\Delta t}{4}) + \underline{u}_{CN}(t - \frac{\Delta t}{4}, \underline{r}_1 \cdot \frac{\Delta t}{4} \tag{9.10}$$

$$\tilde{\underline{r}}_o(t - \frac{\Delta t}{2}) = \underline{r}_{CN}(t - \frac{\Delta t}{4}) - \underline{u}_{CN}(t - \frac{\Delta t}{4}, \underline{r}_2) \cdot \frac{\Delta t}{4} \tag{9.11}$$

These two improvements have proved useful when testing the program on a single circular vortex. Because the positions found from eqs.(9.2), (9.3) are correct to first order only they will introduce an expansion δ_i of a circular vortex when applied for the first order time ($\underline{r}_C$ being the initial position). For a circular vortex (see Fig.8) this expansion is approximately

$\delta_i \approx R \cdot \frac{1}{2}\,(u\,\frac{\Delta t}{4} \cdot \frac{1}{2\pi R})^2$. With $R = 7.2$,

$\mu \cdot \Delta t = 0.6$, (the values used in the numerical experiment), we get $\delta_i \simeq 1.4 \cdot 10^{-4}$, which is in agreement with the measured value $1.45 \cdot 10^{-4}$. The new centring (eq.9.7) puts however $\delta_i = 0$.

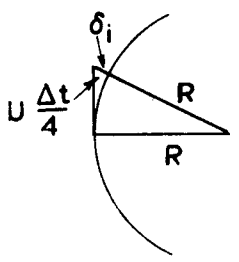

Fig.8.

10. INACCURACIES IN THE DIFFERENCE SCHEME

Although the time integration can be made sufficiently accurate for $\Delta t \to 0$, the integration of eqs.(3.2) and (3.3) as approximated by eqs.(5.1) and (5.2) introduces a

significant overall inaccuracy.

Consider a vorticity distribution

$$f = \cos \frac{2\pi k q}{N} \tag{10.1}$$

where N is the number of meshpoints in the q-direction. The analytical solution to eq.(3.2) is

$$H = \left(\frac{N}{2\pi k}\right)^2 \cos \frac{2\pi k q}{N} \tag{10.2}$$

Inserting (10.2) in (5.1) we get for $\Delta q = 1$,

$$\frac{\Delta^2 H}{(\Delta q)^2} = \left(\frac{N}{2\pi k}\right)^2 \left(\cos\left(-\frac{2\pi k}{N}\right) + \cos\frac{2\pi k}{N} - 2\right)\Big) = f_\Delta \tag{10.3}$$

Comparing f and f_Δ we see that

$$D = \frac{f_\Delta}{f} = \left(\frac{N}{2\pi k}\right)^2 2\,(1 - \cos\frac{2\pi k}{N}) \tag{10.4}$$

Program VORTEX uses $N = 64$. From (10.4) we can calculate the truncation of a mode and as examples we get

k-value	ratio	error
k = 1	D = 0.999	-
k = 4	D = 0.99	1 %
k = 8	D = 0.955	4.5 %
k = 16	D = 0.815	19.5 %
k = 32	D = 0.405	59.5 %

The approximation (5.2) will truncate the higher harmonics in a similar way.

The truncation errors become significant in regions where $\frac{\partial f}{\partial q}$, $\frac{\partial f}{\partial p}$ are large. In program VORTEX we normally consider distributions in f which are Heaviside functions. This means that at the borders where ∇f is very large (theoretically infinite) care must be taken to observe whether or not "diffusion" occurs because of the numerical instabilities which are likely to arise there.

11. TEST RUNS WITH VORTEX

It is important to carry out controlled numerical experiments on simulation codes, both to eliminate programming errors and also to determine the accuracy of the difference approximations. Testing a computer simulation code is often very difficult because of the number of parameters involved, as well as the range of values which they can take. A meaningful series of tests would comprise a suite of "like" runs in which each parameter is varied independently. It therefore seems appropriate to record our experience with the VORTEX code, for a number of successful and unsuccessful runs. This section will deal with a number of numerical tests, and the starting point is a very simple problem.

One Circular Vortex

Consider a circular vortex of radius R. The velocity field due to this vortex is

$$V_\theta = \tfrac{1}{2} F_0 r \ , \ V_r = 0, \ (0 \leqslant r \leqslant R),$$

$$V_\theta = \tfrac{1}{2} F_0 \frac{R^2}{r} \ , \ V_r = 0, \ (R \leqslant r < \infty).$$

where F_0 is the total vorticity defined by $F_0 = \pi R^2 f_0$, f_0 being the constant vorticity density. This system is in stable equilibrium. Program VORTEX has simulated this situation in a variety of ways.

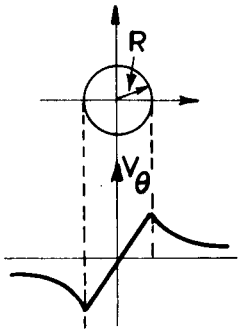

Fig.9.

A. First order time integration, nearest grid point approximation

The vorticity distribution is set up by distributing point vortices at random within a circle of radius R. After approximately 200 timesteps with $\Delta t = 0.50$ the circle has expanded to twice its original radius, thus showing the necessity of using a better scheme.

B. Second order scheme, (Taylor-expansion scheme), nearest grid point approximation

The vorticity distribution is set up as in A. After approximately 250 timesteps with $\Delta t = 0.25$ (2nd order) the original circular shape is still retained. However the energy has decreased by 6%, and the enstrophy (vorticity squared) by a similar amount. The nearest grid point approximation cannot conserve energy sufficiently well and it introduces fluctuations which can be interpreted as "numerical viscosity". Particle trajectories are not exactly circles.

C. Second order scheme (leapfrog), with area-weighting

The vorticity distribution is set up as in A. The circular shape is still retained after 100 timesteps with $\Delta t = 0.25$. The energy shows a variation of about 0.6%, a considerable improvement on B. The random distribution however still introduces fluctuations although the area-weighting implies a smoothing of the distribution, (truncation of higher harmonics).

D. Second order scheme (leapfrog), area-weighting

In this case a uniform f_0 is set up by distributing points on equidistantly spaced concentric circles. 1000 timesteps with $\Delta t = 0.25$ have been calculated. Energy varies by $\sim 0.02\%$ between its maximum and minimum values, an improvement from C, while the enstrophy varies by 0.06%. Each circle of points retains its shape virtually unaltered until 600-700 timesteps have elapsed. The area and circumference of the outer circle have been examined by an analyser program. The result is that the area as function of time oscillates with an amplitude of order 10^{-5} and a period of order 0.1 - 0.2 T, where T is the rotation time for the vortex ($T = \frac{4\pi}{F_0}$). The circumference as a function of time oscillates in a similar way. The conclusion is that a number of "false" m modes ($e^{im\theta}$) are being superimposed by the approximations which have been made. Because of the square shaped region of calculation (see Fig.I) the equilibrium streamlines will not be circles. All modes $m = 4, 8, 12, 16, \ldots\ldots$ will therefore be present as false modes and a quantitive estimate by an analysis program (MODANA) reveals that the amplitudes of these modes grow from 0.02 ($t = 0$) to 0.3 ($t = 2T$) in units of one mesh cell. Other modes $m = 1, 2, 3, 5, 6, 7, 9$ have amplitude less than 0.001. A comparison between the initial state (Fig.II)

and the state after 750 timesteps (Fig.III), which is approximately 5 revolutions of the circular vortex, shows how the circumference has changed. Since the amplitudes of a mode m varies as r^m the effect should be more pronounced at larger r values. A boundary particle will be displaced $\delta\underline{r}$ from r = R because the hodograph for the present problem is not a circle. $\delta\underline{r}$ is initially of order 0.002 if R = 7.2, i.e. $\frac{\delta r}{R} \approx 3\ 10^{-4}$. δr will however increase with time (Section 8) until matching is applied. If this is done every 16 timesteps $\delta\ r/_R$ might on average be of order 10^{-3}. After 10^3 timesteps a particle is therefore likely to have arrived at a position which is off by an amount up to 1 mesh cell. Experience with this run, as well as with a number of related simulations, suggests that the code can be run for 500 - 750 timesteps with $\langle \underline{u} \cdot \frac{\Delta t}{2} \rangle = \frac{1}{4}$ before accumulation of errors become too significant. In other words when a particle on average has travelled a distance of the order 2 - 3 period the accumulated errors can be of the order of cell-length. In the example with the circular vortex $\langle \underline{u} \cdot \frac{\Delta t}{2} \rangle = 0.3$, so that $(\underline{u} \cdot \frac{\Delta t}{2})_{max} = 0.6$ at the boundary of the vortex.

Two Circular Vortices

A more complex problem is the flow generated by two finite vortices of the same or opposite polarity, both being initially circular. Depending on parameters such as the relative polarity, radius, separation distance etc, a situation can arise in which the system takes up a stable large-amplitude oscillatory state. Such a case has been simulated by setting up a distribution of vorticity similar to that of D. It is found that, while energy is conserved to within 10^{-4} over 700 - 1000 timesteps, the enstrophy and the energy of the point vortices oscillate with a definite period, the period of the system. This latter effect is due to the finite number of point vortices

12. CONCLUDING REMARKS

Program VORTEX has at present simulated 10 different hydrodynamic problems with a variety of data. These problems are being examined analytically and results generated by the program as well as by a suite of analyser programs are being studied to explain the behaviour of the computer model used. The outcome of this work will be published elsewhere, but it may be mentioned that the following physical situations have been studied:

1. Kelvin - Helmholtz instability.
2. Formation of a Karman Vortex street.
3. Interaction between two circular clouds of vorticity.
4. Simulation of turbulence problems.
5. Kirchoffs elliptic vortex.
6. Mode - mode coupling on the surface of a circular vortex.

The program has also been used by J.B. Taylor and B. McNamara to simulate the diffusion of plasma in two dimensions using the guiding centre model.

PART II. THE COMPUTER CODE

13. INTRODUCTION

This second part is best read in conjunction with the clarified documented listing which is available in the Culham Library, or from the author. Lists of subroutines and variables as well as numbering of routines will not be given here. It is thus assumed that

the reader is familiar with the notation of the program, and names and symbols will be used without any further explanation.

In the following two sections the structure of the program is explained by diagrams which should not need further comments.

Section 16 explains the printed output which is normally produced by the program, while Section 17 explains briefly the input required. Section 18 discusses the techniques used for coding, mainly the Usercode portion of the program (KDF9 assembler language), and Section 20 describes a suite of analyser programs some of which have been clarified. Listings are available in the Culham Library, or from the author.

14. BLOCK STRUCTURE

Broadly speaking program VORTEX can be divided into 8 blocks or sections as shown on the next page apart from Block VIII. These blocks are centred around subroutines with the following names:

I	MAIN
II	F DATA
III	INITAL
IV	CHECK
V	START
VI	COTROL
VII	CONVEC

Block VIII includes several segments.

15. FLOW DIAGRAMS

On the following pages we show the logical structure of each block by means of flow diagrams. On the left are written the names and numbers of the routines concerned, together with the page number of each routine in the clarified listing. Routines are either written in FORTRAN, ALGOL or KDF9 USERCODE. Two segments need further explanation. POT1 is the Hockney-Poisson solver program which is described elsewhere[14]. MOVIE is the high-speed movie-making package written by J.P. Boris and P. Hodges. Neither of these are included in the listing of the program. At the end of the clarified listing there is a subroutine map or 'program tree' which will help the understanding of the flow diagrams.

16. OUTPUT FROM PROGRAM

The clarified listing includes a test run with typical output generated by the code. This output can be divided into 2 parts:

I. Diagnostic comments during initialisation, starting, and closing down of a run.

II. Diagnostic results as the simulation proceeds.

Part I consists of labelling the job, checking the number of point vortices and checking the value of the timestep DT. 5 pages with results from initialisation, a test run (automatically performed) and the starting conditions follow, and a page with the values of certain common variables completes the first part of the output.
Part II consists of information which is printed before and after each matching has occurred. This printout is performed by routine MPRINT which also produces the 5 pages mentioned above.

I. OVERALL FLOW DIAGRAM

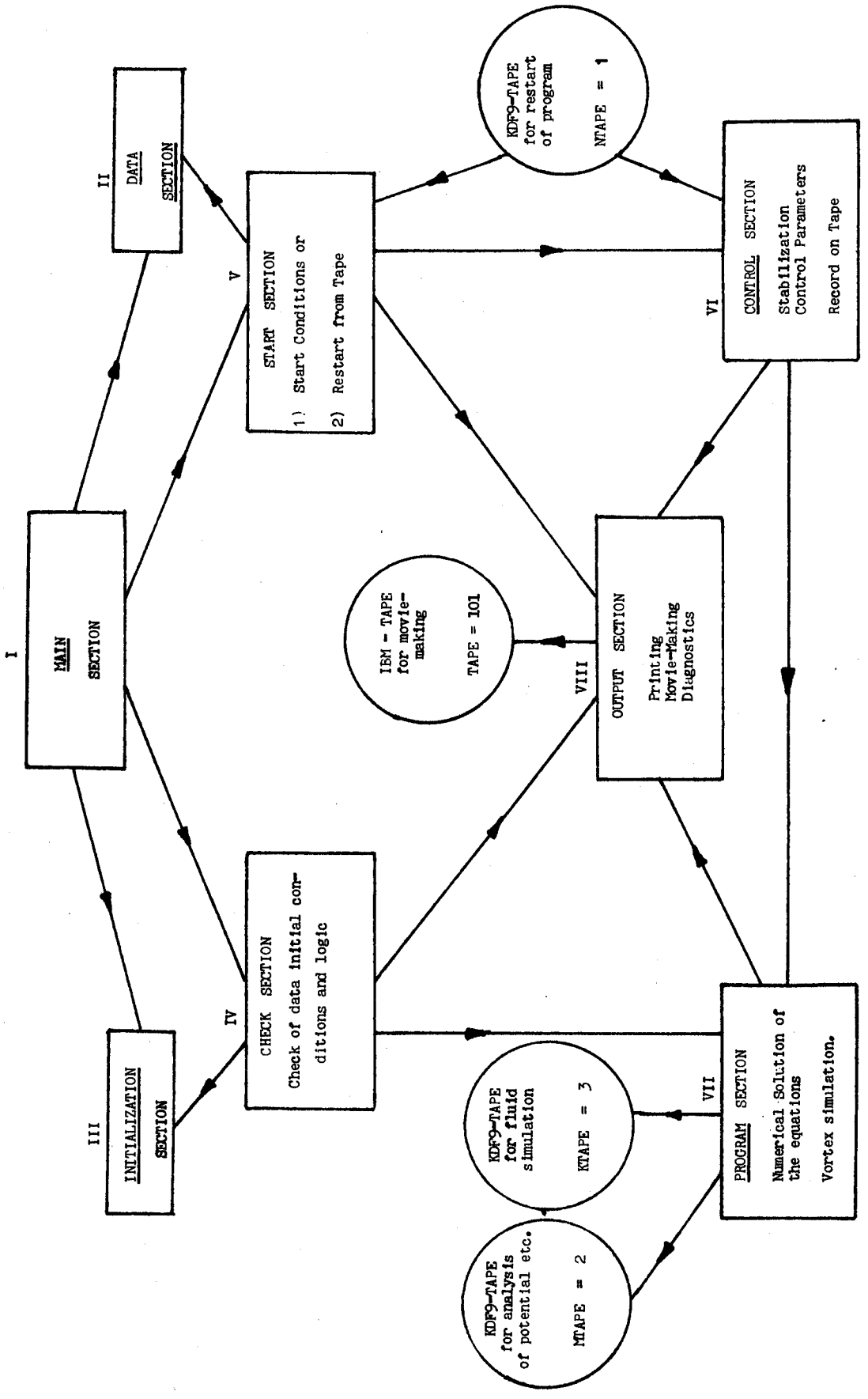

II. DATA

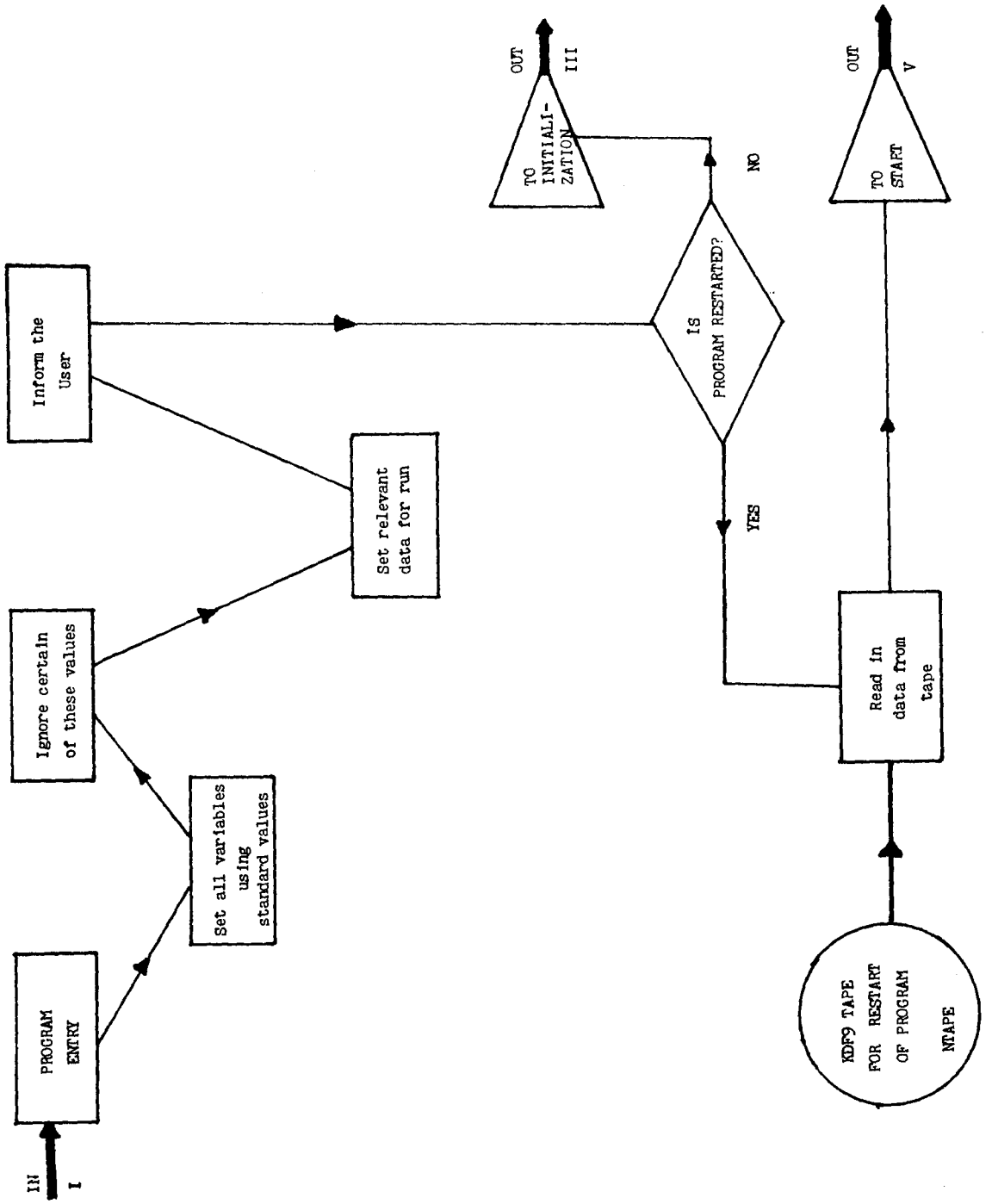
IN
I
PROGRAM ENTRY
Set all variables using standard values
Ignore certain of these values
Inform the User
Set relevant data for run
IS PROGRAM RESTARTED?
NO
YES
OUT
III
TO INITIALI-ZATION
OUT
V
TO START
Read in data from tape
KDF9 TAPE FOR RESTART OF PROGRAM
NTAPE
1. MAIN
20. IGNORE
32. FDATA
21. INITAL
1 MAIN
25 START

III. INITIALIZATION

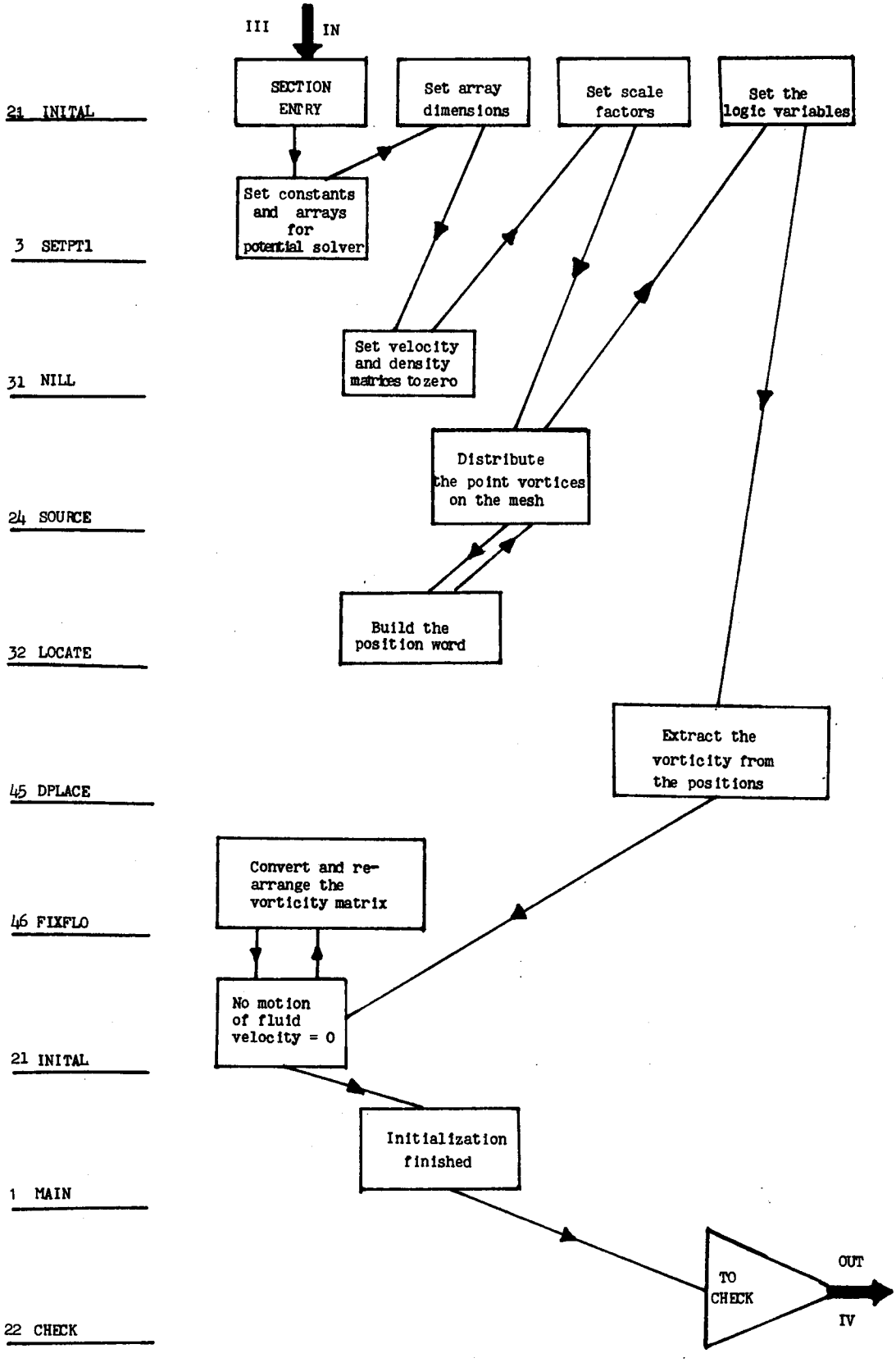

IV. CHECK 'a'

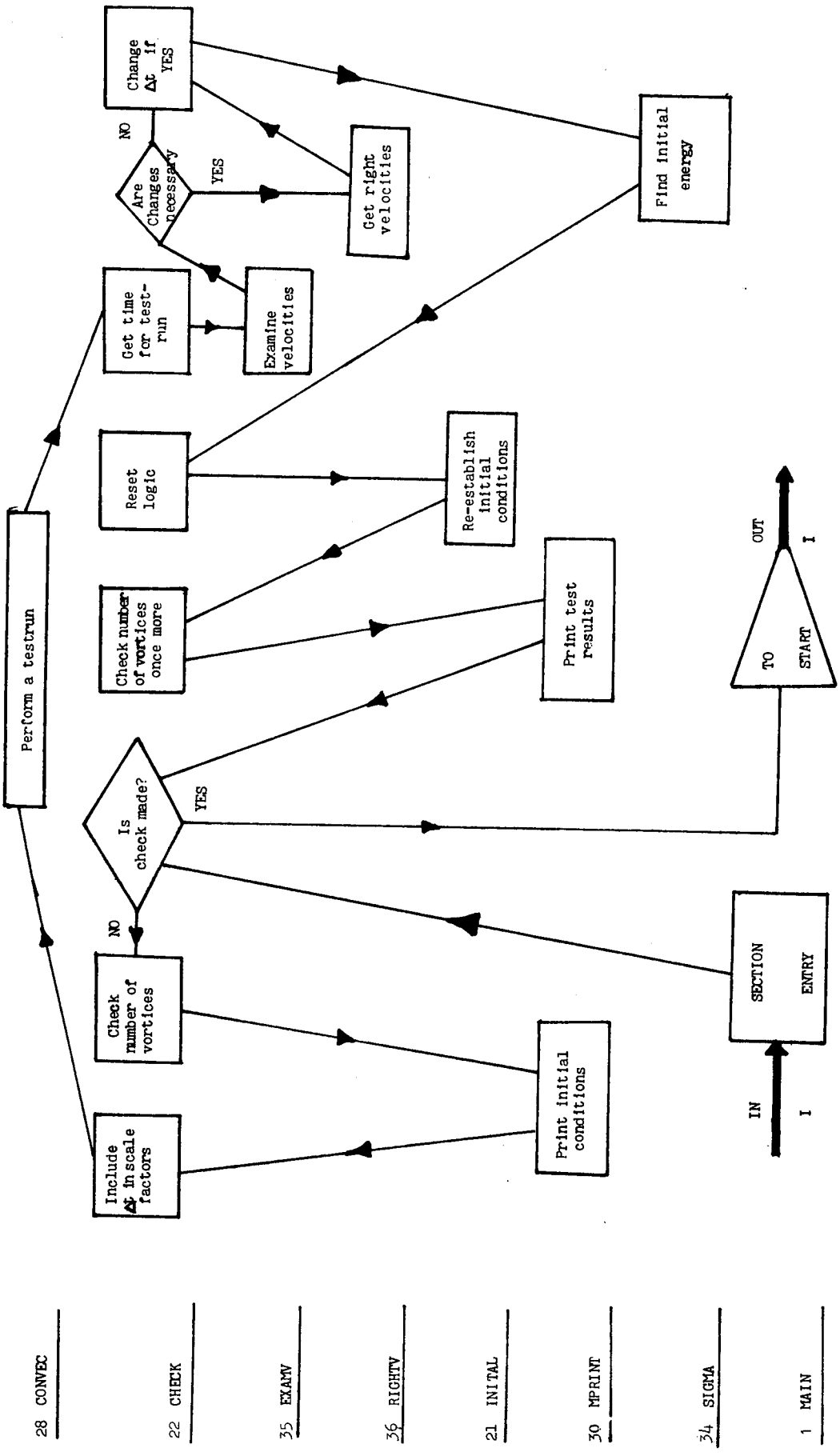
Change Δt if YES
NO
Are Changes necessary
YES
Get right velocities
Find initial energy
Get time for test-run
Examine velocities
Reset logic
Re-establish initial conditions
Perform a testrun
Check number of vortices once more
Print test results
OUT
I
TO
START
Is check made?
YES
NO
Check number of vortices
SECTION
ENTRY
Include Δ scale factors
Print initial conditions
IN
I
28 CONVEC
22 CHECK
35 EXAMV
36 RIGHTV
21 INITAL
30 MPRINT
34 SIGMA
1 MAIN

IV. CHECK 'b'

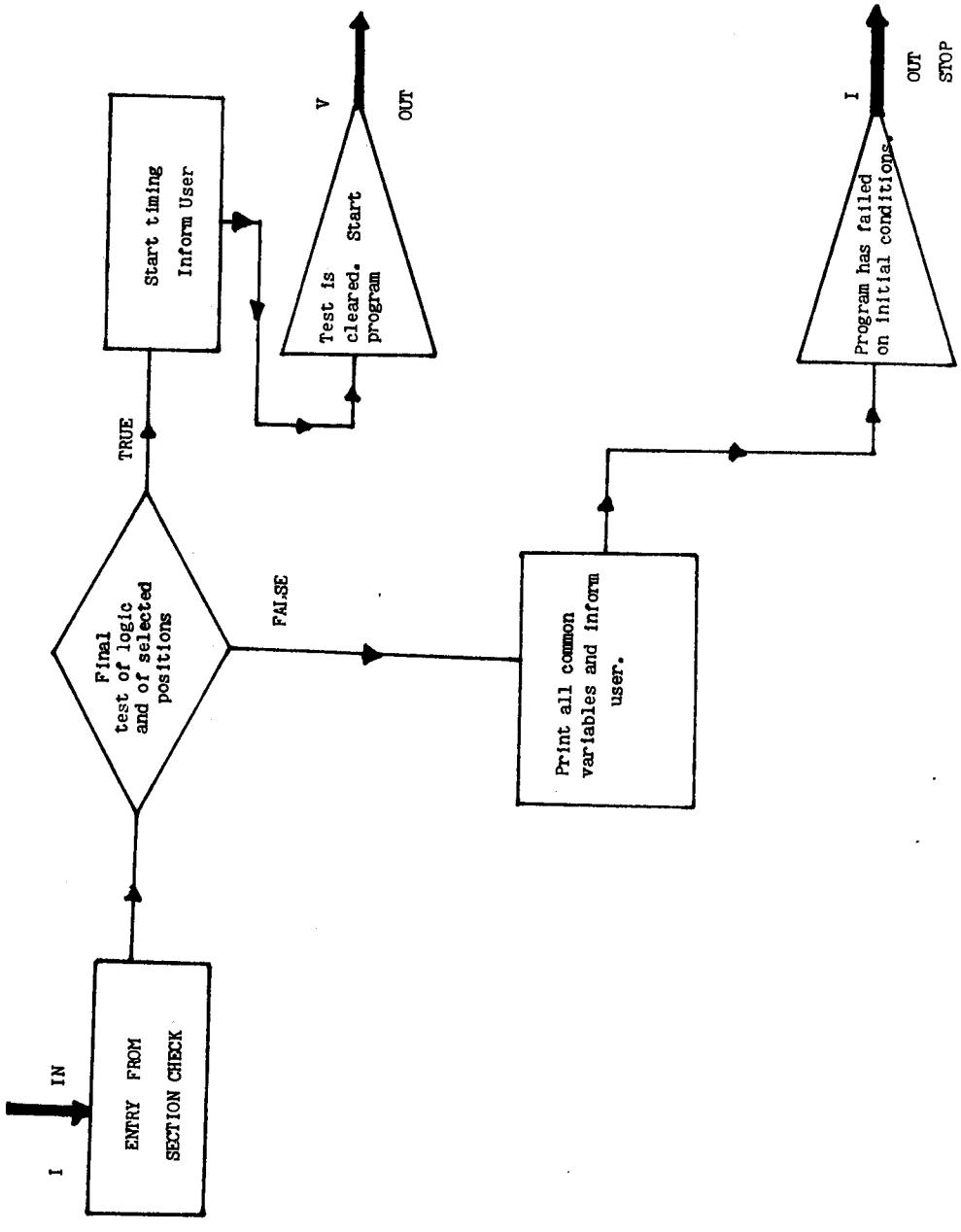

1. MAIN

25. START

23. CLIST

EXIT STOP

V. START

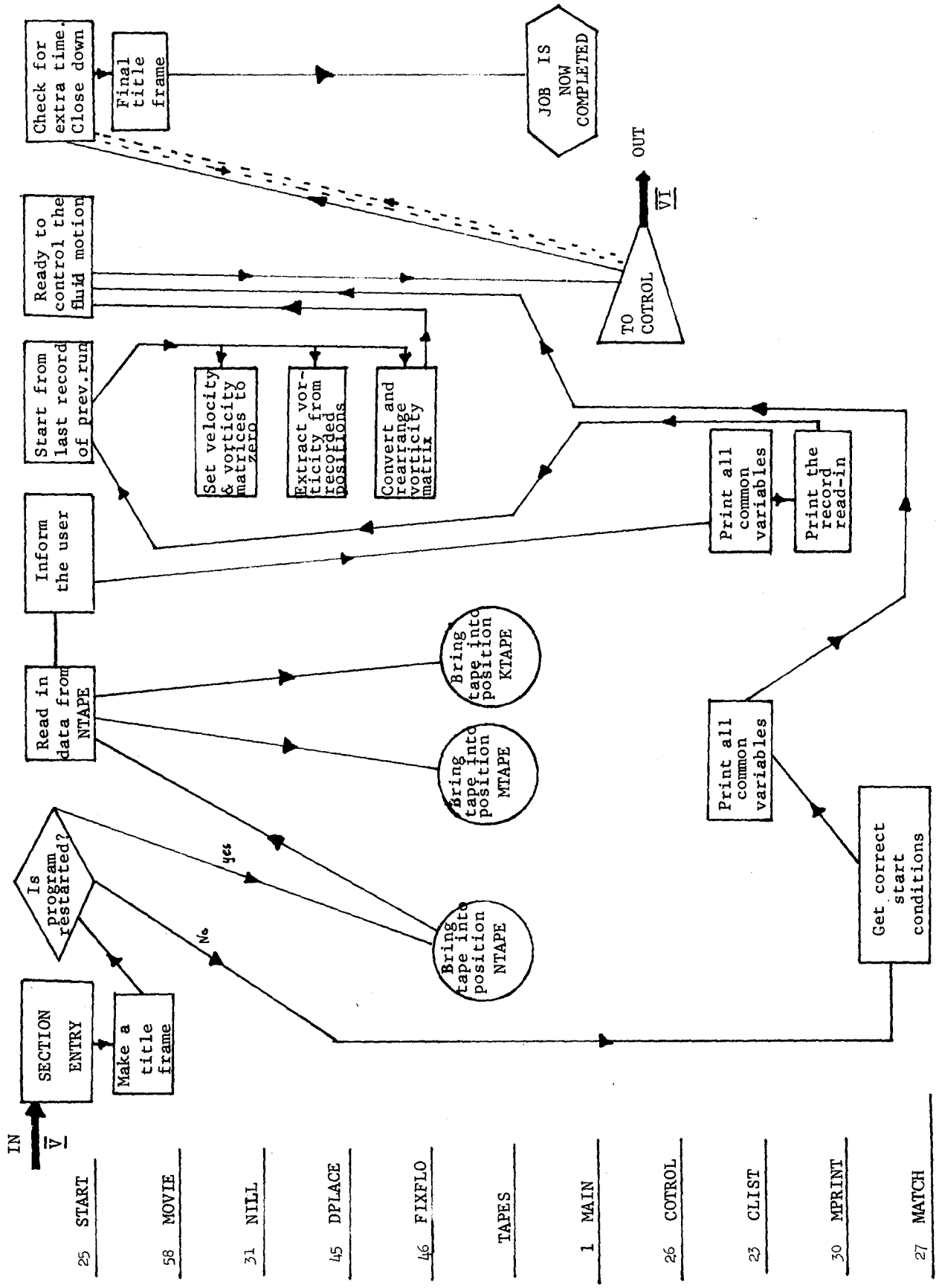
IN
V
SECTION ENTRY
Make a title frame
Is program restarted?
yes
No
Read in data from NTAPE
Bring tape into position NTAPE
Bring tape into position MTAPE
Bring tape into position KTAPE
Inform the user
Start from last record of prev.run
Set velocity & vorticity matrices to zero
Extract vorticity from recorded positions
Convert and rearrange vorticity matrix
Ready to control the fluid motion
Check for extra time. Close down
Final title frame
JOB IS NOW COMPLETED
OUT
VI
TO COTROL
Print all common variables
Print the record read-in
Print all common variables
Get correct start conditions
25 START
58 MOVIE
31 NILL
45 DPLACE
46 FIXFLO
TAPES
1 MAIN
26 COTROL
23 CLIST
30 MPRINT
27 MATCH

VI. CONTROL

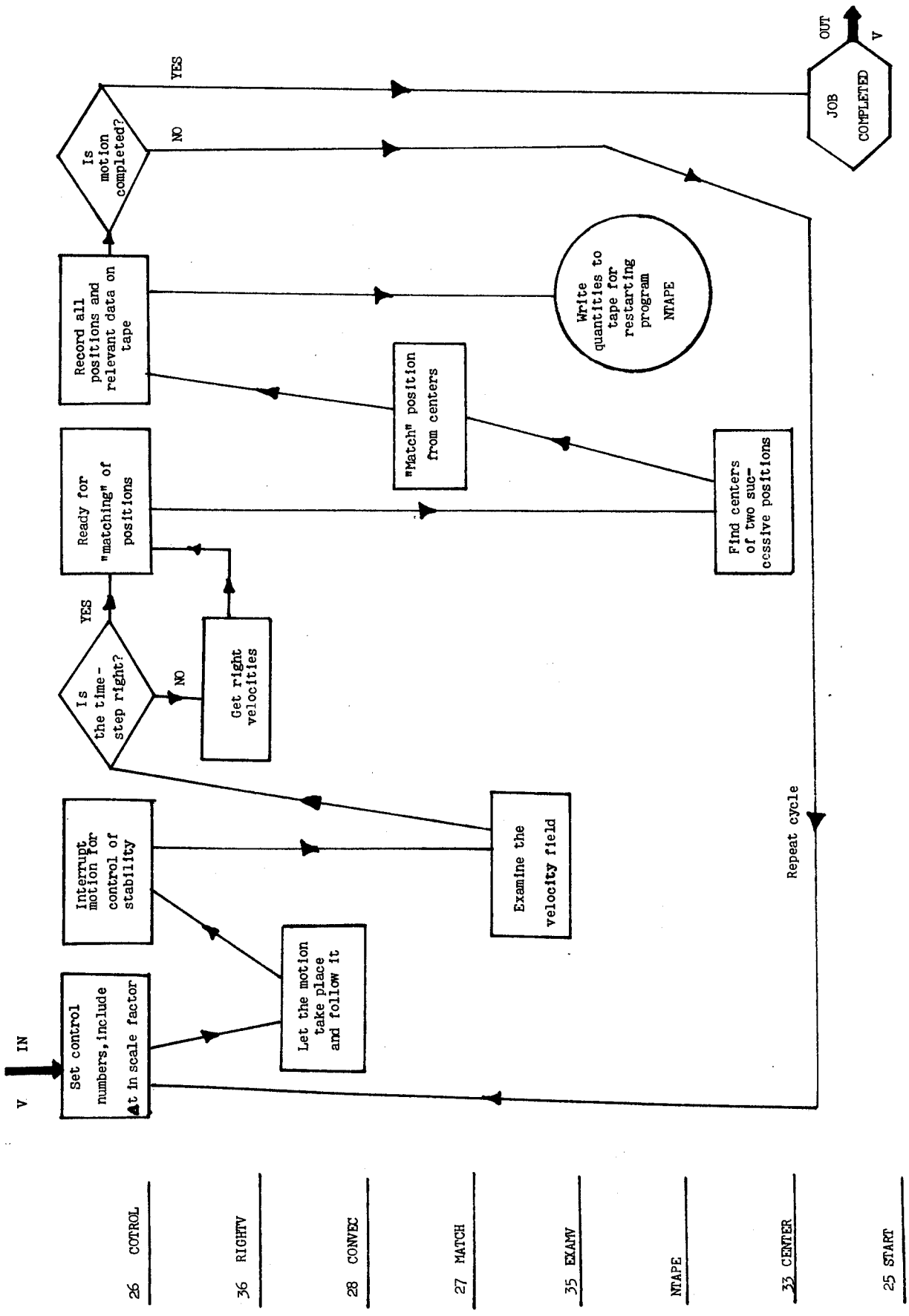
IN
Set control numbers, include Δt in scale factor
Interrupt motion for control of stability
Let the motion take place and follow it
Examine the velocity field
Is the time-step right?
YES
NO
Get right velocities
Ready for "matching" of positions
"Match" position from centers
Find centers of two successive positions
Record all positions and relevant data on tape
Write quantities to tape for restarting program NTAPE
Is motion completed?
YES
NO
JOB COMPLETED
OUT
Repeat cycle
26 CONTROL
36 RIGHTV
28 CONVEC
27 MATCH
35 EXAMV
NTAPE
33 CENTER
25 START

VII. FLUID MOTION

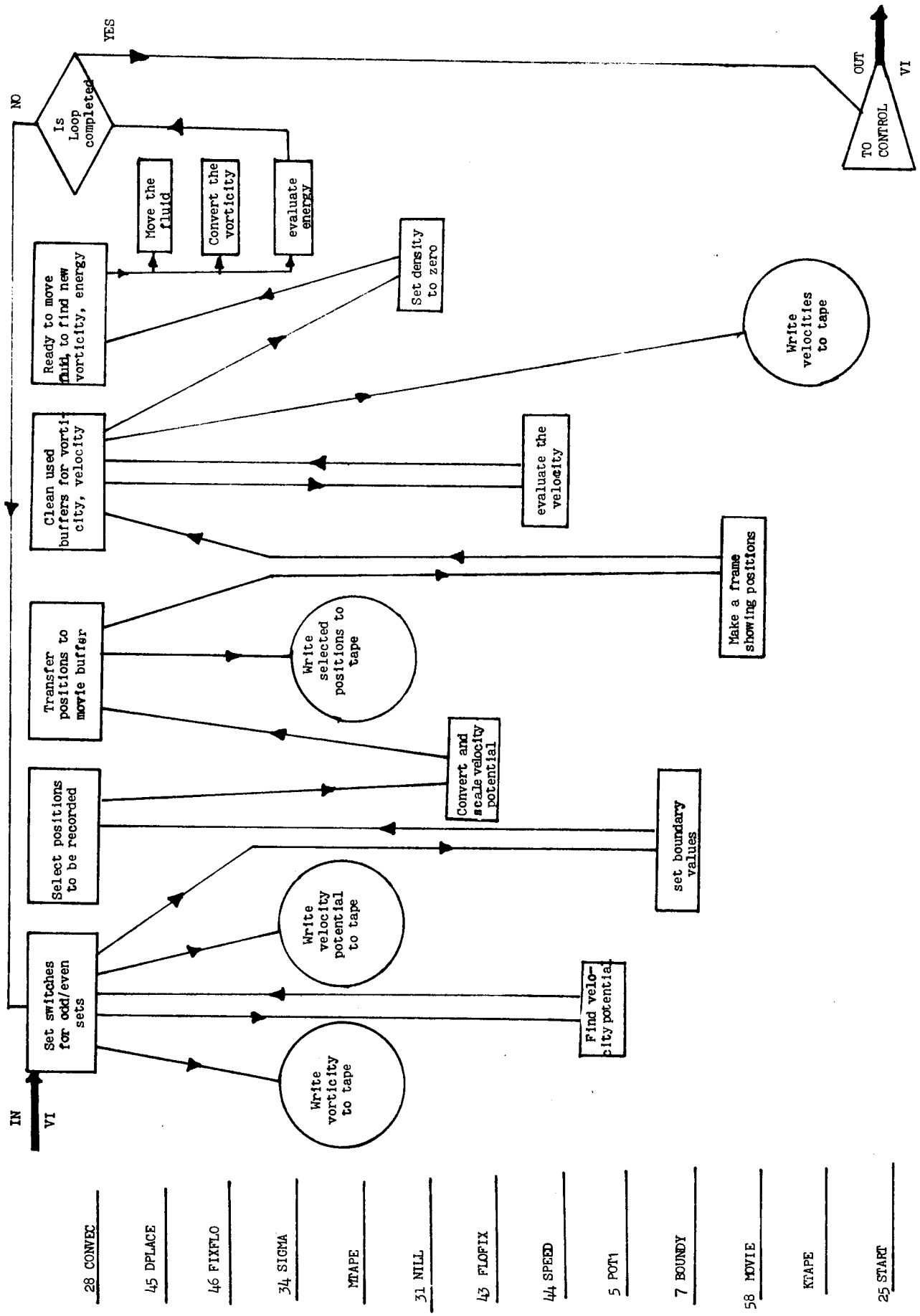

VIII. MATCH

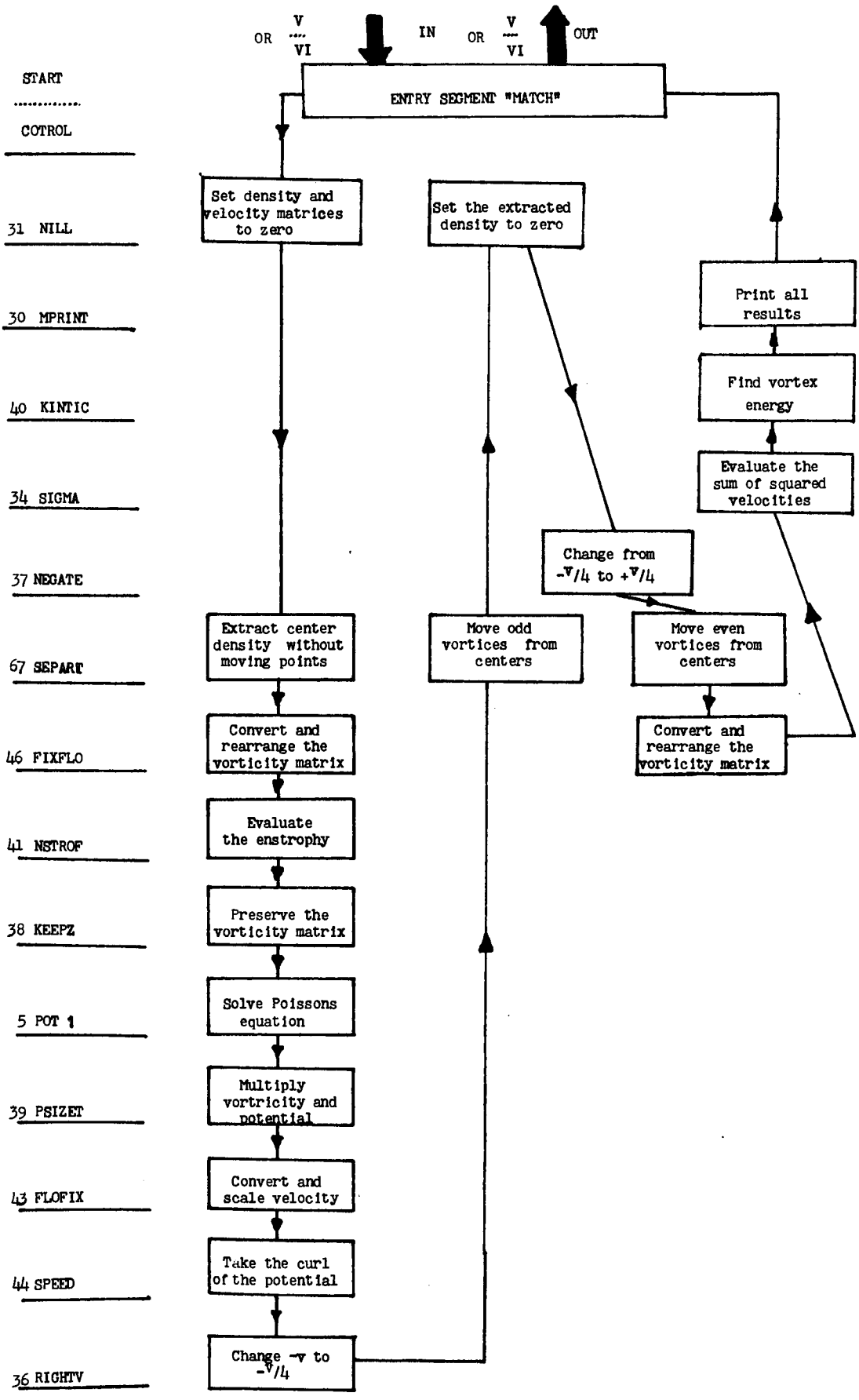
OR V/VI
IN
OR V/VI
OUT
START
COTROL
ENTRY SEGMENT "MATCH"
31 NILL
Set density and velocity matrices to zero
Set the extracted density to zero
Print all results
30 MPRINT
Find vortex energy
40 KINTIC
Evaluate the sum of squared velocities
34 SIGMA
Change from $-^{V}/_{4}$ to $+^{V}/_{4}$
37 NEGATE
67 SEPART
Extract center density without moving points
Move odd vortices from centers
Move even vortices from centers
Convert and rearrange the vorticity matrix
46 FIXFLO
Evaluate the enstrophy
41 NSTROF
Preserve the vorticity matrix
38 KEEPZ
Solve Poissons equation
5 POT 1
Multiply vortricity and potential
39 PSIZET
Convert and scale velocity
43 FLOFIX
Take the curl of the potential
44 SPEED
Change -v to $-^{V}/_{4}$
36 RIGHTV

The information comprises the positions of selected odd/even vortices and selected velocities. Printing can be done in octal or decimal format according to whether the common variables LPRINT is .TRUE. or .FALSE. respectively. The fluid energy has been calculated at each timesteps prior to the matching and an array with these values is printed.

After the matching process, the fluid energy, the sum (zeta x psi), mean fluid velocities, vortex energy, enstrophy, and mean vortex velocities are printed. These are calculated as follows:

$$\text{Fluid energy} = \sum_{\text{Mesh}} u_m \, u_m = E_1$$

$$\text{Sum (zeta x psi)} = \sum_{\text{Mesh}} f_m \cdot H_m = E_2$$

$$\text{Mean fluid velocity} = \frac{1}{M} \sum_{\text{Mesh}} u_m = U$$

$$\text{Vortex energy} = \sum_{\text{particles}} u_{pt} \cdot u_{pt} = L$$

$$\text{Enstrophy} = \frac{1}{M} \sum_{\text{Mesh}} f_m \cdot f_m = F$$

$$\text{Mean Vortex velocities} = \frac{1}{N} \sum_{\text{particles}} u_{pt} = V$$

where M is the number of meshpoints (4096), N is the number of point vortices, subscript 'm' indicates a value at a meshpoint, subscript 'pt' a value for a point vortex.

In order to convert to physical values, i.e. to find the scaling, we imagine a system of units as follows:

Quantity	symbol	value	computer model value
length	L	1	Mesh spacing
vorticity	T^{-1}	1	1 vortex particle
density	ML^{-2}	1	Mass of fluid within a cell.

If a particle is meant to simulate a charged particle in a plasma, (electron, ion), then that particle possesses a unit charge which is either positive or negative.

In order to calculate the value of the timestep in physical units we assume that the average velocity of the particles is known denoting this by $\langle \mu \rangle$ (in the right units) we get

$$\Delta t = \frac{\sqrt{L}}{2 \langle \mu \rangle} \frac{M}{N^3}$$

where L is the vortex energy as printed. This relation will give Δt in physical units, which can be compared with the value of Δt in program units.

In addition to the printed output program VORTEX can produce 4 magnetic tapes. 3 of these tapes contain information to be processed by analyser programs. The 4th tape is an IBM-tape which when run on the Benson-Lehner microfilm recorder will produce film or hard-copy showing the motion of the point vortices.

17. INPUT REQUIRED FOR A RUN

The input required by program VORTEX is the vorticity distribution f as approximated by eq.(3.1). This approximation is made by specifying the coordinates (q, p) of each point vortex. All coordinates are initially calculated in floating point form such that $0. \leqslant (q, p) \leqslant 64. 0$. The (q, p) positions of a point vortex are then packed into one fixed-point word in the array NXY. This array has to be filled up as indicated in Fig.10 assuming the number of point vortices to be NREAL.

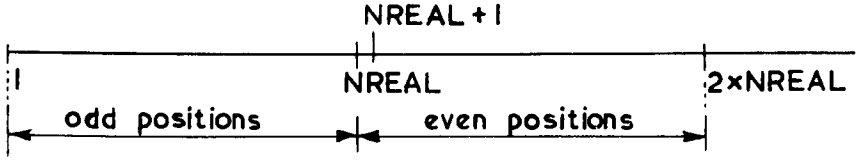

Fig.10.

The array is to be filled with position words starting from the 1st element. Element i and NREAL + i represent the positions of the same physical vortex and initially they are identical. The program checks this as well as the number of positions filled in and if there is an error an abnormal exit will occur.

In the clarified listing as well as in the User Manual (Sec.21) an example is given showing how to distribute points uniformly within a circle. The routine which the user supplies is called SOURCE.

The data for program VORTEX is supplied by the user in a routine called FDATA and the reader is referred to the User Manual.

In case an experienced user wants to change part of the program while maintaining the basic structure, a dummy routine called EXPERT is called for frequently from the routine CONVEC, which does the actual simulation sequence. By introducing his own version of EXPERT, the user is able to control the run or introduce new facilities.

18. PROGRAMMING TECHNIQUES

The most prominent feature of the VORTEX code is its vector integration technique; integer arithmetic has been used wherever possible. The (q, p) components of the positions and velocities are packed into one word NXY as illustrated (NPSI is the velocity word).

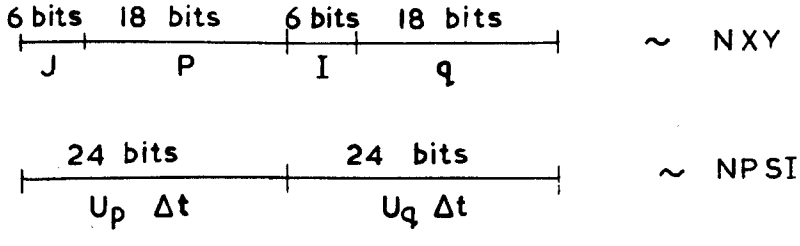

Fig.11.

With this structure most of the coding is done in KDF9 usercode. The 6 bits in a position word containing the mesh coordinate are easy to extract by shift operations. The most obvious advantage of this packing is the simultaneous time integration of (q, p) by adding the two words shown in the figure.

The potential-solver program POT1 works in floating point form, however, so that conversion routines FIX FLO, FLO FIX are used as indicated in the structure diagrams.

A careful study of the execution times for different instructions in KDF9 usercode has led to optimum design of the high speed loops in the routines which perform the time integration.

The next section briefly describes how a relatively simple routine is coded.

19. EXAMPLES OF OPTIMUM CODING

Suppose that the $2N$ positions of the odd/even point vortices are stored in an array called NXY. The first half of NXY contains N values of $\underline{r}_o$, the second values of $\underline{r}_e$.

Suppose that we wish to find $\underline{r}_C = \frac{1}{2}(\underline{r}_e + \underline{r}_o)$ the socalled centre position encountered in Section 9.

The following three criteria have been set for this subroutine (CENTER):

1. Although we write $\underline{r}_C = \frac{1}{2}(\underline{r}_e + \underline{r}_o)$ it is necessary to calculate $\underline{r}_C = \frac{1}{2}\underline{r}_e + \frac{1}{2}\underline{r}_o$. Referring to Fig.11 we see that if $IY_{o,e} \geqslant 32$ the y-interval will be lost because of over flow if addition is done before division.

2. Furthermore as each component has 24 bits we must make sure that division does not involve "flow" of bits from Y to IX.

3. To optimise the speed we examine the actual times for KDF9 instructions. Integer addition or division take 1 or 47 μsec respectively if done in the nesting store. A shift instruction (~ x 2" or /2") takes 5-6 μsec. A loop which scans over all N = NREAL point vortices must be as fast as possible.

The routine which performs this calculation is called CENTER. When the call occurs the addresses of its 2 arguments are left in the top two cells of the KDF9 nesting store, N1 and N2.

CENTER (NXY(1), NREAL)

```
= M15,      (Put address of NREAL in modifier of Q15      )
MOM15,      (Bring value of NREAL to nesting store N1     )
DUP,        (Make a duplicate in N2                       )
= RC15,     (Put NREAL in counter of Q15 and 1 in         )
            (incrementer, 0 in modifier                   )
= RM12,     (Put the other value of NREAL in the          )
            (modifier of Q12                              )
DUP,        (Make a duplicate of the address of           )
            (NXY(1) in N2                                 )
= M15,      (Put one copy of the NXY(1) in the modifier   )
            (of Q15                                       )
= + M12,    (Add the other copy of the address of MXY(1)  )
            (to the current contents in the modifier of Q12)
```

This section of code takes about 55 μsec and it is only executed once for one call of CENTER.

It results in the following contents of the Q-stores

	Counter	Incrementer	Modifer
Q12	0	1	Address of NXY(1+NREAL)
Q15	NREAL	1	Address of NXY(1)

THE LOOP IN CENTER

Execution time in μsec	Command	Number of used cells in nesting store	Explanation
9	1,MOM12,	1	Bring value of NXY(JE) (evenvortex) to top cell of nesting store
2	DUP,	2	Make a duplicate of this value
9	MOM15,	3	Bring value of NXY(JO) (odd vortex) to top of cell of nesting store
1	- ,	2	Make NXY(JE) - NXY(JO) ~ N1
5	SHA-1,	2	Shift the bit pattern in N1 arithmetic 1 bit down preserving the sign bit
7	SHC-23,	2	Shift the bit pattern in N1 (cyclic) 23 bits, i.e. y-part into x-part and vice-versa
5	SHA-1,	2	Shift the bit pattern in N1 arithmetic 1 bit down, i.e. x-part/2
6	SHC-24,	2	Shift the bit pattern in N1 (cyclic) 24 bits, i.e. y-part/2 into old position and x-part/2 into old position
1	- ,	1	Form NXY(JE) - (NXY(JE)-NXY(JO))/2 This gives $\underline{r}_C$
2	DUP,	2	Duplicate the value of $\underline{r}_C$
10	= MOM12Q,	1	Store this value and update address to NXY(JE + 1)
10	= MOM15Q,	0	Store this value, update address to NXY(JO + 1) and subtract 1 from counter in Q15
11	J1C15NZ,	0	Jump to label 1 if counter in Q15 is not zero
	VR,	0	Reset overflow register.
	EXIT1,END,	0	Return to the calling routine

We notice that the total execution time for the instructions in this loop is 78 μsec for one vortex particle. (0.4 sec ~ for 5000 particles).

The most "expensive" commands are the fetches and stores.

The 4 shift instructions are necessary because the first shift, SHA-1, may result in the flow of a non-zero bit from Y to IX.

The number of instructions words for this loop is $3\frac{4}{6}$, $\frac{4}{6}$ meaning 4 syllables out of the 6 syllables in one word. (1 syllable = 8 bits). Written in FORTRAN or ALGOL the same code would be rather complicated, time consuming, but perhaps easier to interpret.

20. SUITE OF ANALYSER PROGRAMS

The analyser programs developed so far are:

A. MODANA, mode analyser program
B. SPECTRUM, spectrum values of matrix
C. TELESCOPE, examine Vortex structures under magnification
D. FERMI, statistical properties
E. MARKER, exhibit the fluid motion
F. SURFACE, 3-D surface plots

MODANA examines m-modes excited on the surfaces of a vortex. It produces either phase-plane diagrams or growth rates.

SPECTRUM evaluates the frequency distribution of a mesh function and is meant to explain clustering phenomena occurring during simulation.

TELESCOPE magnifies the pictures produced by MOVIE thus enabling the user to see how a given distribution develops in time.

FERMI evaluates the functional relationship between f and H, and is used for examining the statistical properties of the computer model.

MARKER shows the motion of the physical fluid by introducing dummy particles moving with the velocities calculated by VORTEX.

SURFACE was written by Dr J.P. Boris and is able to produce pictures of 3-D surfaces for either f or H.

21. USERS MANUAL FOR PROGRAM VORTEX

Contents of Users Manual

21.1 Input Deck

The input deck for the Culham KDF9 is quite simple. It can be divided into 3 groups of cards:

I. Control cards

II. Fortran cards which formulate the problem

III. Data cards, (including Fortran data)

In order to illustrate this an example is given below, in which we assume that the problem to be solved is that of a single finite circular vortex placed in the centre of a square region, the boundaries of which have no normal component of the fluid velocity. To set up a circular region of constant vorticity we distribute point vortices in equidistantly spaced rings.

In the job deck listed below all cards underlined are necessary for any problem, that is they are independent of our particular example.

GROUP I

```
1.   * JOB ........
2.   * IOD TAPE 1/COMMON/SAVE * FOR USER
3.   * IOD TAPE 2/  "  /  "       "   "
4.   * IOD TAPE 3/  "  /  "       "   "
5.   * SUBSTITUTE VORTEX // CHRIS J
6.   * SUBSTITUTE DELSQPHI // CP GROUP
```

GROUP II

```
7.   * IDENTIFIER SOURCE
8.   * FORTRAN
9.   X SUBROUTINE SOURCE
10.  * SUBSTITUTE VORCOM
11.      IODD = NINDXY
12.      DR = 0.3
13.      NDR = 24
14.      NPR = 10
15.      XC  = 32.0
16.      YC  = 32.0
17.      DO 102 JR = 1, NDR
18.      R = FLOAT (JR) * DR
19.      NTHETA = JR * NPR
20.      DTHETA = 2.0 * PI/FLOAT (NTHETA)
21.      DO 101 JJ = 1, NTHETA
22.      THETA = FLOAT (JT) * DTHETA
```

```
23.             X = XC + R * COS (THETA)
24.             Y = YC + R * SIN (THETA)
25.         CALL LOCATE (X,Y, NXY(1), IODD)
26.         IEVEN = IODD + NREAL + 1
27.         NXY (EVEN) = NXY (IODD + 1)
28.     101 IODD = IODD + 1
29.     102 CONTINUE
30.         NI NDXY = IODD
31.         RETURN
32.         END
                                        GROUP III
33.     *   IDENTIFIER FDATA
34.     *   FORTRAN
35.     *   SUBROUTINE FDATA
36.     *   SUBSTITUTE VORCOM
37.             NRUN = 192
38.         RETURN
39.         END
40.     *   DATA
41.     T.H.I.S.  T.H.E.  L.A.B.E.L.L.I.N.G.  O.F.
42.     A  S.P.E.C.I.A.L.  T.E.S.T.  R.U.N.  T.O.
43.     D.E.M.O.N.S.T.R.A.T.E.  T.H.E.  U.S.E.
44.     O.F.  L.A.B.E.L.S.
45.     R.U.N.  1.2.(3).2  9./.1.2./1.9.6.9.
46.     *   END JOB
```

21.2 "Default mode" as opposed to "users mode"

The inclusion of cards 2-4 and 7-39 constitutes a deviation from the default mode, which comprises for the three parts:

I. Cards 1,5,6 SUPPLIED BY USER
II. Cards 7,8,9, 31 and 32. DUMMY SOURCE
III. Cards 33,34,35, 38 and 39. DUMMY FDATA
Cards 40-46. SUPPLIED BY USER

The program initially sets all common variables to default values (section 21.7), some of which are overwritten by the user in Groups II and III. Unless this is done, the default mode runs without any formulation of the problem to be solved, and so abnormal exit from the program will occur.

It is thus necessary to deviate from the default mode. In the following three sections we shall briefly describe the consequences of the deviations which have been made in our example. (DM "Default Mode").

21.3 Comments on Group I: "Control Cards"

A. Card 1 is an obvious necessity

B. Cards 2-4 supply the program with three magnetic tapes, because DM requires this.

C. Card 5 calls in the following cards:

```
47.  *   SUBFILE FLUID // CHRIS J
48.  *   SUBFILE OF LIBRARY // CP GROUP
49.  *   SUBFILE EG 3 LIBRARY
50.  *   SUBFILE CUL LIB
51.  *   TABLES
52.  *   CARD LIST
53.  *   STORAGE /6912
54.  *   IODTAPE 101/IBM-SC/SAVE
55.  *   XEQ
56.  *   PRELUDE
57.  *   RLB * ..... 3/12/1969 .. PRELUDE
58.  *   CHAIN 1
59.  *   RLB * ..... 3/12/1969 ... DUMMY. MAIN. PROGRAM
```

D. Card 6 calls in the Hockney-Poisson solver program.

21.4 Comments on Group II: "Formulation of Problem"

In the example discussed here, the particle positions are defined in loops. No matter how the user formulates the problem, the card 25 is used to define each single set of coordinates (x, y) in floating point form, with $0.0 \leqslant (x, y) \leqslant 64.0$, and cards 26, 27 and 28 must follow immediately after.

21.5 Comments on Group III: "Data"

In this example we have accepted all DM values except NRUN, the number of timesteps.

On cards 41-45 we have labelled our run by symbols starting in column 1 and proceeding in every other column until column 55.

21.6 Epilogue

Because we have accepted DM data it seems appropriate to explain what this is. In the following section the name of a variable, its significance and its DM value are shown. For logical variables the value .TRUE. causes action, the value .FALSE. causes the opposite. The table also shows the range of values;

A-B meaning that the variable varies continuously from A to B.

I1/12/13 meaning that the variable varies discontinuously from I1 to I2 in steps of I3.

Blank meaning no variation and

\+ meaning arbitrary variation.

21.7 TABLE OF DEFAULT VALUES

NAME	SIGNIFICANCE	RANGE	DEFAULT VALUE
DT	Value of delta t	+	1.0
HX	Mesh spacing in x	+	1.0
HY	Mesh spacing in y	+	1.0
IBCX	Parameter for boundary conditions in x	1/3/1	1
IBCY	Parameter for boundary conditions in y	1/3/1	1
KTAPE	Channel number of tape containing the velocities		3
MTAPE	Channel number of tape containing the potential		2
MTRY	Frequency of printing/matching	2/32/2	16
MVELOC	Number of bits representing V (average)	1/23/1	17
NHDPY	Frequency of hardcopy production	2/NRUN/1	16
NMINUS	Number of negative vortices	0/3200/1	0
NP1	Starting point of position printing	1/3199/1	1
NP2	End point of position printing	2/3200/1	8
NP3	Increment between NP1 and NP2	1/3200/1	1
NREAL	Total number of point vortices	1/3200/1	3200
NRUN	Number of timesteps to be done	1/200/1	2
NSKIP	Number of blocks to be skipped for restart of program from NTAPE	2/ /1	0
NTAPE	Channel number of tape for restarting program		1
NV1	Starting point of velocity printing	1/4224/1	1820
NV2	End point of velocity printing	2/4225/1	1827
NV3	Increment between NV1 and NV2	1/4225/1	64
POTCON	Potential value on boundaries	+	0.0
ZAD	Switch for adjusting the charges	0.0/1.0/1.0"	0.0
ZFAC	Scale Factor	+	64.0
LANA	Potential/vorticity to MTAPE		.TRUE.
LBEGIN	Start from initial conditions		.TRUE.
LCOPY	Make hard copies		.TRUE.
LFILM	Make film		.TRUE.
LMATCH	Stabilise the numerics		.TRUE.
LPRINT	Print diagnostic results in octal or decimal		.TRUE.
LRECOR	Record history on NTAPE		.TRUE.
LTROL	Control DT		.TRUE.
LVELOC	Eulerian velocities to KTAPE		.TRUE.

21.8 Comments on table

I. The two magnetic tapes MTAPE and KTAPE contain information dumped from core during simulation. They are meant to be used by a suite of analyser programs.

II. The tape NTAPE contains all the information required for a restart of the program from a problem time T_p

where $T_p = N * MTRY * MTRY * DT$, N arbitrary

At time T_p the tape NTAPE has recorded 2N blocks. A restart from time T_p is thus implemented by the following two cards (if N is say 30).

LBEGIN = FALSE
NSKIP = 2 * 30

If a tape is not required the appropriate control card can be omitted.

III. The variables IBCX and IBCY determine 1 set out of 9 possible sets of boundary conditions in (x,y) according to:

IBCX = 1	VX = 0	at x-boundaries
IBCX = 2	VY = 0	at x-boundaries
IBCX = 3	(VX,VY)	are periodic in X,

and similarly for IBCY at the Y-boundaries.

IV. The variable DT is automatically changed by the program according to the value of MVELOC, if LTROL = .TRUE.
With LTROL = .FALSE. the value of DT is not changed. MVELOC is equal to the number of bits occupied by the average velocity, that is 17 ~ ¼, 18 ~ ½, 19 ~ 1 etc.

V. The indexes NP1, NP2, NP3, NV1, NV2, NV3 can be set by the user according to which particles/which meshpoints he wants to examine with diagnostics.

VI. POT CON is the potential value at the boundaries. It is only required if either IBCX or IBCY or both are equal to 1.

VII. ZAD is a switch for adjusting the charges in double periodic geometry in such a way that the total charge is zero. ZAD is normally equal to 0.0, but if IBCX = IBCY = 3 (doubly periodic geometry) and if NMINUS ≠ NREAL/2, then ZAD must be set to 1.Ø by the user.

21.9 Users control of program VORTEX

The users control of a particular simulation consists of 3 distinct parts:

A. He has to define the problem concerned by setting up a distribution of point vortices in routine SOURCE (Section 21.1 and Section 21.4).

B. He has to provide the program with data relevant to his problem in routine FDATA (Section 21.5 and Section 21.7).

C. He can if he wishes interrupt the simulation cycle at 14 stages in the program, at which a routine EXPERT(I) is called. EXPERT(I), I = 1,14 is a dummy routine in the DM mode, but the user can write

his own version, allowing for the appropriate entries. EXPERT(I) is called at stages 1-9 from subroutine CONVEC, at stage 10 from subroutine START (Section 2.6) and at stages 11-14 from subroutine MATCH.

21.10 Conclusion of manual

Timing shows that a timestep performed by program VORTEX when run with appropriate DM - DATA takes approximately 20 secs. By cutting out all options this figure can be reduced to 12 secs. Relocation, initialisation and implementation of 300 timesteps for a typical run with appropriate DM - DATA takes 70 minutes.

22. CONCLUSION

A number of different goals have been aimed at in project VORTEX. In order of importance, these are briefly:

I. Production of physical results

II. Experience in programming and numerical technique

III. Documentation

It is left to the reader to judge the success of III and the author will welcome criticism of this topic.

ACKNOWLEDGEMENTS

This report was originally written in June 1969. Because substantial improvements to the VORTEX code have been made since, it was decided to publish the report after results had been obtained.

The Author is grateful to Dr K.V. Roberts who is the originator and supervisor of the project. The Author would also like to thank Dr Roberts and Mr B. McNamara for reading this report and suggesting some modifications.

REFERENCES

1. TRUESDELL, C., The Kinematics of vorticity. Indiana University Press (1954).

2. LAMB, H., Hydrodynamics. 6th Ed. Cambridge University Press (1932).

3. CHANDRASEKHAR, S., Hydrodynamics and Hydrodynamic stability. Oxford University Press (1961).

4. LIN, C.C., The theory of hydrodynamic stability. Cambridge University Press (1955).

5. FROMM, J.E., HARLOW, F.H., Phys. Fluids, 6, 975 (1963).

6. ABERNATHY, F.H., KRONAUER, R.E., J. Fluid Mech., 13, 1 (1962).

7. BERK, H.L., ROBERTS, K.V., Phys. Fluids, 10, 1595 (1967).

8. De PACK, D.C., J. Electronics Control, 13, 417 (1962).

9. DORY, R.A. J. Nuclear Energy (Pt.C), 6, 511 (1964).

10. ONSAGER, L., "Nuovo Cim. Suppl. VI, 130 (1949).

11. CHRISTIANSEN, J.P., ROBERTS, K.V., Proc. of Computational Physics Conference Culham Laboratory, paper 40. (1969).

12. CHRISTIANSEN, J.P., Roberts, K.V., Proc. of Computational Physics Conference Culham Laboratory, paper 52. (1969).

13. HOCKNEY, R.W., J.A.C.M., 12, No.1, (1965).

14. CHRISTIANSEN, J.P., HOCKNEY, R.W., Delsqphi, A. 2-dimensional Poisson solver program. Computer Physics Communications (to be submitted).

15. LYNDEN-BELL, D., M.N.R.A.S. 136, 101, (1967).

16. MORIKAWA, G.K., J. of Meteorlogy, 17, (1960).

17. TRUESDELL, C., TOUPIN, R.A. The classical field theories. Handbuch der Physik, vol.III/1 Springer Verlag, Berlin 1960.

18. BERK, H.L., NIELSEN, C.E., ROBERTS, K.V., Phys. Fluids. 13, 980, (1970).

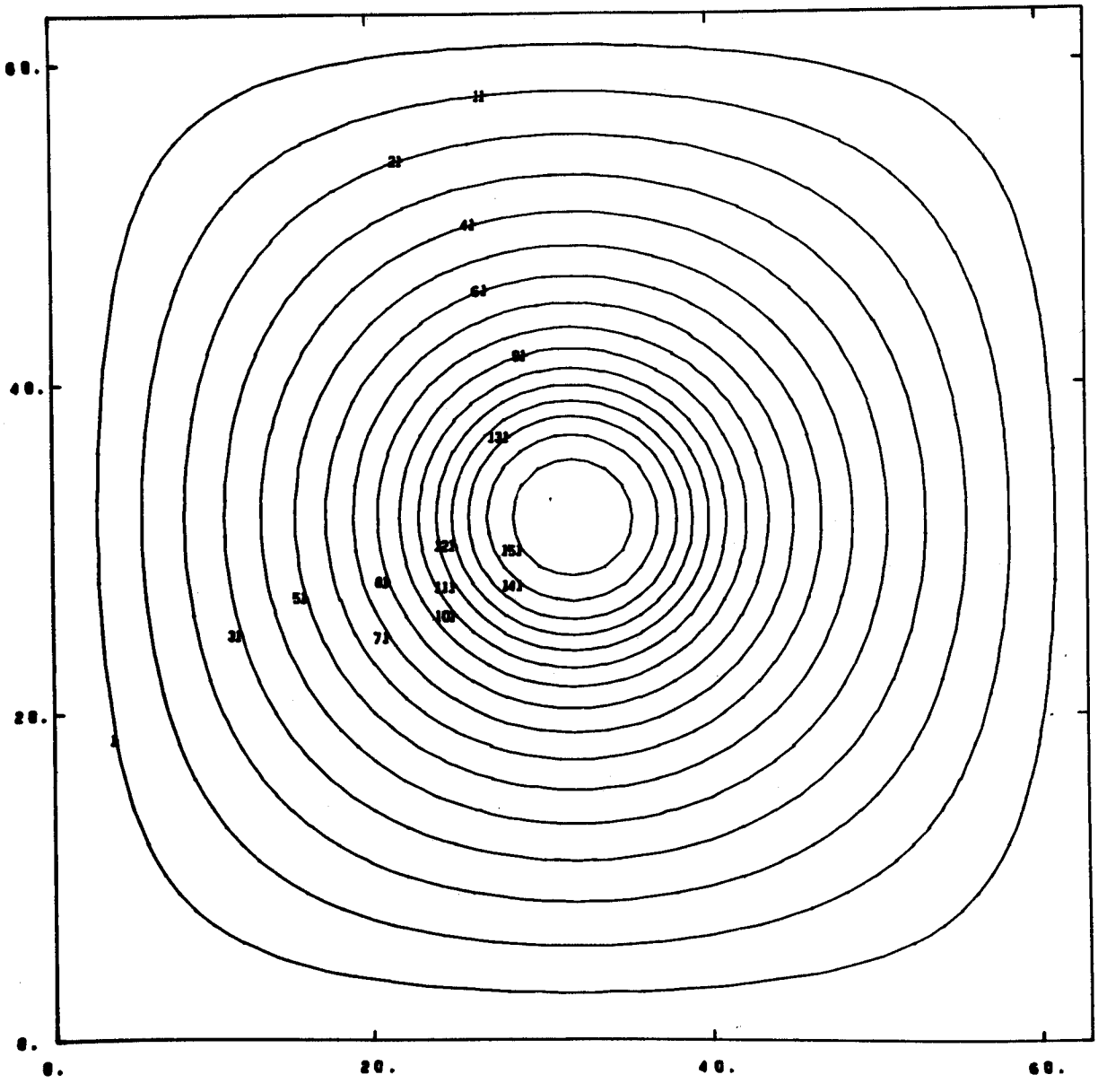

Fig. 1 Streamlines arising from a single circular vortex. Mesh size 64 x 64

CLM - R106

THE PICTURE IS PRODUCED BY PROGRAM TELESCOPE

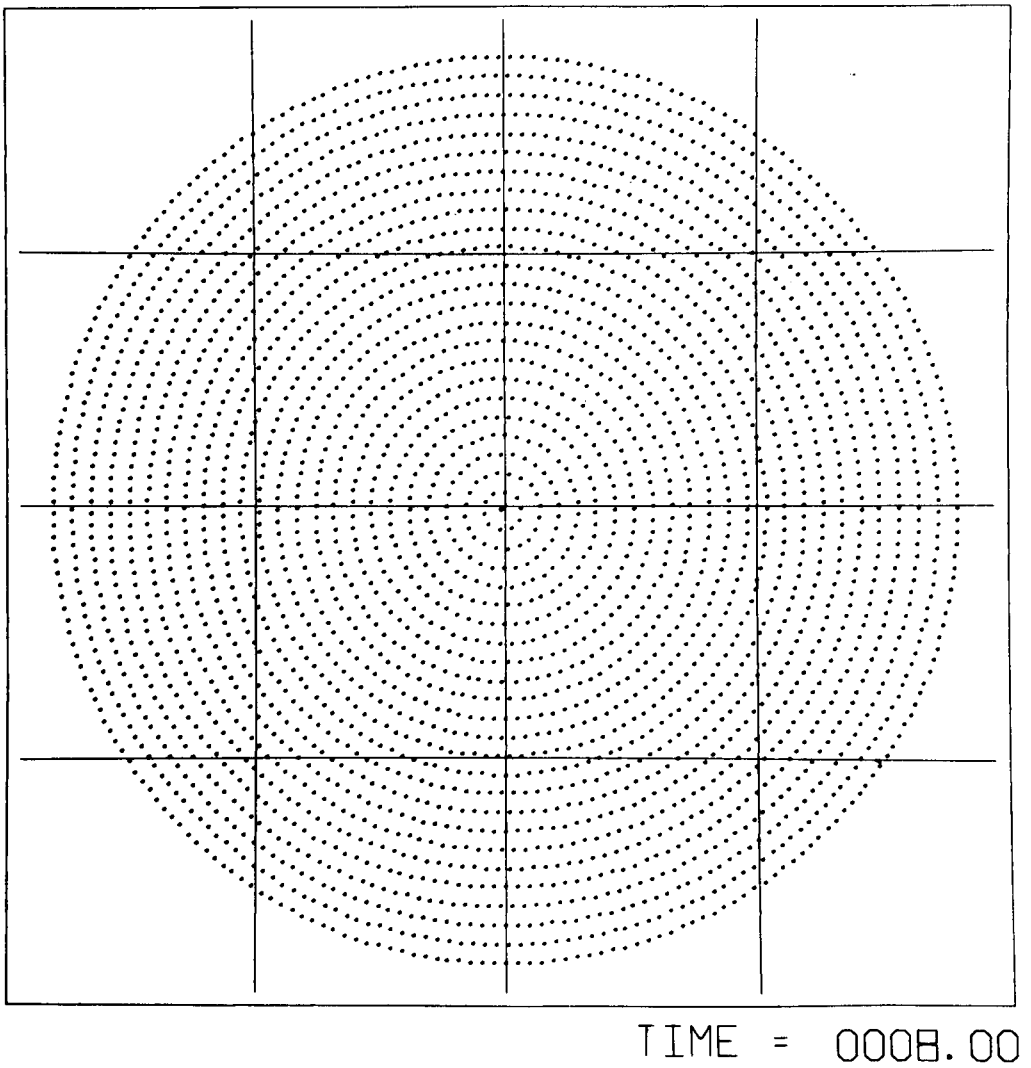

Fig. II Single circular vortex made up of point vortices. Mesh size 16 x 16

CLM-R106

THE PICTURE IS PRODUCED BY PROGRAM TELESCOPE

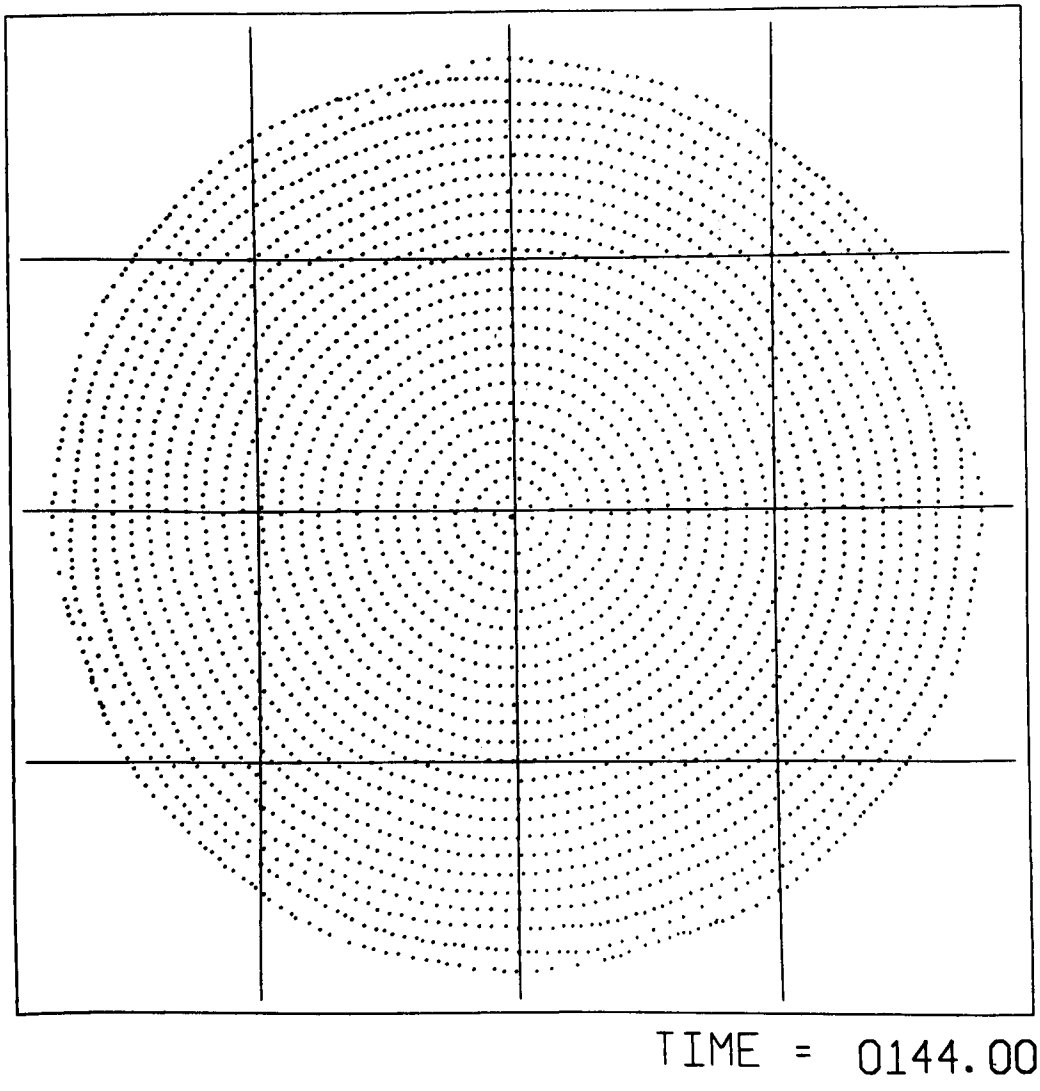

Fig. III Single circular vortex made up of point vortices. Mesh size 16 x 16

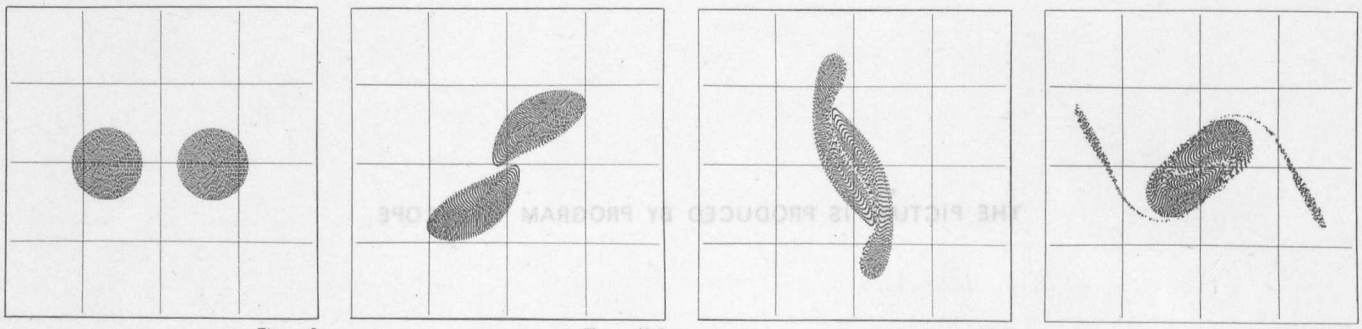

Two vortices coalescing because of sufficient initial proximity

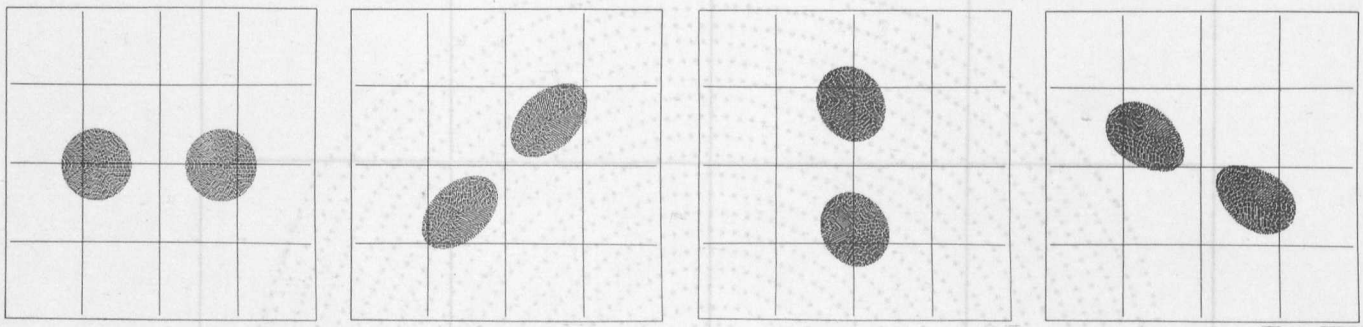

Two vortices precessing around each other. Large amplitude oscillations on their surfaces

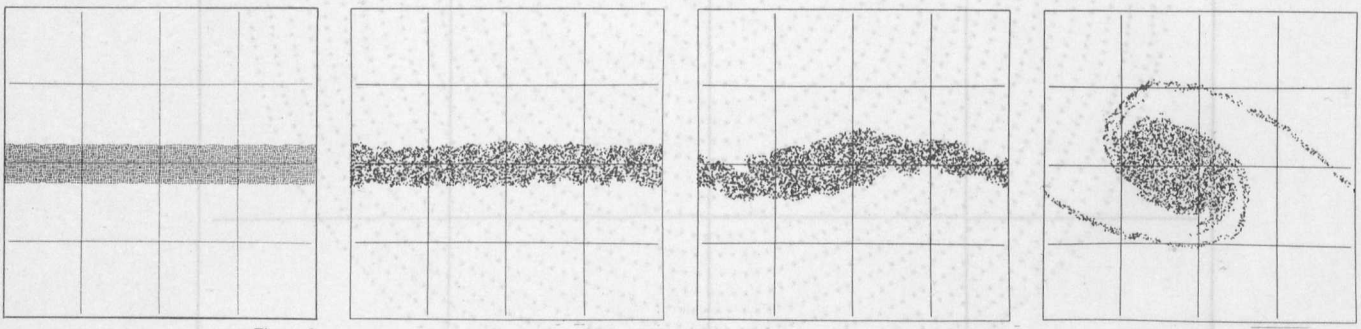

The onset of the Kelvin-Helmholtz instability

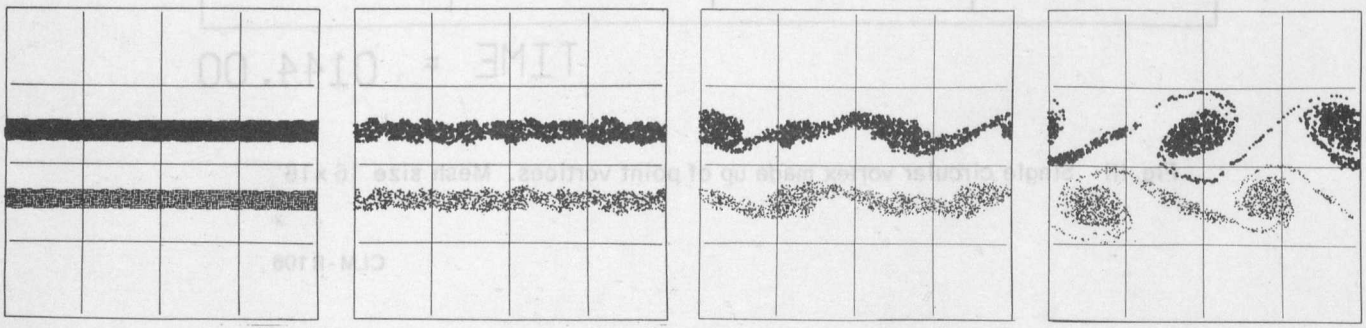

The formation of the von Karman vortex street

Fig. IV Flow problems simulated by program VORTEX